

HOCHSCHULE MÜNCHEN  
UNIVERSITY OF APPLIED SCIENCES



---

MASTER'S THESIS  
FACULTY FOR APPLIED NATURAL SCIENCES AND MECHATRONICS  
MASTER MICRO- AND NANOTECHNOLOGY

---

**Evaluation of novel piezoelectric actuators for metal based  
micro diaphragm pumps**

---

Julia Staude  
Matriculation nr.: 55677318  
e-Mail: staude@hm.edu

1. Academic supervisor: Dr. Karin Bauer
2. Academic supervisor: Prof. Dr. Alfred Kersch

External supervisor at the insitute: M. Sc. Nivedha Surendran  
Fraunhofer Institute for Electronic Microsystems and Solid State  
Technologies EMFT  
Hansastraße 27 c, 80686 München

*Date*  
June 27, 2025

## Declaration of Authenticity

I hereby declare on my honour that I have written this thesis independently and without the use of any aids other than those specified; any ideas taken directly or indirectly from external sources (including electronic sources) are identified as such without exception.

München, June 27, 2025

A handwritten signature in black ink, appearing to read "J. Heude". The signature is written in a cursive style with a large initial "J".

---

Signature of the student

## Confidentiality

The present Master Thesis contents has confidential information of Fraunhofer EMFT. Any publication or copying without permission of Fraunhofer EMFT is not allowed. Access to this document is limited to persons, involved into the examination procedure. These persons are bound to keep the information confidential. It should be noted, that in case of an applied legal review of the grading, this thesis has to be submitted to the court having jurisdiction.

München, June 27, 2025

A handwritten signature in black ink, appearing to read "J. Heude". The signature is written in a cursive style with a large initial "J".

---

Signature of the student

## Abstract

The development of micro metal diaphragm pumps (MMDP) represents a significant area of research in medical technology, particularly with regard to implantable drug delivery systems. Conventional piezoelectric actuators used to date, such as those based on lead zirconate titanate (PZT), contain lead and are therefore potentially harmful to both humans and the environment.

To promote a more sustainable alternative, lead-free piezoelectric actuators based on potassium sodium niobate (KNN) are to be integrated into the further development in this Thesis. To investigate the functionality of these lead-free actuators, electromechanical tests, including static and dynamic measurements as well as performance evaluation in both air and water media, are being conducted. A central part of this work also involves analyzing the actuators load capacity and their impact on the pump's performance. For this purpose, robustness tests followed by functional tests are carried out. The results demonstrate the feasibility of employing KNN-based actuators in MMDPs, offering promising alternative to conventional PZT ceramics.

Another challenge in the further development of piezoelectric MMDPs is their optimization for medical applications, such as precise control and monitoring of the flow rate. However, the fluidic system may be subject to various failure modes, such as blockages or air bubbles, which cannot be detected without external sensing. To address this issue, a piezoelectric actuator with an integrated sensing layer is being investigated. The aim is to evaluate the potential of this actuator design to detect fluidic disturbances in the pumping system. The experimental results confirm that piezoelectric actuators with integrated sensing capabilities can successfully detect such disruptions. The findings of this work contribute to a deeper understanding of the functionality and potential of various piezoelectric actuators and aim to identify new approaches for optimizing and expanding the functionalities of MMDPs.

Keywords: micro pump, piezoelectric actuators, micro dosing, self-sensing micro pump

## Kurzfassung

Die Entwicklung von Mikro Metall Membran Pumpen (MMDP) stellt ein bedeutendes Forschungsfeld in der Medizintechnik dar, insbesondere im Hinblick auf implantierbare Systeme zur Wirkstoffverabreichung. Bisher konventionell verwendete piezoelektrische Aktuatormaterialien wie Blei-Zirkonat-Titanat (PZT) enthalten Blei und sind daher sowohl für den Menschen als auch für die Umwelt potentiell schädlich.

Um eine nachhaltigere Alternative zu fördern, sollen bleifreie piezoelektrische Aktuatoren auf Basis von Kalium-Natrium-Niobat (KNN) in die Weiterentwicklung von MMDPs integriert werden. Zur Untersuchung der Funktionalität dieser bleifreien Aktuatoren werden elektromechanische Tests, darunter statische und dynamische Messungen, sowie Charakterisierungen mit Luft und Wasser durchgeführt. Ein zentraler Bestandteil der Arbeit ist zudem die Analyse der Belastbarkeit der Aktuatoren und deren Einfluss auf die Leistung der Pumpe, wozu Langzeit-Belastungstests und anschließende Funktionstests erfolgen. Die Ergebnisse deuten darauf hin, dass bleifreie piezoelektrische Aktuatoren eine vielversprechende Alternative zu den herkömmlichen PZT-Keramiken darstellen.

Eine weitere Herausforderung bei der Weiterentwicklung piezoelektrischer MMDPs besteht in der Optimierung für medizinische Anwendungen. Dazu zählt insbesondere die präzise Steuerung und Überwachung der Durchflussrate. Im fluidischen System kann es zu verschiedenen Fehlerzuständen, wie Blockierungen oder Luftblasen im System kommen, die ohne die Verwendung externer Sensoren nicht erfasst werden können. Zur Lösung dieser Herausforderung wird ein piezoelektrischer Aktuator mit integrierter Sensorschicht untersucht. Ziel ist es, das Potenzial dieses Aktuator-Designs zur Erkennung möglicher fluidischer Störungen im Pumpsystem zu evaluieren. Die experimentellen Ergebnisse zeigen, dass piezoelektrische Aktuatoren mit bereits integrierten Sensoreigenschaften solche Störungen erfolgreich detektieren können. Die Ergebnisse dieser Arbeit sollen dazu beitragen, ein tieferes Verständnis der Funktionalität und des Potenzials verschiedener piezoelektrischer Aktuatoren zu entwickeln und neue Ansätze zur Optimierung und Erweiterung der Funktionalitäten von Mikropumpen aufzuzeigen.

## Acknowledgement

My special thanks go to my supervisor, Nivedha Surendran, who provided me with great commitment, professional expertise and constant support throughout the entire process. Her valuable suggestions and constant willingness to help have contributed significantly to the success of this thesis.

I would also like to thank Dr. Karin Bauer, my first supervisor, for her helpful advice and food for thought, which opened up new perspectives and enriched the depth of my work.

I would also like to thank Prof. Dr. Alfred Kersch, who kindly took on the role of second supervisor and thus made it possible to review this thesis.

A further thank you goes to Martin Richter, whose impulses and ideas have repeatedly provided me with new insights into the topic and allowed me to gain even deeper knowledge about the topic.

For the support of the work in the lab, I want to thank Martin Wackerle, who was always available for kindly helping with the devices and measurement programs in the laboratory. Last but not least, I would like to thank Nina Martin (work bestie), who, as a valued office colleague, was always available to answer my questions and made my day-to-day work easier through her exchange of mind.

# Contents

<b>1</b>	<b>Introduction</b>	<b>1</b>
1.1	Background and context . . . . .	1
1.2	Problem statement and research objectives . . . . .	1
<b>2</b>	<b>State of the art</b>	<b>3</b>
2.1	Piezoelectric micro pumps in medical technology . . . . .	3
2.2	Piezoelectric actuators . . . . .	5
2.2.1	Piezoelectric effect in lead-based and lead-free materials . . . . .	5
2.2.2	Bulk piezoelectric actuators . . . . .	7
2.2.3	Stack piezoelectric actuators . . . . .	7
2.3	Self-Sensing in micro pumps . . . . .	8
2.4	Fraunhofer EMFT micro pumps . . . . .	9
<b>3</b>	<b>Materials and methods</b>	<b>10</b>
3.1	Materials . . . . .	10
3.1.1	Piezoelectric micro pumps . . . . .	10
3.1.2	Piezoelectric actuators . . . . .	11
3.1.3	Additional equipment and materials . . . . .	14
3.2	Methodologies . . . . .	15
3.2.1	Fabrication of micro pumps . . . . .	15
3.2.2	Mounting of the piezoelectric actuators onto the micro pumps . . . . .	16
3.2.3	Housing of the micro pumps . . . . .	17
3.3	Methods of analysis . . . . .	18
3.3.1	Electro mechanical characterization . . . . .	18
3.3.2	Air characterisation . . . . .	20
3.3.3	Water characterisation . . . . .	21
3.3.4	Robustness test . . . . .	22
3.3.5	Surface and structural analysis . . . . .	24
<b>4</b>	<b>Results and discussion</b>	<b>26</b>
4.1	Initial quality assessment of the piezoelectric actuators . . . . .	26
4.2	Evaluation of the lead-free bulk piezoelectric actuators . . . . .	27
4.2.1	Electro mechanical characterization - static stroke measurement . . . . .	27
4.2.2	Electro mechanical characterization - dynamic stroke measurement . . . . .	30
4.2.3	Air characterization . . . . .	33
4.2.4	Water characterization . . . . .	39

4.2.5	Robustness test . . . . .	47
4.2.6	Surface and structural analysis . . . . .	56
4.3	Evaluation of lead-based stack piezoelectric actuators with self-sensing properties	61
4.3.1	Optimization of the micro pump fabrication process . . . . .	61
4.3.2	Electro mechanical characterisation - static stroke measurement . . . . .	64
4.3.3	Evaluation of the self-sensing properties . . . . .	65
4.4	Failure mode and effects . . . . .	68
<b>5</b>	<b>Summary and outlook</b>	<b>72</b>
<b>6</b>	<b>Appendix</b>	<b>I</b>
6.1	Material data for different piezoelectric actuators . . . . .	I
6.2	Measurement results of the preliminary examination of the piezoelectric actuators	III

## **Acronyms**

**KNN** potassium sodium niobate

**MEMS** micro electro mechanical systems

**MMDP** micro metal diaphragm pumps

**MPB** morphotropic phase boundary

**PT** lead titanate

**PZT** lead zirconate titanate

**SEM** scanning electrode microscopy

# 1 Introduction

## 1.1 Background and context

The increasing demand for compact and energy-efficient micro fluidic systems in medical and industrial applications has led to a growing interest in micro metal diaphragm pumps (MMDP). These miniature pumps rely on piezoelectric actuators for fluid transport using passive check valve to control the flow direction, offering precise control, low energy consumption, and miniaturized design. However, improving the performance and sustainability of such systems remains a key challenge in advancing their practical use.

This Master’s thesis focuses on the evaluation of novel piezoelectric actuators for use in MMDPs, with the aim of enhancing performance while exploring environmentally friendlier and functionally advanced alternatives.

Piezoelectric actuators have long been a core component in micro fluidic systems due to their fast response time and precision. Traditionally, lead-based PZT piezoelectric ceramics have been the industry standard, owing to their high piezoelectric coefficients and mechanical stability. However, concerns about lead toxicity and regulatory restrictions have spurred research into lead-free alternatives.

In addition, conventional actuator systems lack integrated feedback mechanisms, making it difficult to detect anomalies such as blockages or flow irregularities during operation, without external sensors. Recent developments in self-sensing piezoelectric actuators promise to bridge this gap by enabling simultaneous actuation and condition monitoring in real-time.

This research builds upon these advancements by investigating both lead-free and self-sensing lead-based piezoelectric actuators for their suitability in MMDPs.

## 1.2 Problem statement and research objectives

While existing MMDPs perform reliably using conventional lead-based PZT piezoelectric actuators, there are two major limitations: Firstly, environmental concerns due to the use of lead, and secondly lack of integrated sensing capabilities for real-time monitoring. Lead-free actuators often suffer from reduced performance, and their feasibility in practical micro pump applications remains insufficiently explored. Furthermore, although self-sensing actuators have been proposed, their integration into micro pumps and practical sensing accuracy under dynamic conditions have not yet been thoroughly validated.

The primary objective of this Master’s thesis is to evaluate the applicability and performance of two novel piezoelectric actuator types in MMDPs:

- a lead-free bulk piezoelectric actuator, and
- a lead-based stack actuator with self-sensing capabilities.

The study involves the electro mechanical, and fluidic characterization of both actuator types under various test conditions, including a robustness test of the lead-free piezoelectric actuators. The goal is to assess their performance in comparison to standard actuators and to determine their potential for future implementation in environmentally friendly and intelligent micro pump systems.

## 2 State of the art

### 2.1 Piezoelectric micro pumps in medical technology

Micro pumps play an important role in the medical technology and the engineering fields, as they are suitable to deliver small volumes at high precision [1]. Therefore, they attracted a lot of attention for different applications, like micro fluidic sensors or high heat flux cooling [[2], [3]]. After the introduction of the first micro electro mechanical systems (MEMS) based micro pump for insulin delivery, many more use cases were found out for the use in the medical field [4]. This includes MEMS-based micro pumps and many more [[5]].

Micro pumps are commonly categorized based on their working principle, with a general distinction between mechanical and non-mechanical types [6]. Since this work focuses on piezoelectric micro pumps, the emphasis will be placed on mechanical micro pumps. These include piezoelectric micro pumps, among others [6], [7]. Mechanical micro pumps operate using physical actuators or mechanical components to drive fluid movement. In addition to piezoelectric actuators, other types of mechanical micro pumps include electrostatically actuated pumps, thermally actuated pumps, and several other variants [[8], [9], [10]].

Micro pumps are characterized by the delivery of fluids in the nano and lower micro litre range and are usually very small. Especially in medical technology, mechanical micro pumps are the preferred option, as non mechanical micro pumps often times use magnetic fields or electric fields for driving the pump. These forces may interact with the chemical properties of the drug that is pumped through the micro pump, which makes these types of pumps unsuitable. Among mechanical micro pumps, piezoelectric micro pumps show a very fast response, drive at low energy and are easy to integrate. [11]

Piezoelectric micro pumps usually consist of a pump chip with passive check valves, to control the flow direction. On the pump chip, the actuator is mounted to build a fully functionalized pump [[12], [13], [14]]. The pump chamber is defined by the inlet and outlet valve and a diaphragm. The diaphragm is moved laterally through the piezoelectric disk actuator, which then moves the fluid inside through negative and positive pressures in the pump chamber. The flow rate is proportional to the number of movement cycles the piezoelectric actuator goes through. The piezoelectric actuator is driven with an alternating input signal. Thus, the flow rate can be adjusted with the actuation frequency.

There are many ways to characterize micro pumps. Some of the key characteristics are as follows:

- Flow rate: Volume, that is transported through the pump per time
- Blocking pressure: Maximum pressure a pump can generate in the pump chamber, measured by applying a pressure to the outlet of the pump, the so called backpressure

- Self-Sensing: The system being able to recognize and handle any disturbances such as bubbles or blockages, without the use of external sensing devices

For the actuation of piezoelectric micro pumps, different kinds of piezoelectric actuators are suitable for different applications. There are different kinds of piezoelectric micro pumps, that fulfil different purposes. For very low flow rates, micro pumps are used, that work with piezoelectric thin films at a thickness of  $1,5\ \mu\text{m}$  to achieve flow rates in the nano litre range at a very low energy consumption [15]. Another piezoelectric actuator for example is a folded vibrator with piezoelectric sheets to improve the efficiency in terms of deflection and power consumption [7].

Further developments of piezoelectric actuators are forwarding in the direction of stack piezoelectric actuators, that combine multiple layers of piezoelectric sheets. Compared to the bulk piezoelectric actuators, the stack actuators drive at lower voltages, are higher in cost but also higher in precision [16]. In Figure 1 the difference between bulk and stack actuator is depicted.

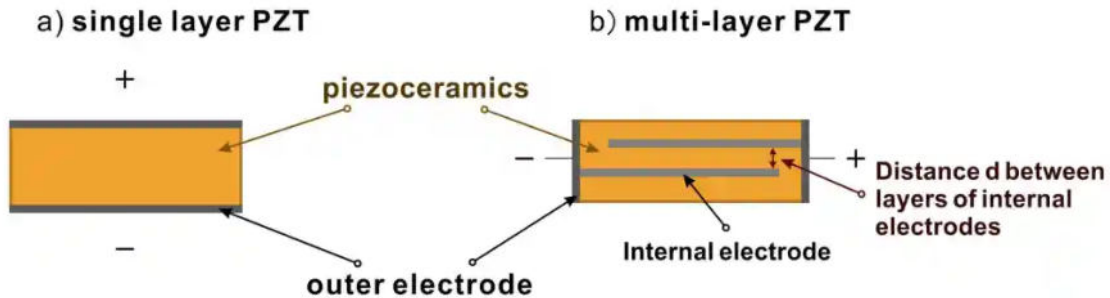


**Figure 1** Schematic of bulk (single-layer) vs. stack (multi-layer) piezoelectric actuators [16]

PZT is the most common actuator ceramic. This material shows a good piezoelectric efficiency, low fabrication cost and it can be fabricated into different shapes [17]. However, PZT contains lead, which is toxic and environmentally hazardous. Therefore, other alternatives for efficient piezoelectric actuators are being investigated. One proposed alternative is barium titanate ( $\text{BaTiO}_3$ ) nanoparticles which are embedded into a polymer matrix of polyvinylidene fluoride (PVDF) [18]. Other researches focus on potassium sodium niobate (KNN) as an alternative [[19], [20], [21], [22]].

## 2.2 Piezoelectric actuators

### 2.2.1 Piezoelectric effect in lead-based and lead-free materials

The piezoelectric effect describes the bidirectional coupling between mechanical stress and electrical polarization in certain crystalline solids. [23]. Specifically, the direct piezoelectric effect occurs when a crystalline solid generates temporary electrical energy in response to mechanical loading. This phenomenon is explained by polarization: the displacement of the internal positive and negative charge centers results in opposite charges appearing on the surfaces of the dielectric material [19]. In contrast, the indirect piezoelectric effect involves the temporary mechanical deformation of a solid when subjected to an external electrical voltage [24]. Both effects require an asymmetric molecular structure and a band gap within the material [25].

A special class of piezoelectric materials is ferroelectric materials, which exhibit not only piezoelectricity but also spontaneous and reversible polarization. Ferroelectric materials consist of regions, called domains, where the polarization spontaneously aligns in the same direction. By applying a high electric field, known as the coercive field strength, these domains can be oriented in a uniform direction. This process is referred to as the poling of the material. After the material undergoes poling, a remanent polarization remains, meaning the reorientation of the domains is preserved. Domain reorientation can also be induced by mechanical stress, with compressive stress potentially leading to partial or complete depolarization. In piezoelectric materials, polarization occurs during production when the material is heated above the Curie temperature, and applying a strong electric field during the cooling process. Depending on the specific composition, the materials have different domain mobilities and also different polarization and depolarization behaviours. Materials with low domain mobility are difficult to pole but can withstand high electrical or mechanical loads without significant loss of their piezoelectric properties. [26]

Regarding piezoelectric materials, three key parameters significantly influence their performance and operating mode: the output strain  $\delta$ , the polarization field  $\mathbf{P}$ , and the actuation field  $\mathbf{E}$ . The relative orientations of these parameters determine the working mode of the piezoelectric actuator. Common modes include the longitudinal, transverse, and shear modes. The material is first polarized in a specific direction by the polarization field  $\mathbf{P}$ . When an actuation field  $\mathbf{E}$  is applied, either in the same or a different direction, it causes the material to deform accordingly, depending on the mode of operation [27].

One of the most used piezoelectric materials is perovskite PZT. It is a monolithic piezoelectric ceramic [28]. PZT ceramics offer advantages such as ease of fabrication, application-specific shaping, low production costs and more [29]. Another reason for the widespread use of PZT is the extensive isomorphism allowed by the perovskite structure, enabling property tailoring

through compositional adjustments. PZT ceramics show excellent piezoelectric performance, inducing high charge and voltage coefficients, large dielectric constants, strong electro mechanical coupling coefficients, high charge density and high energy density [30]. Just as in lead titanate (PT), the same perovskite structure forms in PZT (see Figure 2).

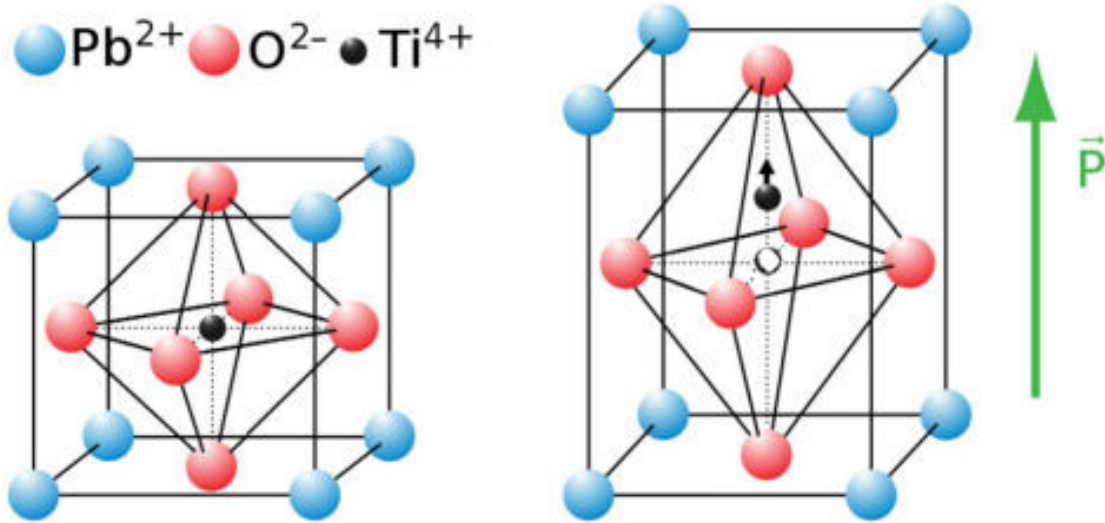


**Figure 2** Perovskite structure of PT before and after polarization [31]

The ferroelectric phase of PZT changes to a non-ferroelectric phase below the Curie temperature (cubic), so it is important to operate this piezoelectric material at temperatures below the Curie temperature [31]. In comparison to PT, PZT shows superior piezoelectric performance, as the piezoelectric coefficient  $d_{33}$  is higher [32]. Another special feature about this material is the occurrence of morphotropic phase boundary (MPB). This is due to the composition of the material: It consists of lead zirconate ( $PbZrO_3$ ) and lead titanate ( $PbTiO_3$ ). Compositions of PZT, that are close to the MPB show excellent piezoelectric characteristics, due to the composition induced ferroelectric-to-ferroelectric phase transitions. [33]

However, due to environmental concerns and potential hazards to human health and the environment, it is desirable to incorporate lead-free materials in future developments.

One promising alternative is KNN. Compared to other lead-free alternatives this material has good ferroelectric properties and electro mechanical coupling factors, that are still below the values of PZT. Also the curie temperature is typically high at around  $420^\circ\text{C}$  [34], making this material suitable for a high temperature range. KNN has a complex perovskite structure, in which the A-site is shared between Na and K. It is a mixture of potassium niobate ( $KNbO_3$ ;  $KN$ ) and orthorhombic antiferroelectric sodium niobate ( $NaNbO_3$ ;  $NN$ ). [31]

For most of the application in mechanical micro pumps, these different piezoelectric materials are shaped into a disc form and can be categorized as either bulk piezoelectric actuators or stack piezoelectric actuators, depending on the design and actuation requirements.

**2.2.2 Bulk piezoelectric actuators**

Bulk piezoelectric actuators consist of a single layer of piezoelectric material with single electrodes on the top and bottom of the disc. These actuators can vibrate at nanometer to micrometer amplitudes with extremely high speed and precision. They show a very fast response, high precision displacement and a low power consumption. [35]

Figure 3 shows the schematic design of a bulk piezoelectric actuator with top electrode, piezoelectric disc and bottom electrode.

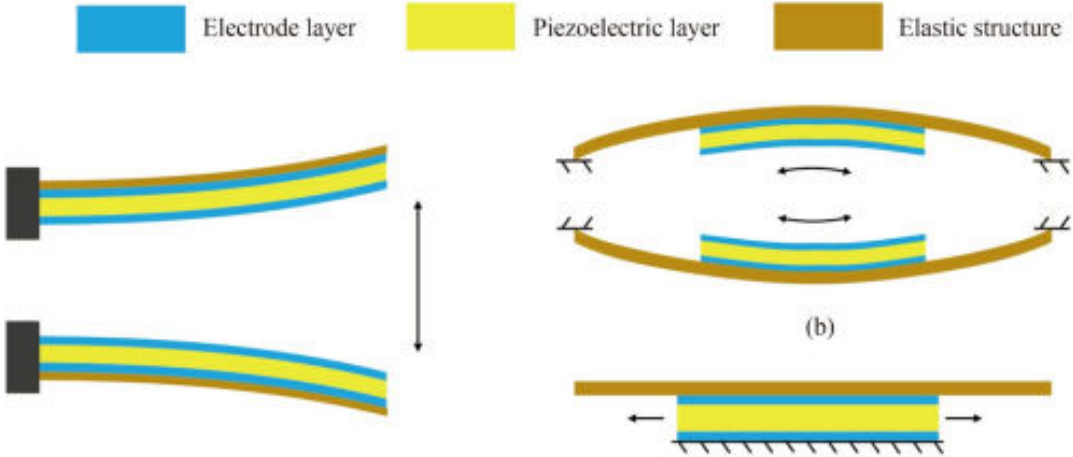


**Figure 3** Schematic design of bulk piezoelectric actuators [27]

Regarding the use of these piezoelectric actuators on micro pumps, the transversal piezoelectric effect  $d_{31}$  is the most important. Since disc actuators are bonded to the diaphragm of the pump, the expansion and contraction of the material in the planar direction under actuation causes a change in the volume of the pump chamber [27].

**2.2.3 Stack piezoelectric actuators**

To enhance deformation and strength of the piezoelectric actuators, a common approach is to put multiple piezoelectric layers in one single layer structure. All of the piezoelectric layers are oriented in the same direction and are connected to the electrical input. The different layers are isolated from each other. When voltage is applied, each layer contributes to the overall displacement. As a result the total displacement is the cumulative effect of all

individual piezoelectric layers. The maximum voltage application to the actuator depends on the specific design and the thickness of each layer. [36]

The schematic of a piezoelectric stack actuator is given in Figure 4.

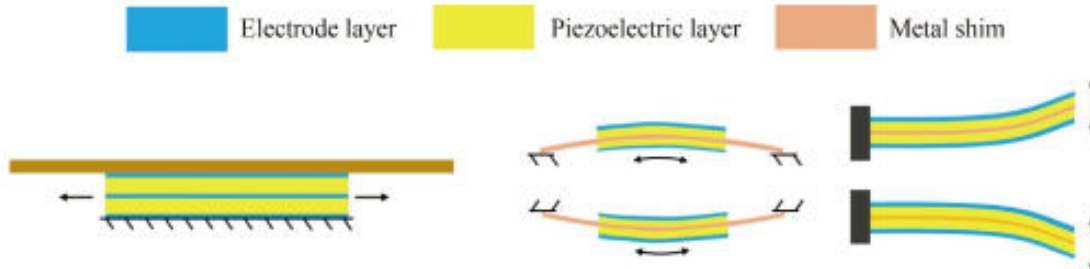


**Figure 4** Schematic design of stack piezoelectric actuator [27]

### 2.3 Self-Sensing in micro pumps

Another critical area of research is the evaluation of the safety and reliability of micro pumps. In medical applications, precise control and continuous monitoring of the delivered volume are essential. A major challenge in such systems is the occurrence of various failure modes that can disrupt flow and compromise dosing accuracy. Issues like blockages in the fluidic pathway or the presence of air bubbles can lead to significant deviations from the intended delivery volume, potentially resulting in severe consequences. Currently, real-time monitoring typically requires the use of external measurement devices.

To overcome this limitation, current research explores the use of self-sensing techniques to detect flow disruptions or potential failure states within the system [37]. This approach aims to integrate sensing functionality directly into the micro pump, thereby enhancing system reliability and reducing the reliance on external sensors.

Regarding piezoelectric micro pumps, efforts are focused on utilizing the direct piezoelectric effect to monitor actuator displacement during operation. The direct piezoelectric effect refers to the generation of an electrical voltage in response to mechanical deformation. When the actuator bends during actuation, a measurable voltage is generated, which can then be used to infer the displacement of the actuator. This self-generated signal enables real-time condition monitoring without the need for additional sensor components [38].

## 2.4 Fraunhofer EMFT micro pumps

Fraunhofer EMFT piezoelectric micro pumps are made of stainless steel and use a piezoelectric actuator to pump fluids. The piezoelectric actuator converts an electrical input signal into a mechanical movement with which the fluids are moved through the pump. Figure 5 shows the schematic cross-section of a micro pump in its non-functional state without voltage applied. The micro pump consists of different stacks of metal parts, such as 1,3 mm thick metal base plate with inlet and outlet openings, two valve foils with spring arm structures that are each 50  $\mu\text{m}$  thick, and a 100  $\mu\text{m}$  thick diaphragm foil (see Figure 5: 2, 3, 4, 5). To create an impermeable pump chamber for a fully functional metal micro pump, all elements mentioned above are laser welded together. On top of the micro pump a piezoelectric actuator is mounted by gluing with a two-component epoxy glue. While curing of the glue takes place, the ceramics are exposed to a defined electric field. Therefore, bonding takes place in the contracted state of the piezoceramic. After curing, the voltage is removed, and expansion of the ceramic bulges out the pump chamber. This specific mounting process introduced by Herz et al ([39]) establishes a large compression ratio, which leads to self-priming and bubble-tolerant micro pumps [40]. This method is applied to all piezoelectric micro pumps manufactured at EMFT [41].

The micro pump is usually located in a housing (Figure 5: 7), into which the pump is pressed with seals (Figure 5: 6). [42]

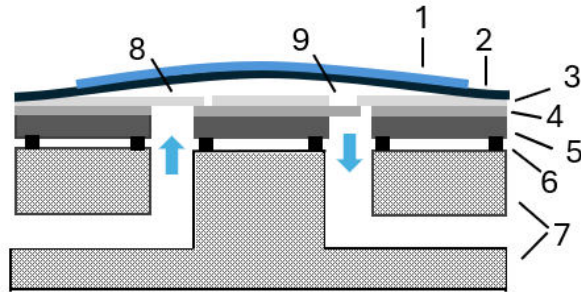


**Figure 5** Schematic cross-section of a micro pump in its non-functional state. Pump components: 1) piezoelectric actuator 2) Diaphragm 3) 1st valve foil 4) 2nd valve foil 5) Metal base plate 6) Sealing rings 7) Housing 8) Inlet 9) Outlet

Positive and negative voltages can be applied to the piezoelectric actuator to operate the micro pump. Due to its piezoelectric properties and the utilisation of the indirect piezoelectric effect, the application of a voltage leads to a contraction or expansion of the actuator. The voltages required for this depend on the respective piezoelectric actuator. When a negative voltage is applied, the expansion of the piezoelectric actuator is maximised so that a vacuum is generated in the pump chamber, which ensures that the non-return valve at the inlet opens and the fluid flows into the chamber (see Figure 7a).

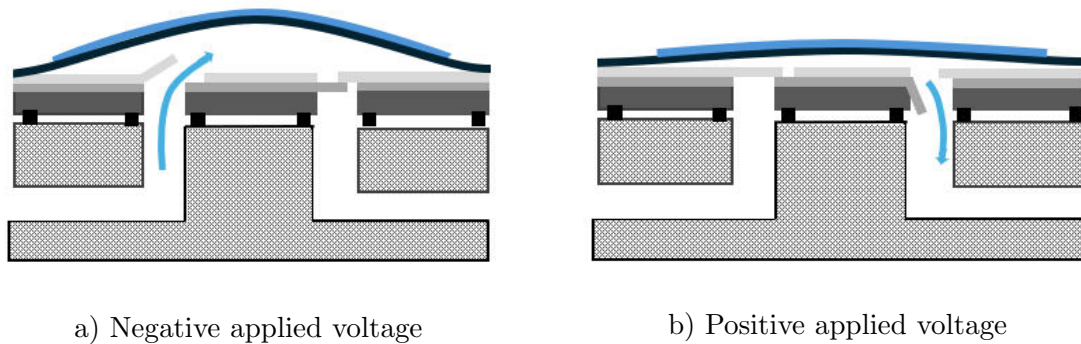


**Figure 6** Schematic cross-section of a metal micro diaphragm pump with applied voltages

As soon as sufficient fluid has flowed in and the vacuum has stabilised, the valve closes. If a positive voltage is then applied to the piezoelectric actuator, the material contracts and excess pressure builds up in the pump chamber, causing the non-return valve at the outlet to open. The fluid flows out of the chamber (see Figure 7b).

### 3 Materials and methods

In the following sections, all materials and methods used in this work are described. This includes the materials themselves, working principles, fabrication processes, and experimental procedures. The aim of this chapter is to provide a comprehensive overview of the data acquisition process in alignment with the objectives of this thesis. The chosen materials and experimental methods are discussed with a focus on explaining the rationale behind their selection. Furthermore, this section is intended to ensure the reproducibility of the experiments conducted.

#### 3.1 Materials

##### 3.1.1 Piezoelectric micro pumps

The piezoelectric micro pump used in this work are made of stainless steel and have a diameter of 20 mm. Depending on the configuration of the individual layers used to build the pump, the total thickness of the base body is approximately 1,5 mm.

The pump body consists of multiple layers. The first layer is the metal base, which includes two holes for the inlet and outlet. The second and third layers are valve foils containing laser-cut structures that form passive check valves. These foils are positioned with a rotational offset of  $180^\circ$  relative to each other. Each valve foil has a thickness of  $50\ \mu\text{m}$ . Above these, the diaphragm is placed, with a thickness of either  $100\ \mu\text{m}$  or  $150\ \mu\text{m}$ , depending on the type

of piezoelectric actuator used [43].

The individual layers of the base body are joined using laser beam welding.

The type of piezoelectric actuator bonded on top of the pump significantly influences its performance characteristics, such as the actuation voltage range, maximum flow rates for air and water, and the stroke volume.

### 3.1.2 Piezoelectric actuators

This study investigates three distinct types of piezoelectric disc actuators relevant for micro pumps: a standard lead-based bulk actuator, a lead-free bulk variant, and a lead-based stack actuator with integrated self-sensing functionality.

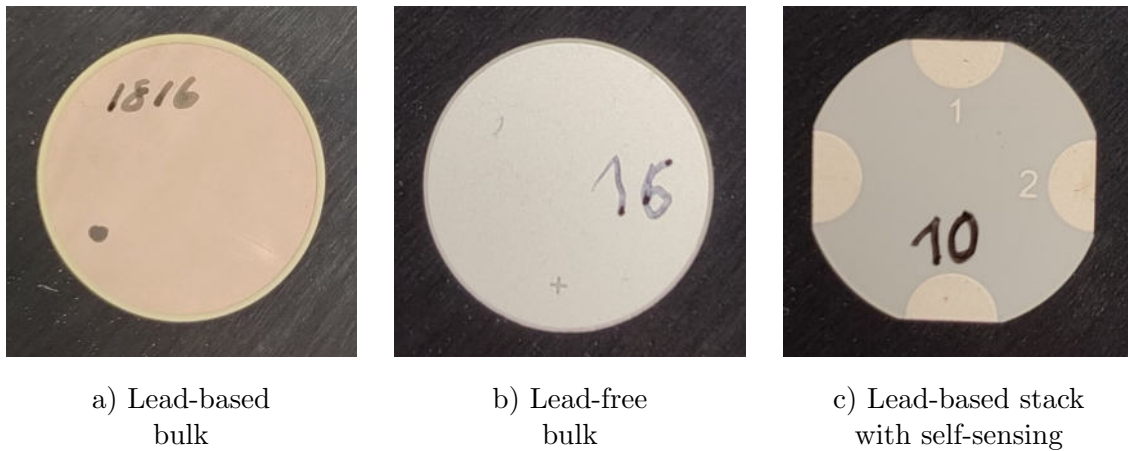


**Figure 7** Overview of selected piezoelectric disc actuators used in this work

The manufacturing process of bulk piezoelectric actuators, both lead-based and lead-free, follows a similar workflow. It begins with granulate of the desired ceramic material, which is pressed into cylindrical forms. These are then sintered at temperatures up to 1300 °C, resulting in approximately 15 % shrinkage and forming a dense, stable ceramic. After sintering, the cylinders are precision cut into thin discs using special saws. Next, electrodes are applied using screen printing technology, producing layers approximately 10 μm thick. These electrode pastes, typically containing silver or silver-palladium alloys, are fired at temperatures above 800 °C. For thinner layers (around 1 μm), sputtering technology is used, employing materials such as gold, copper, or copper-nickel alloys. Finally, the ceramic discs are polarized. This critical step aligns internal dipoles, enabling the material to deform upon subsequent exposure to an electric field below the coercive field strength. [44]

In the following sections, each of these actuators will be presented in more detail.

### **Lead-based bulk piezoelectric actuator**

The lead-based bulk piezoelectric actuators (PI Ceramic GmbH, Auburn, USA) are of type PIC151. These actuators are used as the standard actuator in MMDPs due to its advantageous material properties, as summarized in Table 12 in Appendix 6.1. The material exhibits high piezoelectric coefficients, excellent mechanical strength, and good elasticity. The recommended operating temperatures are going up to 50% of the Curie temperature. The top electrode is a copper-nickel-alloy. [45]

Since lead-based actuators contain lead, which is known to be harmful to humans and the environment, this work aims to investigate a lead-free alternative.

### **Lead-free bulk actuators**

The lead-free bulk piezoelectric actuators (PI Ceramic GmbH, Auburn, USA) are made from KNN or of type PIC753. This material exhibits decent piezoelectric charge coefficients, although they are generally lower than those of lead-based actuators. Similarly, the electromechanical coupling factors are acceptable, but still inferior compared to lead-based. The values of the elastic compliance and stiffness coefficients indicate that KNN is mechanically more brittle than PZT (see Table 13, Appendix 6.2). The top electrode is made of silver. [45]

It should be noted that lead-free materials must be re-evaluated for each specific application, as their reliability and long-term performance may differ from that of lead-based materials.

### **Lead-based stack self sensing actuators**

The lead-based stack self-sensing piezoelectric actuators (PI Ceramic GmbH, Auburn, USA) are made from a lead-based material known as PIC252 (see Table 14, 6.1). In this stack configuration, multiple thin ceramic layers are stacked vertically. The actuator consists of 14 active piezoelectric layers, complemented by two additional top layers that serve control and self-sensing functions. Insulating layers are positioned at the bottom of the actuator, between the active and sensing layers, and on the top surface to ensure proper electrical isolation.

The thickness of the individual layers is approximately 30 nm, as is the thickness of the insulating layers. The electrodes on top of the piezoelectric material are made from a silver-palladium alloy, which is commonly used as a conductor or electrode material due to its good electrical conductivity and thermal stability. Recommended operating temperatures for this piezoelectric actuator lie between  $-20^{\circ}\text{C}$  and  $150^{\circ}\text{C}$ . [45]

### Comparison of the three investigated piezoelectric actuators

A comparison of the different piezoelectric actuators and their most important properties are shown in Table 1.

**Table 1** Comparison of properties of different piezoelectric actuators used in this work [45]

Characteristic	PIC-151	PIC-753	PIC-252
	bulk, lead-based	bulk, lead-free	stack, lead-based
<b>Physical and dielectric properties</b>			
Material	PZT	KNN	PZT
Electrode material	Copper-nickel	Silver	Palladium-silver
Curie temperature	250 °C	300 °C	350 °C
Coercive field strength in $kV/mm$	1.0	1.1	1.5
<b>Electro-mechanical properties</b>			
Piezoelectric charge coefficient $d_{31}$ in $10^{-12}C/N$	-210	-118	-180
Coupling factor $k_p$	0.62	0.53	0.62
<b>Acousto-mechanical properties</b>			
Elastic stiffness coefficient $C_{11}^D$ in $10^{-10}N/m^2$	15.7	17.2	15.4
<b>Advantages and Disadvantages</b>			
Advantages	Industrial standard  High performance	Environmentally friendly	Self-sensing  Stack for higher vis- cous fluids
Disadvantages	Harmful to environ- ment	Moderate perfor- mance  more brittle material	Harmful to environ- ment

### 3.1.3 Additional equipment and materials

#### Adhesive glue

The conductive glue evaluated as a substitute for soldering the piezoelectric actuators is Elecolit 3661 (Panacol-Elosol GmbH, Steinbach, Germany). This adhesive is a modified, one-component epoxy resin that does not require mixing through a static mixer prior to application. It is solvent-free as well as both thermally and electrically conductive.

The base material consists of a grey epoxy matrix filled with silver particles, with a D90 particle size of 10  $\mu\text{m}$ . The filler content amounts to 71%. The viscosity of the adhesive ranges between 20 000 mPas to 40 000 mPas, ensuring dimensional stability in the uncured state.

Curing process is still needed for this glue. In order to minimise the thermal load on the piezoelectric actuators, an adhesive that cures at comparatively low temperatures was selected. Typical curing conditions are temperatures between 80 °C to 150 °C with curing times ranging from 6 h to 10 min. Higher curing temperatures generally lead to shorter curing times. However, curing times can vary depending on the adhesive volume and initial temperature conditions. Full mechanical strength is typically achieved after at least 24 hours.

After curing, the adhesive exhibits a temperature resistance ranging from  $-40\text{ }^{\circ}\text{C}$  to  $180\text{ }^{\circ}\text{C}$ . The volume resistivity is between  $1 \times 10^{-3}\ \Omega\ \text{cm}$  to  $5 \times 10^{-3}\ \Omega\ \text{cm}$ .

In order to achieve optimal adhesion, all bonding surfaces must be cleaned prior to adhesive application. Surface pre-treatment is carried out to degrease the surfaces, remove dust and clean them of other contaminants. Typically Isopropanol is used for this step. [46]

#### Adhesive Epoxy Foil

The double-sided adhesive epoxy foil Ablestik 563K (Henkel AG & Co. KGaA, Düsseldorf, Germany) is being evaluated as a replacement for adhesive glue in attaching piezo elements to the pump. The foil has a thickness of 50  $\mu\text{m}$ , and it is both thermally conductive and electrically insulating. Curing is required and can be performed either for 30 min at 150 °C or for 2 h at 125 °C. These curing schedules are recommended but may vary depending on handling or other influencing factors.

Prior to applying the epoxy foil, all surfaces must be thoroughly cleaned and free of grease or dust to ensure optimal adhesion. The foil should be handled with care, as it lacks a supporting structure. Surfaces are recommended to be preheated to approximately 45 °C. To avoid air bubbles beneath the foil, the adhesive film should be gently pressed down. [47]

#### Additional measurement equipment

In addition to the main components, some auxiliary measuring devices were also used. These were mainly used for general measurements.

The Acculab Atilon ATL-840 (Sartorius AG, Göttingen, Germany) precision scale was used for various gravimetric measurements. This precision scale can measure mass up to an accuracy of 0,1 mg.

The multimeter 138 TRMS (Keithley Instruments GmbH, Germering, Germany) was used for various electrical measurements. This allows important measured values to be recorded quickly and easily. In the context of this work, the multimeter was mainly used to measure various capacitances, such as the capacitance of the piezoelectric actuators themselves or the pump as a whole. The multimeter was also used to assist with troubleshooting in the event of short circuits, for example.

The oscilloscope RTB2002 (Rohde & Schwarz GmbH & Co. KG, Munich, Germany) was used to record the self-sensing properties of the multilayer piezoelectric actuators. With a bandwidth of 70 MHz to 300 MHz, a sampling rate of up to 2,5 Gsamples/s are possible. [48] Another smaller portable oscilloscope was used for measurements in the laboratory. The Analog Discovery 3 (Digilent C/O NI, Austin, USA) can easily be connected to a laptop and measure up to a sampling rate of 125 Msamples [49].

## 3.2 Methodologies

### 3.2.1 Fabrication of micro pumps

The production of the metal micro diaphragm pump requires several key components, as illustrated in Figure 8.



**Figure 8** Components of the micro pump base body [50]

The manufacturing process itself is very fragile. The valve foils and diaphragm of the pump are very thin, making these foils very sensitive to thermal stress during the welding process.

Only a slight change in the welding set up and parameters can change the welding results significantly. The quality of the welding process is very important, as bad welding seams result in leakages in the micro pump.

Firstly, the valve structures are positioned so that they precisely cover the inlet and outlet opening holes of the metal base plate. Then the foils are tacked to the base plate with multiple micro tack weld spots to ensure a minimum air gap, thereby achieving close contact of the foils. Later, a circular, hermetic weld of 6,5 mm joins the valve structure to the base plate. This circular weld is crucial as it prohibits pumping liquid from having a free leakage fluidic path between inlet and outlet openings. As a final step, a circular weld of 18 mm joins the deflecting actuator diaphragm to the pump chamber. All the welding seams should be hermetically tight and free of blown welds, as it aids in having a leak-free micro pump. Thus, leading to optimal micro pump efficiency and pressure build-up ability.

For the attachment of the piezoelectric actuator onto the diaphragm, various bonding methods can be applied. However, liquid adhesive bonding is the most likely and practical approach for this step, as described in the next chapter.

### **3.2.2 Mounting of the piezoelectric actuators onto the micro pumps**

The mounting process of the piezoelectric actuators onto the base bodies of the micro pumps involves several carefully executed steps. First, all materials must be prepared. Both the welded micro pump base bodies and the piezoelectric actuators are thoroughly cleaned and dried to ensure optimal adhesion.

Special tools are used to ensure precise and accurate placement of the actuators at the exact centre of the base bodies. These tools, like the components, are also cleaned beforehand to maintain cleanliness and accuracy. Isopropanol is used for all cleaning steps, ensuring a contamination-free environment for the assembly process.

Before placing the fixture with the cleaned pump base bodies into the Vieweg glue dispensing machine, the glue must be prepared. The glue used is a specialized two-component adhesive (353ND, Epoxy Technology, Inc., Billerica, USA) with a mix-to-weight ratio of 10:1. After thoroughly mixing the components in a small container, the adhesive is transferred to a syringe. To eliminate any air bubbles in the mixture, the syringe is placed in a centrifuge. Once degassed, a needle tip is attached to the syringe, which is then mounted in the Vieweg machine.

After placing the pump bodies correctly into the fixture as seen in Figure 9, the fixture tool can be put in the Vieweg glue dispensing machine (I&J7300-LF, Fisnar GmbH, Germantown, USA).

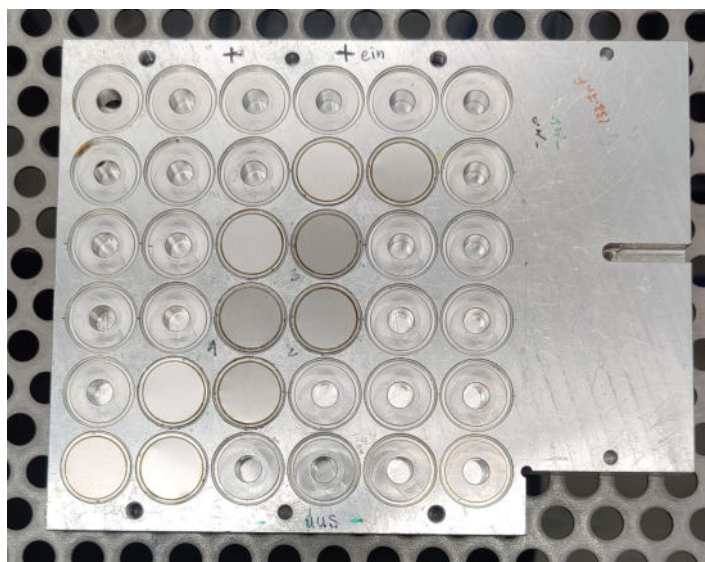


**Figure 9** Fixture for holding pump base bodies for use in the Vieweg glue dispensing machine

Two pump base bodies are used to test the application of the correct amount of glue onto their surfaces. To operate the Vieweg glue dispensing machine, pre-programmed settings are available, allowing users to input the parameters required for precise glue placement. These parameters include, for instance, the height of the pump base bodies and the dispensing speed of the syringe. To verify the accuracy of glue application, the test pump base bodies are weighed. The desired amount of glue should fall within the range of 3 mg to 5 mg. After applying the correct amount of glue onto the base bodies, the piezoelectric actuators can be positioned on them using a specialized tool. Once the actuators are placed on the base bodies, another tool will be used to secure the actuators in place. The actuators are then pressed onto the pump base bodies using a press (Schmidt ServoPress 416, SCHMIDT Technology GmbH, St. Georgen, Germany) to ensure a uniform spread of the glue. Following this, each pump will be contacted with a pin to measure the overall capacity and give an input voltage to create the pretension while curing. Finally, everything is placed in an oven to cure the glue. The glue needs to be cured for around 2 h at 120°C while receiving an input voltage of 165 V, which creates the necessary pretension.

### 3.2.3 Housing of the micro pumps

After the production of the micro pump base bodies and the subsequently mounting of the piezoelectric actuators on top, the pump is ready to be put in the housing to complete the fabrication of the micro pump.

The materials, that are used for the housing of the micro pumps are depicted in Figure 10.



**Figure 10** Housing materials for the metal micro pumps

Before assembly, all components must be thoroughly cleaned with isopropanol to ensure a dust-free and contaminant-free environment. This step is particularly important for the black sealing rings, as any residue may compromise the sealing integrity of the inlet and outlet.

Once cleaned, the sealing rings are placed into the designated slots in the plastic bottom piece. The micro pump body is then positioned correctly on top of this base. Attention must be paid to the orientation of the pump: the passive check valves must align with their corresponding openings in the plastic body. The inlet is identified by the smaller opening.

Next, the pump is secured in place using the green PCB, which is mounted on top of the pump. Screws are used to fasten the PCB tightly, ensuring that the pump body is firmly pressed against the sealing rings to maintain an effective seal. The final step is to connect the outlet to the inlet using a tube to prevent particles from entering and damaging the pump or the valves.

Finally, the micro pump is enclosed with the lid, completing the assembly.

### **3.3 Methods of analysis**

#### **3.3.1 Electro mechanical characterization**

For the electromechanical characterization of piezoelectric actuators, the FRT MicroProf 300 (FRT GmbH, Bergisch Gladbach, Germany) is utilized. This precision measurement device is specifically designed for highly accurate optical topographic measurements of surfaces. In our application, it measures the stroke height of the piezoelectric actuator under various applied voltages, enabling an evaluation of the actuator's efficiency. Depending on the selected sensor, the measurable height range extends from 300  $\mu\text{m}$  to 50 mm, with a resolution as fine as 2 nm. The MicroProf 300 is composed of several key components, including sensors, a probe table, sensor electronics, and more. The system is controlled via the Acquire software, which also

supports the creation of custom measurement programs, offering flexibility for specialized applications.

The sensor in the MicroProf 300 employs a patented measurement method based on chromatic aberration to deliver precise and reliable results. The sample is illuminated with focused white light, which is vertically dispersed into a spectrum of focal points due to significant chromatic aberration. When this dispersed light interacts with the surface of the sample, the optimally reflected light beams are captured by the sensor. Using a calibration table that correlates wavelength to distance, the sensor accurately determines the distance between itself and the sample. This method ensures exceptional accuracy in height measurements. It is a non-contact and absolutely non-destructive measuring method. [51]

To control the pump via an input signal, a combination of a waveform generator and a piezo amplifier is used. The Trueform waveform generator 33500B (Keysight Technologies Deutschland GmbH, Böblingen, Germany) serves as the waveform generator. It offers high precision and low-noise signal generation with jitter as low as 1 ps. It includes various built-in waveform types such as sine, square, and ramp. With a total harmonic distortion of just 0,03 %, Trueform waveform generators provide up to five times better signal fidelity than conventional generators [52].

To drive the piezoelectric actuators, the signal from the waveform generator is amplified using the SVR1000 piezo amplifier (piezosystem jena GmbH, Jena, Germany), which is capable of generating the high voltages required. The amplifier accepts input signals in the range of 1 V to 10 V and amplifies them by a factor of 120. [53]

### **Static stroke height measurement**

For the static stroke height measurement, a specialized measurement program is employed. To provide the micro pump with an electrical input signal, it must be connected to the signal generator and the amplifier. This program also automatically controls the signal generator and thus the input signal for the micro pump as long as the measurement is running. Prior to initiating the actual measurement, a surface scan is performed using the piezoelectric actuator to ensure the correct positioning of the sensor and the pump sample.

During static stroke measurement, voltages between  $-80\text{ V}$  and  $400\text{ V}$  are applied to the piezoelectric bulk actuators. For the stack piezoelectric actuators, a different voltage range is needed going from  $-12\text{ V}$  to  $100\text{ V}$ . The measurement starts at  $0\text{ V}$  and goes up to  $400\text{ V}$  or  $100\text{ V}$  in steps of  $10\text{ V}$  and then goes down to  $-80\text{ V}$  or  $-12\text{ V}$ . This cycle is completed twice before the measurement ends with going directly from the highest voltage down to  $0\text{ V}$  and up again to the highest voltage. The height of the piezoelectric actuator is measured each time a new voltage is applied. The entire measurement only takes a few minutes in total.

### **Dynamic stroke height measurement**

In contrast to static stroke measurements, dynamic measurements involve applying a continuous input signal to the piezoelectric actuator. In this setup, sine wave signals with amplitudes ranging from  $-80\text{ V}$  to  $300\text{ V}$  for bulk piezoelectric actuators and from  $-12\text{ V}$  to  $88\text{ V}$  for stack piezoelectric actuators were used, along with varying frequencies. Additionally, rectangular waveforms with the same voltage ranges were applied at different frequencies. This approach allows for continuous observation of the actuator's response, enabling the evaluation of how the stroke amplitude reacts to rapid input changes. The scan rate of the MicroProf300 is at  $10\,000\text{ Hz}$  for this measurement.

To assess the influence of pressure in the pump chamber on the actuator's behaviour, dynamic stroke measurements were also performed under different pressure conditions. For this, the inlet and outlet of the pump were connected to a pressure controller. Measurements were taken at pressures of  $10\text{ kPa}$ ,  $20\text{ kPa}$ , and  $50\text{ kPa}$ . In an additional test, a pressure of  $10\text{ kPa}$  was applied only to the outlet to investigate its effect on stroke height and valve functionality. Contrary to the static stroke height measurements, where stroke height is observed under relatively slow input signal variations, giving the actuator time to respond fully, dynamic stroke height measurements capture the reaction of the actuators to continuous and rapid signal changes.

### **3.3.2 Air characterisation**

In addition to the electromechanical characterisation, the air characterisation provides valuable insights into the pump's functionality, valve performance, and dynamic behaviour.

Various measurements are carried out to evaluate the pump's performance with respect to the working fluid air. These include flow rate measurements at different actuation frequencies, a measurement of the mean airflow at a certain frequency, as well as measurements under increasing backpressures at different frequencies. The following test setup is used to conduct these experiments:

The micro pump is connected in series with a mass flow measurement device and a pressure controller. The flow meter is connected to the inlet side of the pump, while the pressure controller is attached to the outlet side. For flow rate measurements, a differential pressure mass flow meter (Bronkhorst Deutschland Nord GmbH, Kamen, Germany) is used. This device is specifically designed for gases at very low differential pressures. It achieves minimal flow resistance by combining a large-bore capillary with a cylindrical flow splitter [54].

The mass flow sensor operates on the principle of heat transfer. Inside the sensor, a heating element and two temperature sensors are integrated, positioned upstream and downstream of the heater. The first temperature sensor measures the initial gas temperature before the flow passes the heating element, where the gas is heated. The second sensor measures the

resulting temperature. The temperature difference between the two sensors is proportional to the mass flow, as it reflects the amount of thermal energy absorbed by the gas. The sensor ensures laminar flow conditions throughout the measurement path [55].

For the backpressure measurements, the CPC3000 pressure controller (Mensor LP, San Marcos, USA) is employed. It is a high-speed, digital pneumatic controller designed for precise pressure regulation. The CPC3000 achieves a precision of 0,025 % of full scale (FS) and can regulate pressure within this range in under three seconds, assuming a test volume of 150 mL. Its operating temperature range spans from 10 °C to 50 °C [56].

To control the pump via an input signal, the same combination of a waveform generator and amplifier are used as in 3.3.1 Electro mechanical characterization .

For all subsequent tests, the same input voltage range of  $-80\text{ V}$  to  $300\text{ V}$  is applied to the piezoelectric bulk actuators.

The first experiment is a frequency sweep, conducted to evaluate the pump's flow rate as a function of the actuation frequency. For lead-free piezoelectric actuators, the sweep starts at 1 Hz and increases up to 550 Hz. Between 1 Hz and 100 Hz, the frequency is incremented in steps of 5 Hz; above 100 Hz, the step size increases to 50 Hz. For the lead-based piezoelectric actuators, the frequency sweep stops at a frequency of 300 Hz.

The second measurement focuses on determining the mean airflow at a fixed frequency of 200 Hz. The flow rate is recorded five times under identical conditions to ensure repeatability. Next, the backpressure test is performed. Several test runs are carried out at different input frequencies. Initially, a low frequency of 10 Hz is applied to the pump. A defined pressure is then applied to the outlet of the pump with the pressure controller to determine the pressure at which the outlet pump valve closes, this is the so called backpressure. The backpressure is increased from 0 kPa to 50 kPa in increments of 2,5 kPa. For each pressure level, the resulting airflow is measured. As soon as the airflow reaches 0 mL/min, the corresponding blocking pressure of the micro pump is identified.

The test is then repeated with an input frequency of 30 Hz. For standard lead-based bulk piezoelectric actuators, the test sequence ends here. In contrast, for lead-free bulk actuators, an additional measurement is carried out at an input frequency of 100 Hz.

### **3.3.3 Water characterisation**

For both air and water tests, the micropump is connected in series with a flow rate measurement device and a pressure controller. The mini CORI-FLOW M14 (Bronkhorst Deutschland Nord GmbH, Kamen, Germany) is used to measure flowrate. This compact and precise sensor operates based on the Coriolis principle, which offers a key advantage: it measures mass flow independently of fluid pressure, temperature, density, conductivity, or viscosity. It is suitable for both water and air applications [57].

The principle is as follows: as the fluid passes through a vibrating tube, the Coriolis force causes a phase shift. This shift is detected and translated by the sensor's electronics into a signal proportional to the mass flow rate. This method allows for fast and highly accurate measurements.

The pressure controller used is the CPC3000, which is the same as in the air characterization. Similar to the air characterization, various measurements are also conducted during the water characterization. For the subsequent tests that require an input signal, the input voltage range applied to the bulk piezoelectric actuators is set to  $-80\text{ V}$  to  $300\text{ V}$ .

The first measurement is a frequency sweep. For both lead-free and lead-based bulk piezoelectric actuators, the flow rate is recorded at input frequencies up to  $150\text{ Hz}$ .

The second measurement is the backpressure test. Defined input frequencies of  $10\text{ Hz}$ ,  $30\text{ Hz}$ , and  $100\text{ Hz}$  are applied to the pump. The test follows the same principle as in 3.3.2 Air characterisation, the test is stopped when the water flow rate decreased to  $0\text{ g/min}$ .

The third measurement is a water leakage test, which assesses the functionality of the passive check valves. In this test, no input signal is applied to the pump. Instead, different backpressures ranging from  $0\text{ kPa}$  to  $5\text{ kPa}$  are applied to the outlet. The objective is to verify whether the valves close properly and prevent any water flow under these conditions.

### 3.3.4 Robustness test

The robustness tests are carried out to investigate the influence of mechanical stress on the performance of the piezoelectric actuators.

The micro pump is connected to a wave form generator, which provides a defined input signal. For these tests, the input signal is set to a sine wave ranging from  $-80\text{ V}$  to  $300\text{ V}$  at a frequency of  $30\text{ Hz}$ . This voltage range is typically used for piezoelectric actuators with the corresponding properties such as thickness and piezoelectric coefficient. The operating frequency was selected based on the following considerations. While the highest flow rates for the combination of these actuators with the micro pump occur at around  $100\text{ Hz}$ , practical applications typically demand lower flow rates. Therefore, a reduced frequency was chosen. Additionally, continuously operating the pump at maximum capacity would impose excessive mechanical stress, leading to accelerated wear and a significant decline in performance over time. For these reasons, a more moderate operating frequency was deemed more suitable for real-world use.

The inlet of the micro pump is connected to a reservoir, which contains the desired test fluid. The outlet of the micro pump is connected to a tube which leads to a small reservoir.

In general, different stresses can cause fatigue in the piezoelectric actuators, such as specific waveforms like rectangular, higher electric fields, or touch down of the actuator. As this

This thesis focusses on the application of the pumps in the medical field, the test modes chosen for this test simulate the practical drug dosing. Three different test modes were chosen.

- **Test mode 1:** High mechanical load is achieved by operating the pump with water, while the outlet is closed. Pressure builds up progressively in the pump chamber over time. Since water is significantly less compressible than air, this leads to a continuous state of high mechanical stress
- **Test mode 2:** Moderate mechanical load is achieved by operating the pump with air, while the outlet is closed. Pressure builds up progressively in the pump chamber over time. Since air is more compressible than water, the actuator experiences a lower deflection while operating
- **Test mode 3:** Reference mode, which is continuous water pumping under normal operating conditions, without clamping the outlet

The test procedure is as follows: the waveform generator first sends the input signal to the pump, initiating fluid flow from the reservoir. The pump is operated for one minute to ensure proper functionality and to fully fill the pump chamber with fluid. For test modes simulating a closed outlet, the outlet tube is then sealed using a clip. In the continuous water pumping mode, the outlet tube is connected back to the inlet reservoir to allow recirculation. Figure 11 shows the experimental setup used for the robustness test in the closed-outlet configuration.

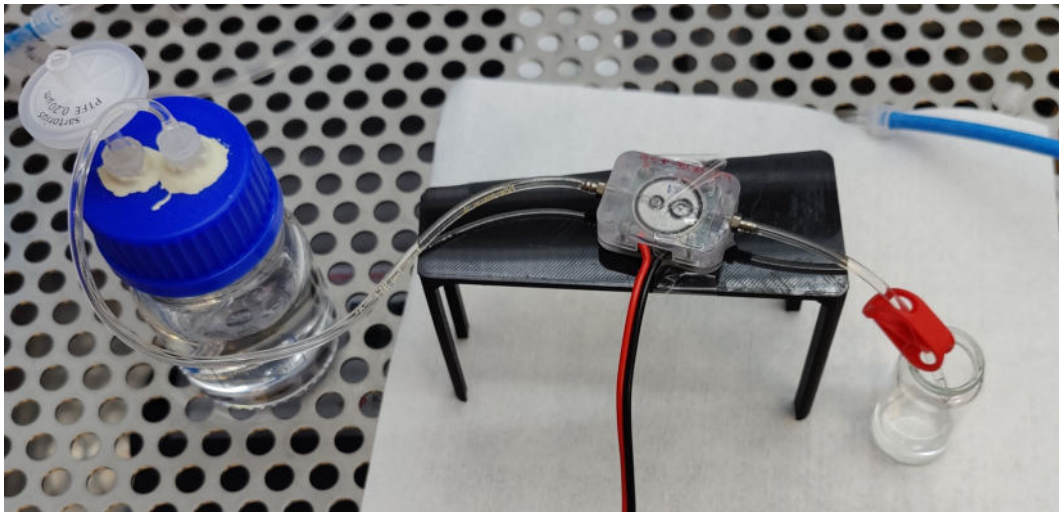


**Figure 11** Experimental setup for robustness testing of micro pumps in closed-outlet configuration

The robustness test was conducted in 24-hour intervals. Initially, the pump was tested for 24 hours, followed by extensions to 48 and 72 hours, with each stage adding an additional 24-hour

operating period. After each interval, both electromechanical and water characterizations were performed to evaluate any changes in the pump's performance over time.

### **3.3.5 Surface and structural analysis**

#### **Scanning electron microscopy**

With the help of the scanning electrode microscopy (SEM) insights into the surface structure of the piezoelectric actuators are gained. With the SEM insights up to the scale of 300 000 x magnification can be observed. This is achieved by an electron beam, which is concentrated by condensing lenses. Spot sizes of 10 nm and a penetration depth of 1  $\mu\text{m}$  can be attained. The electron beam is generated by a so called electron gun. There are different electron voltages modes which can have influence on the provided details. Common voltage ranges are between 5 kV to 30 kV. A higher voltage on the electron beam will influence the penetration deepness into the material. An electron detector is used to detect the emitted electrons from the sample. There are two different types of emitted electrons which are mainly used to understand the surface of the sample. One of them are the so called secondary electrons. These are electrons, which are emitted through the ionization of specimen atoms by the electron beam. They have a low energy typically in the range of 3 eV to 5 eV. They can only emit from the region that is a few nanometers in the material. Secondary electrons are usually used for the topographic contrast in the SEM like the visualisation of the texture and roughness. One other source of information are collected through the so called backscattered electrons, which have undergone a single or multiple scattering events and escape the surface with energies higher than 50 eV. [58]

The microscope which is used for SEM is the Gemini 3 (Carl Zeiss Microscopy Deutschland GmbH, Oberkochen, Germany). It is designed for working conditions ranging from 1 kV to 30 kV. This microscope enables efficient signal detection by detecting secondary and backscattered electrons in parallel. It uses a special Nano-twin lens which is an optimized electromagnetic objective lens. It permits sub nanometer resolution at low voltages. [59]

#### **Profile measurements with Keyence microscope**

For 3D measurements, the Keyence VR-6000 (KEYENCE International NV/SA, Mechelen, Belgium) is used. This optical 3D measurement system enables contactless surface analysis using structured light. A pattern of light is projected onto the surface of the sample via a lens, and the reflected light is captured by a receiver lens. Variations in the surface topology cause the projected light to appear distorted or banded. The system employs triangulation to calculate the 3D shape of the object with high accuracy.

With this method, the VR-6000 can achieve precise measurements down to 0,1  $\mu\text{m}$  with a measuring range of 300 mm  $\times$  150 mm  $\times$  70 mm. To maintain high precision across this range,

telecentric lenses are used to minimize optical aberrations. Notably, the system requires no prior calibration. The system automatically detects the sample's position and adjusts the measuring range accordingly, reducing user influence on the results. Thus, ensuring high reproducibility and elimination of measurement errors due to incorrect sample placement. [60]

## 4 Results and discussion

The aim of this work is to further develop already existing micro pumps by investigating two novel types of piezoelectric disc actuators. The first is a lead-free bulk piezoelectric disc actuator, designed as an environmentally friendly alternative. The second is a lead-based stack piezoelectric disc actuator featuring integrated self-sensing capabilities.

To evaluate the performance of both variants and compare them to standardly lead-based bulk piezoelectric actuators, preliminary measurements are included as well as fatigue analysis of the lead-free bulk piezoelectric actuators and a detailed interpretation of the micro pump's performance.

### 4.1 Initial quality assessment of the piezoelectric actuators

A thorough initial quality assessment of the piezoelectric actuators is essential for accurate characterization before their bonding onto the pump base body. This step ensures that the actuators meet the expected specifications and provides a solid foundation for evaluating their overall performance. Key parameters such as thickness, weight, and capacitance are measured and analyzed during this stage. These measurements not only verify compliance with design requirements but also yield valuable insights into the actuators behaviour, forming the basis for subsequent analysis and performance evaluation.

#### Lead-based bulk piezoelectric actuators

For the preliminary examinations, 25 lead-based bulk piezoelectric actuators were analyzed. Thickness measurements were conducted at three distinct points on each actuator, resulting in an overall average thickness of  $198,1 \mu\text{m} \pm 0,78 \mu\text{m}$ . The detailed measurement values are presented in Appendix 6.2, Table 15. Compared to the data given from the manufacturer the value for the thickness is 0,95 % lower than expected.

The weight and capacitance of these piezoelectric actuators were also evaluated, with the following results: a weight of  $310,56 \text{ mg} \pm 0,8 \text{ mg}$  and a capacitance of  $2,17 \text{ nF} \pm 0,02 \text{ nF}$  were measured (see Appendix 6.2, Table 16).

#### Lead-free bulk piezoelectric actuators

A total of 25 lead-free bulk piezoelectric actuators were available for the preliminary examination. Thickness measurements were carried out on three different points on the surface of each actuator. The resulting measurement values are presented in Appendix 6.2 in Table 17. The average thickness of the piezoelectric actuators is  $207,4 \mu\text{m} \pm 3,6 \mu\text{m}$ . This corresponds to a deviation of  $7,4 \mu\text{m}$  or 3,7 % from the specified thickness of  $200 \mu\text{m}$ .

For the weight measurement, an average weight of  $201,2 \text{ mg} \pm 2,5 \text{ mg}$  was determined.

The capacitance measurement yielded an average value of  $9,3 \text{ nF} \pm 0,1 \text{ nF}$ . The measurement values for weight and capacitance are presented in Appendix 6.2, Table 18.

### **Lead-based stack piezoelectric actuators with self-sensing capabilities**

For the preliminary investigation of the lead-based stack piezoelectric actuators with self-sensing properties, a total of 50 specimens were available. For each actuator, the thickness was measured at three different points. The measurement values are presented in Table 19 in Appendix 6.2. The average thickness of the actuators is  $578,4 \mu\text{m} \pm 6,3 \mu\text{m}$ . When compared with the specifications outlined in Table 3.1.2, it becomes evident that the average measured thickness of the actuators falls outside the manufacturer's specified range of  $570 \mu\text{m} \pm 0,06 \mu\text{m}$  by 1,47%.

The following values were recorded for weight and capacitance:  $886,3 \text{ mg} \pm 1,96 \text{ mg}$  for the weight for the piezoelectric actuators and  $141,8 \text{ nF} \pm 1,2 \text{ nF}$  for the capacity for sensing pad 1, and  $1236,8 \text{ nF} \pm 12,2 \text{ nF}$  for pad 2, which is used for actuating the piezoelectric actuator. These values are presented in Appendix 6.2, Table 20.

Piezoelectric actuators with huge deviations from the expected properties were not included in further process steps and testing in order to maintain uniformity among the test samples.

## **4.2 Evaluation of the lead-free bulk piezoelectric actuators**

After the initial quality assessment, the decisive step is to mount the actuators onto micro pump base bodies and evaluate their performance with different tests. The following chapters present the measurement results from the various test procedures for characterizing the lead-free bulk piezoelectric actuators and comparing them to the standardly used lead-based bulk piezoelectric actuators. These pumps as reference have already been extensively tested in various applications, providing a solid and well established understanding of their behaviour and performance. The characterization includes an electromechanical characterization with static and dynamic tests. This is followed by the performance evaluation of the pumps with air and water as working fluids. The final test conducted is the robustness test, which examines the influence of long-term stress on the performance of the pump and is followed by a surface analysis of the actuators.

### **4.2.1 Electro mechanical characterization - static stroke measurement**

One key characteristic of a piezoelectric actuator is its stroke, which describes the transversal movement performed by the piezoelectric actuator attached to the diaphragm under excitation. As this parameter largely determines the volume change in the pump chamber during actuation, and thus directly affects the volume displaced per stroke. A greater stroke height

leads to a higher stroke volume, making it a critical factor in the overall pump performance. Furthermore, a key objective of this work is to investigate whether lead-free actuators can serve as an environmentally friendly alternative to the established lead-based systems, and to assess their potential suitability for real-world applications.

For the static stroke measurement, 20 micro pumps equipped with lead-based bulk actuators were tested. Each pump underwent an individual static stroke measurement.

The stroke height was measured using the FRT MicroProf300, an optical profilometer capable of detecting height variations with extremely high precision. Further details on this measurement procedure can be found in 3.3.1 Electro mechanical characterization .

A representative stroke-height curve for these piezoelectric actuators is shown in Figure 12.

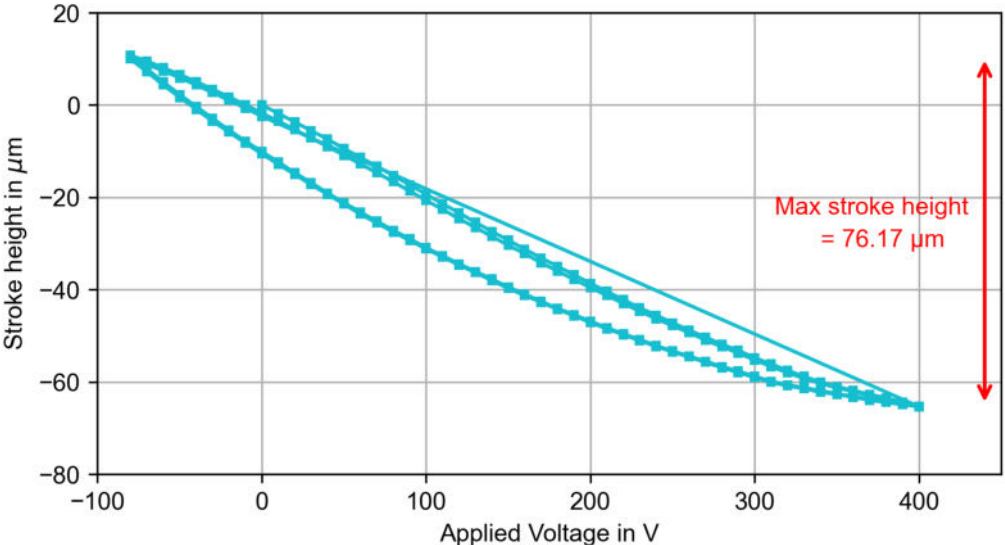


**Figure 12** Static stroke measurement for lead-based bulk piezoelectric actuator on micro pump

This diagram illustrates that the stroke heights differ between increasing and decreasing input voltages, which results in a characteristic hysteresis curve. One important parameter is the maximum stroke, which refers to the total height difference achieved by the actuator. To determine this, the maximum and minimum values are extracted and subtracted from one another. For the pump shown in Figure 12, the maximum stroke was measured to be 76,17 μm. For the 20 pumps, that were tested, the average maximum stroke was 76,74 μm ± 10,8 μm.

Regarding the lead-free bulk piezoelectric actuators, the static stroke measurement was carried

out three times in succession for each pump, to minimize measurement errors. Overall, 8 micro pumps were available for the testing. The results for these measurements are depicted in Table 2.

**Table 2** Results for the static stroke measurement for micro pumps with lead-free bulk piezoelectric actuators

Pump nr.	max stroke 1 in $\mu\text{m}$	max stroke 2 in $\mu\text{m}$	max stroke 3 in $\mu\text{m}$	mean max stroke in $\mu\text{m}$
1	44.25	43.83	43.76	43.95
2	46.33	45.96	45.90	46.06
3	43.34	42.28	37.28	40.97
4	46.02	45.79	41.00	44.27
5	40.46	40.34	37.04	39.28
6	36.67	36.55	36.25	36.49
7	38.81	38.81	38.26	38.63
8	37.96	37.71	37.65	37.77

As the measurement was carried out three times for each pump, deviations between the individual measurements could be observed. It is visible, that the static stroke decreased by  $2,09 \mu\text{m}$  on average over the course of the measurements.

In general, the deviation of the measured stroke height for each pump can be attributed to several factors. Firstly, piezoelectric actuators are subject to electrical and mechanical tolerances during the manufacturing process, which can lead to inhomogeneities between individual components.

In addition, the mounting process of the actuators onto the pumps can significantly affect their performance. For instance, variations in the amount of adhesive applied to the pump diaphragm can influence the mechanical coupling, and thus the resulting stroke height. If there is e.g. very less glue or the glue has some air bubbles, this would affect the pump's performance negatively. Similarly, the positioning of the actuator plays a role: if the piezo is not placed precisely at the center of the diaphragm, the stroke can be reduced due to asymmetric deformation.

Another important factor is the electrical connection between the piezo actuator and the PCB, which is established manually. A copper wire is soldered to both the actuator and the PCB. The quality of this connection directly impacts the signal transmission; better conductivity enables more efficient energy transfer and potentially results in a higher stroke. Additionally, localized thermal stress during soldering may alter the piezoelectric properties of the actuator locally, further contributing to performance variability.

A representative diagram is given in Figure 13 for the micro pumps with lead-free bulk piezoelectric actuators.

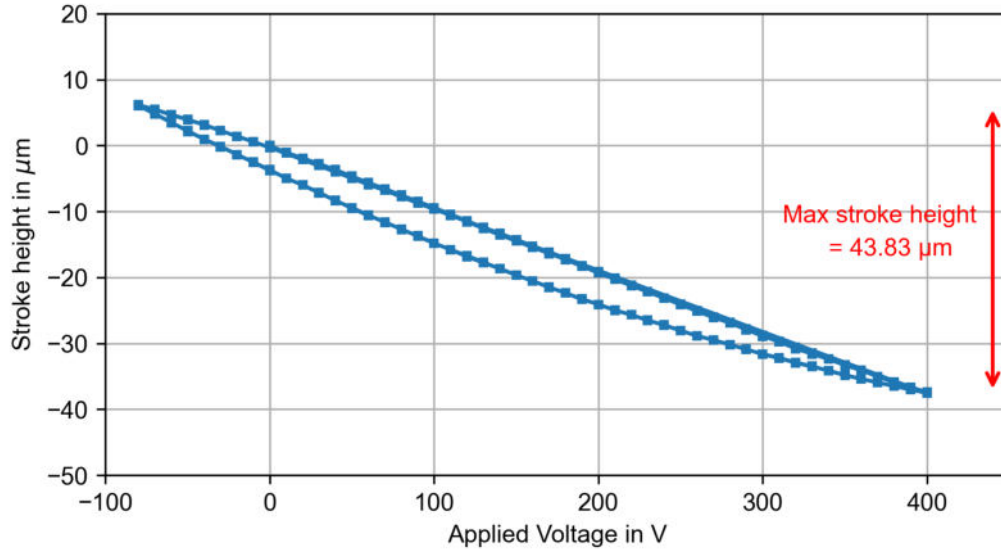


**Figure 13** Stroke measurement for lead-free piezoelectric actuator on metal micro diaphragm pump

The plot exhibits a hysteresis similar to that of the lead-based bulk piezoelectric actuators. However, a notable difference is observed in the maximum stroke height of the lead-free bulk piezoelectric actuators, which is significantly smaller. For all 8 tested pumps, the mean maximum stroke height is  $40,93 \mu\text{m} \pm 3,24 \mu\text{m}$ .

Compared to the micro pumps equipped with lead-based bulk piezoelectric actuators, the maximum static stroke height of the micro pumps with lead-free bulk piezoelectric actuators is  $35,81 \mu\text{m}$  or  $53,34 \%$  lower. This is attributed to the different characteristics of the piezoelectric materials used for the actuators. The material used for the lead-free bulk piezoelectric actuators has a lower piezoelectric coupling factor and a higher stiffness coefficient, leading to a smaller static stroke height.

To gain deeper insights into the behaviour of the lead-free bulk piezoelectric actuators, dynamic stroke measurements are conducted in addition to the static stroke measurements.

#### 4.2.2 Electro mechanical characterization - dynamic stroke measurement

In contrast to static stroke measurements, dynamic stroke measurements apply a continuous input signal to the piezoelectric actuator while its stroke height is recorded. This allows for

the investigation of the time-dependent behaviour of the actuator. Therefore, dynamic stroke measurements provide information on actuator performance under more realistic real-world operating conditions.

Additionally, the testing includes the application of different pressures and input signals to the pump chamber to investigate their effects on the behaviour of the piezoelectric actuators. A sine wave signal at 10 Hz with a voltage range from  $-80\text{ V}$  to  $300\text{ V}$  was applied, as well as a square wave signal at  $1,5\text{ Hz}$  using the same voltage range.

For both input signals, pressure levels of  $0\text{ kPa}$ ,  $10\text{ kPa}$ ,  $20\text{ kPa}$  and  $50\text{ kPa}$  were applied simultaneously at both the inlet and outlet. In addition, a scenario was tested in which only the outlet was pressurized to  $10\text{ kPa}$  while the inlet remained unpressurized.

A detailed description of the test setup and procedure can be found in 3.3.1 Electro mechanical characterization . For comparative analysis, these tests were conducted on micro pumps equipped with both lead-free and lead-based bulk piezoelectric actuators.

A representative result of one of the micro pumps with lead-free bulk piezoelectric actuators with sine wave input signal is presented in Figure 14.

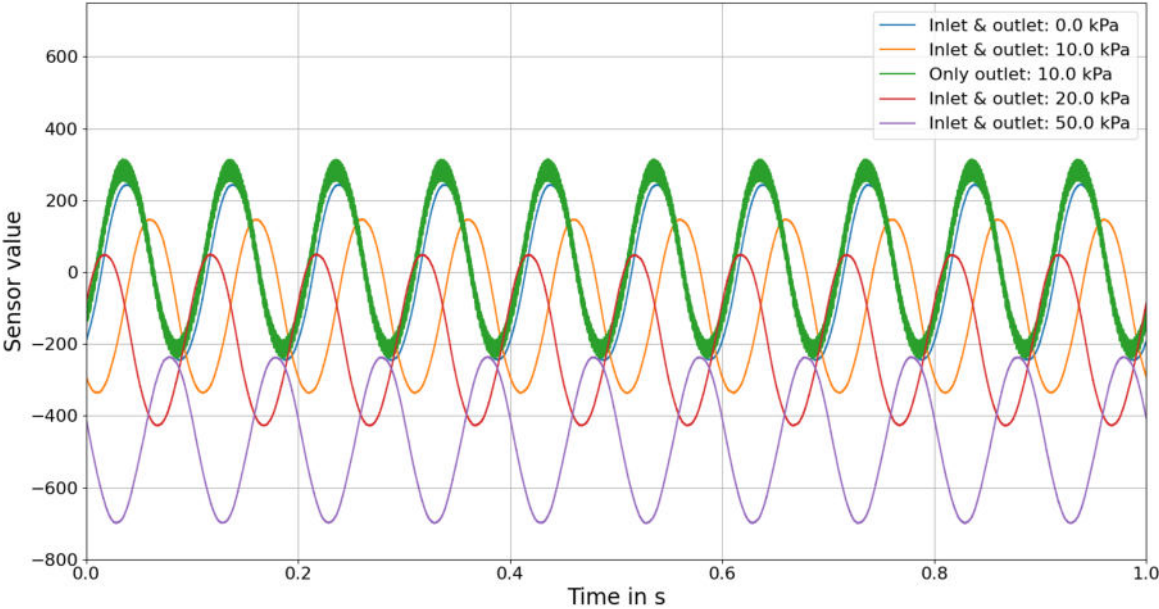


**Figure 14** Deflection of the lead-free bulk piezoelectric actuator in dependence of the adjacent pressure and time in dynamic stroke measurement with sine wave input signal

It seems evident that the dynamic stroke height of the piezoelectric actuators varies with different pressures in the pump. As the pressure in the pump chamber increases, the actuator height changes accordingly. Although the graph appears to show a decrease in the height of the piezoelectric actuator, it actually represents the distance between the actuator and the

sensor of the FRT MicroProf300. The first curve, measured at 0 kPa, is set as the reference zero point, which causes the heights of the curves for other pressures to adjust relative to it. The corresponding pressures applied during the dynamic stroke measurements are shown in the legend of the diagram. The amplitudes for the different pressure conditions were calculated by identifying the maximum and minimum values of the resulting sine curves, with the amplitude defined as the difference between these two values. Due to limitations in the measurement method, these values do not represent absolute amplitudes. Although the exact unit is undefined, the data allow for a relative comparison between different test conditions. Since the measurements only capture the height differences at the very centre of the piezoelectric actuator, it is not possible to draw conclusions about the overall curvature of the actuator.

When examining these relative values, a slight decrease in amplitude can be observed from 491 at 0 kPa to 465 at 50 kPa. This reduction may be attributed to a diminished compression ratio of the piezoelectric actuator under increased pressure. At higher chamber pressures, the actuator is likely pre-deflected, making it more difficult for it to compress further against the opposing force. This initial curvature, caused by the pressure differential, may limit the effective stroke of the actuator.

The green thick line represents the stroke height when pressure is applied exclusively to the outlet. The line appears thicker, which may be attributed to rapid fluctuations in stroke height. This behaviour could result from the outlet pressure acting on the outlet valve, causing it to open and close rapidly. These quick valve dynamics lead to high-frequency oscillations in the measurement, which are visualized as a thicker line in the plot.

For the dynamic stroke measurement with a square input signal, the same procedure was followed as with the sine signal, except that the input frequency was set to 1,5 Hz. This lower frequency was deliberately chosen to observe how quickly the piezoelectric actuator responds to abrupt changes in the input signal. The results are depicted in Figure 15.

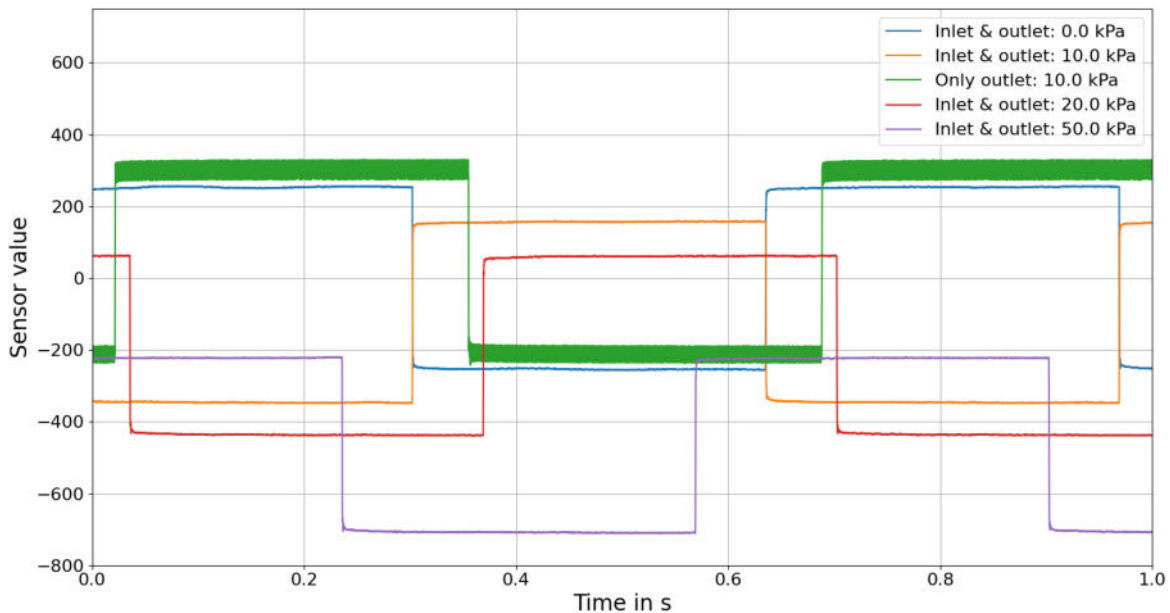


**Figure 15** Deflection of the lead-free bulk piezoelectric actuator in dependence of the adjacent pressure and time in dynamic stroke measurement with square wave input signal

Again it can be observed, that the pump chamber height changes due to the input pressures. Also the amplitude changes slightly. It is decreasing from 514 at 0 kPa to 493 at 50 kPa, which are only relative values, not the absolute amplitude values as explained above.

For comparison reasons, this measurement was also done with standard lead-based bulk piezoelectric actuators. The resulting graphs look the same as for the lead-free bulk piezoelectric actuators. Through the application of pressure on the inlet and outlet, the pump chamber raises. The behaviour of the lead-free bulk piezoelectric actuator is therefore similar to the lead-based bulk piezoelectric actuators.

Overall it shows, that the application of air pressure uniformly to the inlet and outlet or only to the outlet does not hinder the deflection height of the piezoelectric actuators. The piezoelectric actuators are able to withstand 50 kPa of pressure in the pump chamber, without shrinking the deflection significantly.

#### 4.2.3 Air characterization

The air characterization was done with 20 micro pumps with lead-based bulk piezoelectric actuators and 8 micro pumps with lead-free bulk piezoelectric actuators. Even though the aim is to operate micro pumps with liquid media, air characterization is done as it provides an indication about self-priming abilities and bubble-tolerance.

### Frequency sweep

The first measurement conducted in the air characterization is a frequency sweep, in which the air flow rate, generated by the pump, is measured across a range of input frequencies. The input signal has an amplitude of  $-80\text{ V}$  to  $300\text{ V}$ . Different frequency ranges were selected for different types of piezoelectric actuators. For the lead-based bulk piezoelectric actuator, a frequency range of  $0\text{ Hz}$  to  $300\text{ Hz}$  was found to be sufficient. In contrast, the lead-free bulk piezoelectric actuators required a broader range of  $0\text{ Hz}$  to  $550\text{ Hz}$ , as their peak performance occurs at higher frequencies. This difference is illustrated in the following graphs, which show the air flow as a function of input frequency. Figure 16 displays the frequency sweep results for a micro metal diaphragm pump using a lead-based piezoelectric actuator.

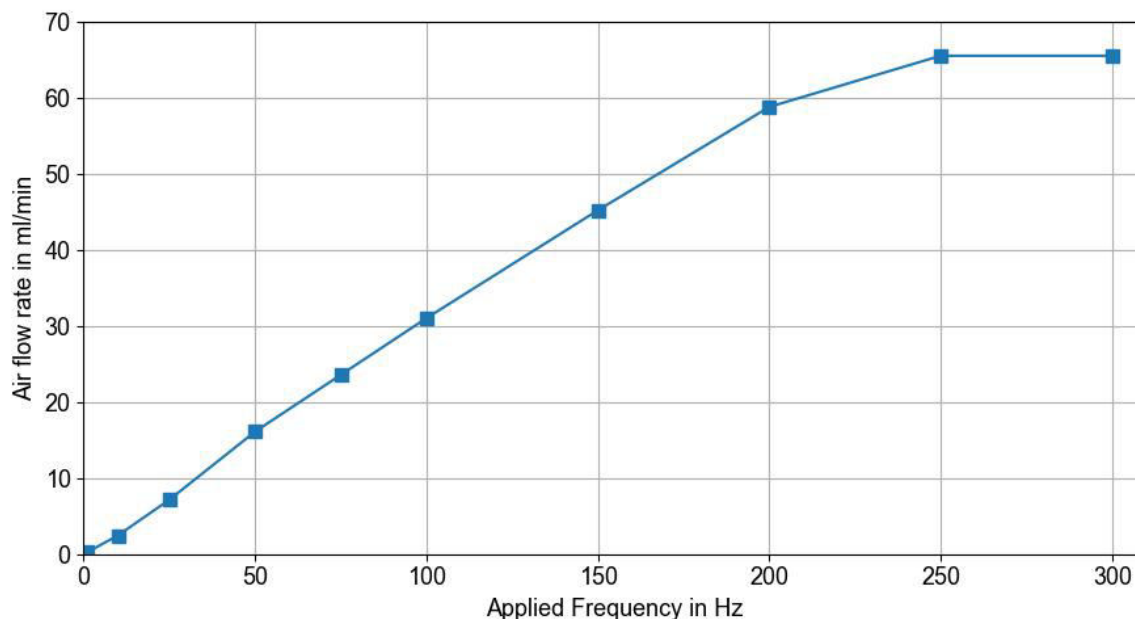


**Figure 16** Frequency sweep for lead-based bulk piezoelectric actuator on MMDP with air

The diagram shows that the air flow rate increases approximately linearly with rising input frequency up to around  $200\text{ Hz}$ , reaching about  $60\text{ mL/min}$ . Beyond  $200\text{ Hz}$ , the increase in air flow begins to level off. The maximum flow rate of  $65\text{ mL/min}$  is achieved at  $250\text{ Hz}$ . For this reason, the measurement range for these pumps is limited to  $0\text{ Hz}$  to  $300\text{ Hz}$ .

In Figure 17 the frequency sweep for a micro pump with lead-free bulk piezoelectric actuator is depicted.

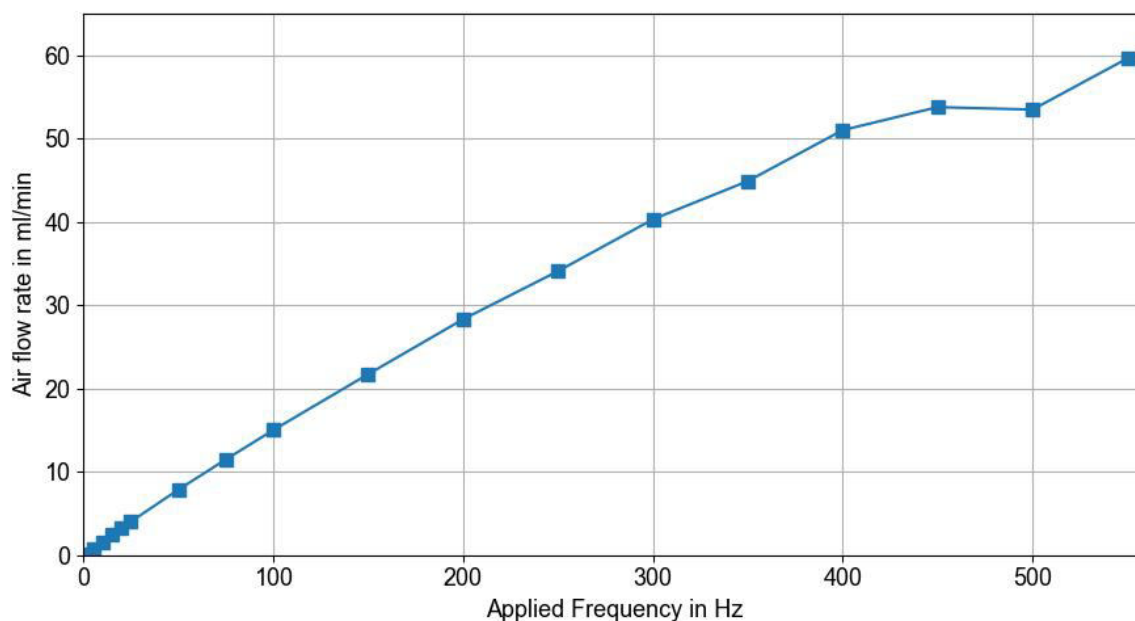


**Figure 17** Frequency sweep for lead-free bulk piezoelectric actuator on MMDP with air

The diagram shows that the air flow increases approximately linearly up to a frequency of 400 Hz, reaching an air flow rate of nearly 60 mL/min. At higher frequencies, there is a slight decrease in flow rate, followed by a further increase to a maximum of 65 mL/min at 550 Hz. This behaviour justifies the selected frequency range for these pumps.

Comparing the two frequency sweeps, it becomes evident that both pump configurations can achieve maximum flow rates of 65 mL/min. However, the lead-based bulk piezoelectric actuator reaches this performance at lower frequencies. This difference is attributed to the distinct material properties of the piezoelectric elements, as detailed in Table 1 in Appendix 6.2. There, it is shown that the piezoelectric coupling factor for the lead-based bulk material is 0.62, whereas for the lead-free bulk material it is 0.52. This coupling factor directly influences the efficiency of converting electrical energy into mechanical deformation. Consequently, the lead-based actuator achieves a higher curvature and therefore a higher flow rate at lower frequencies.

This difference aligns with the observation that micro pumps with lead-based bulk actuators exhibit a higher maximum stroke height than the micro pumps with lead-free bulk piezoelectric actuators. This directly influences the pump chamber volume displaced during each stroke, which is fundamental to the resulting flow rates.

### **Operation against backpressure**

The second measurement assesses the pump's performance under backpressure. In this test, the pump is driven by a defined sine wave input signal at frequencies of 10 Hz and 30 Hz for the lead-based bulk piezoelectric actuators, and 10 Hz, 30 Hz, and 100 Hz for the lead-free bulk piezoelectric actuators. The voltage range used is  $-80\text{ V}$  to  $300\text{ V}$ . The 100 Hz frequency was included for the lead-free actuators, as they require higher frequencies to achieve increased airflow. To assess the pump's performance under load, backpressure is incrementally applied, starting at  $0\text{ kPa}$  and increasing in  $2,5\text{ kPa}$  steps up to a maximum of  $50\text{ kPa}$ .

Initially, the pump generates its typical air flow rate at the given frequency. However, as the backpressure increases, the flow rate gradually decreases. Due to the additional pressure acting on the valve at the outlet, the internal pressure in the pump chamber rises. As a result, it becomes increasingly difficult for the actuator to compress the fluid effectively, leading to reduced flow. Once the external backpressure exceeds the internal pressure generated by the actuator, the outlet check valve closes, and no further flow is possible. As soon, as the air flow rate reaches  $0\text{ mL/min}$ , the test stops.

In Figure 18 the operation against backpressure for a micro pump with lead-based bulk piezoelectric actuator is depicted.

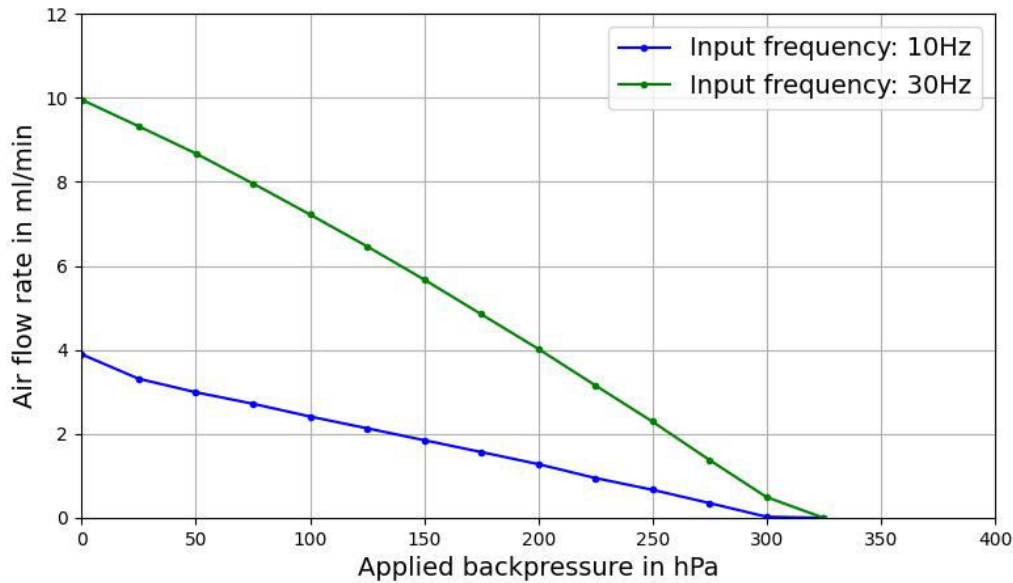


**Figure 18** Air flow backpressure test of lead-based bulk piezoelectric actuator on micro pump

At 0 kPa, the air flow behaves as expected, consistent with the frequency sweep results discussed earlier. As the backpressure increases, the air flow gradually decreases. For both input frequencies, the backpressure reaches approximately 35 kPa before the air flow drops to 0 mL/min. This decline is almost linear.

Out of the 20 micro metal diaphragm pumps tested, only 11 exhibited this regular behaviour. The remaining pumps showed irregularities, such as unusually low backpressure values or unstable declines in air flow. Among the pumps with regular performance, the mean backpressure at an input frequency of 10 Hz was  $35,22 \text{ kPa} \pm 7,34 \text{ kPa}$ , and at 30 Hz, it was  $37,27 \text{ kPa} \pm 6,17 \text{ kPa}$ .

Irregularities observed in this test may result from valve malfunctions. A common cause is the presence of particles obstructing the valves, preventing them from fully closing. In such cases, the air flow does not decrease with increasing backpressure but instead remains constant or fluctuates irregularly. Other possible causes are leakages within the pump, either at the valve inlet or outlet or between the two valve foils. As the laser beam welding process of the valve foils onto the base plate induces thermal stress on the foils, it can not be ruled out, that the initial gap between the valve foils increased, leading to leakages, which can similarly disrupt the expected pressure and flow relationship.

For the micro pumps equipped with lead-free bulk piezoelectric actuators, 8 pumps were subjected to operation against backpressure. Of these, 5 exhibited the expected pressure flow characteristics, while the remaining three displayed irregular behaviour.

In Figure 19 the backpressure test for a micro metal diaphragm pump with lead-free bulk piezoelectric actuator is depicted.

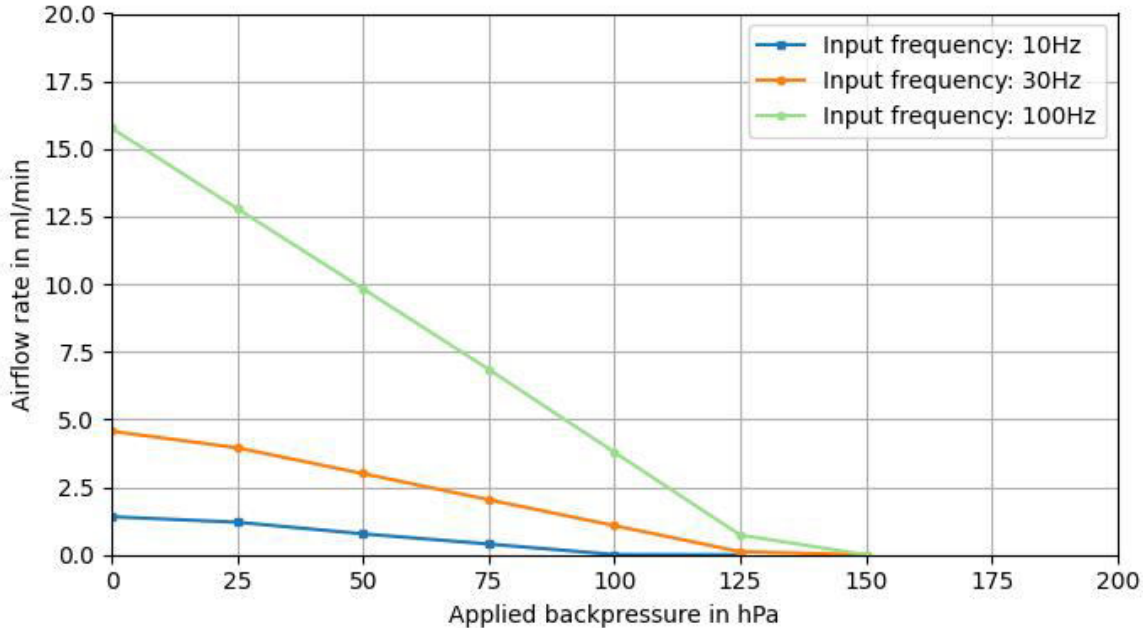


**Figure 19** Air flow backpressure test of lead-free bulk piezoelectric actuator on MMDP

The airflow decreases approximately linearly, reaching zero at around 17,5 kPa. The initial airflow values at 0 kPa are consistent with those observed in the frequency sweep test. The measurement results are summarized in Table 3.

**Table 3** Measurement results for the backpressure testing for lead-free bulk piezoelectric actuators on micro pumps

Pump nr.	Backpressure at 10 Hz in kPa	Backpressure at 30 Hz in kPa	Backpressure at 100 Hz in kPa
1	2,497	4,797	12,497
2	17,498	17,5	17,497
3	2,501	4,998	9,997
4	14,999	14,999	15
5	4,997	10,003	14,998
6	2,495	2,499	4,998
7	2,493	2,493	2,492
8	12,498	14,998	14,998

Overall, the five pumps that operated as expected (pump nr.: 1, 2, 4, 5, 8) exhibited an average backpressure of  $10,5 \text{ kPa} \pm 5,79 \text{ kPa}$  at an input frequency of 10 Hz. At 30 Hz, the average backpressure was  $12,46 \text{ kPa} \pm 4,54 \text{ kPa}$ , and at 100 Hz, it increased to  $15,0 \text{ kPa} \pm 1,58 \text{ kPa}$ . This test shows that the micro pumps with lead-based bulk piezoelectric actuators can achieve higher blocking pressures. This is due to their higher piezoelectric coefficient and also the lower stiffness coefficient.

### Conclusion air characterization

In summary, the lead-free bulk piezoelectric micro pumps were characterized with respect to air performance. During the frequency sweep, a maximum airflow rate of approximately 65 mL/min was observed at 500 Hz.

In the backpressure test, which reflects the actuator's force applied to the pump chamber, the lead-free MMDPs reached a maximum backpressure of  $12,46 \text{ kPa} \pm 4,54 \text{ kPa}$  at an input frequency of 30 Hz. This is 66,58% lower than the according performance of the MMDPs with lead-based piezoelectric actuators.

#### 4.2.4 Water characterization

The water characterization was done with 2 micro pumps with lead-based piezoelectric bulk actuators and with 8 micro pumps with lead-free bulk piezoelectric actuators.

#### Frequency sweep

As in the air characterization, a similar frequency sweep is done in the water characterization. The water flow rate at different input frequencies is measured. The input signal is the same as in the air characterization, which is sine wave signal ranging from  $-80 \text{ V}$  to  $300 \text{ V}$ . The

frequency range is 0 Hz to 150 Hz.

In picture Figure 20 we can see the frequency sweep for a micro pump with lead-based bulk piezoelectric actuators.

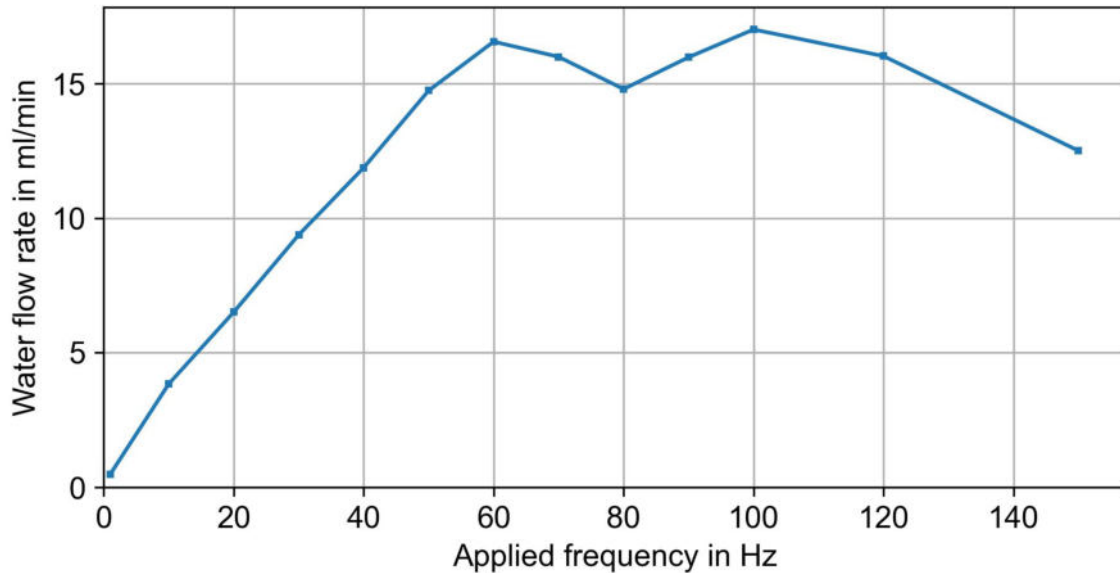


**Figure 20** Frequency sweep for lead-based bulk piezoelectric actuator on micro pump with water

The picture shows that the water flow rate rises with increasing input frequencies up to a maximum water flow rate of around 17 mL/min at 100 Hz for the micro pumps. For further increasing input frequencies, the water flow rate is decreasing.

2 micro pumps with lead-based bulk piezoelectric actuators gone through the water characterization. The mean water flow rate for the frequency sweep at 30 Hz is 9,5 mL/min  $\pm$  0,19 mL/min. A similar observation can be made regarding the micro pumps with lead-free bulk piezoelectric actuators (see Figure 21).

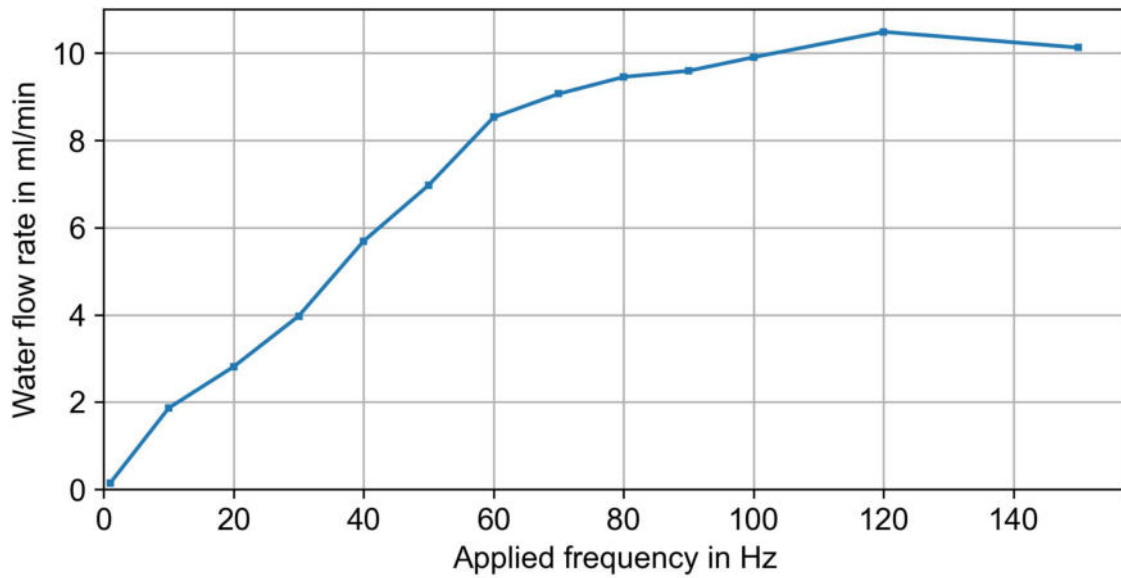


**Figure 21** Frequency sweep for lead-free bulk piezoelectric actuator on micro pump with water

We see a rising water flow rate up to the maximum water flow rate of 10,49 mL/min at 120 Hz. Higher input frequencies lead to lower water flow rates. This is due to inertia effects of the water in the pump chamber.

During the frequency sweep with water it was found, that 1 out of the 8 pumps was leaking water. Leakage can happen due to irregularities in the fabrication process of the pumps. One reason could be, that the welding depth of the pump base bodies is not sufficient or blown.

**Table 4** Measurement results for frequency sweep with lead-free bulk piezoelectric actuators on micro pumps with water

Pump nr.	Water flow rate at 30 Hz in mL/min
1	3.95
2	3.97
3	3.43
4	3.88
5	3.79
6	3.64
7	3.37
8	4.14

In Table 4 some of the test results from the frequency sweep with water are depicted. The

average water flow rate for the lead-free bulk piezoelectric actuators on micro pumps at an input frequency of 30 Hz is  $3,77 \text{ mL/min} \pm 0,25 \text{ mL/min}$ .

As previously mentioned, achieved flow rates of both piezoelectric actuators is lower during the water frequency sweep compared to the air frequency sweep. This shift can be attributed to several factors. One key reason is that the dynamic viscosity and density of water are significantly higher than those of air. In the air characterization, the fluid's low density and viscosity result in minimal inertial and damping effects. In contrast, water exhibits much greater inertia, which causes the system to respond more slowly to the vibrations of the piezoelectric actuators. This delayed response lowers the system's natural frequency. Additionally, the higher dynamic viscosity of water leads to increased frictional losses, particularly at higher frequencies. To minimize these losses and maintain efficient operation, it is advantageous to operate at lower frequencies. In piezoelectric driven micro pumps, the actuator motion is transmitted through the pump diaphragm and into the adjacent fluid. In water, this interaction introduces significant added mass effects, where the surrounding fluid effectively increases the moving mass of the system, further lowering movement of the actuator. Moreover, the acoustic impedance of water is much higher than that of air. This large impedance mismatch reduces the efficiency of energy transmission from the piezoelectric actuator to the fluid in the pump chamber, which can also contribute to a shift toward a flow rate.

### Operation against backpressure

As in the characterization with air, operation against backpressure is part of the characterization with water. The input signal for this test is the same as in the air characterization, which means a sine wave input signal with a voltage range of  $-80\text{ V}$  to  $300\text{ V}$ . The chosen frequency is  $100\text{ Hz}$ . The test procedure is otherwise exactly the same as for air characterization.

As it can be seen in Figure 22, the water flow rate initially starts at the expected values and then decreases approximately linear. For both of the micro pumps with lead-based bulk piezoelectric actuators the water flow rate reaches  $0\text{ mL/min}$  at  $50\text{ kPa}$ .

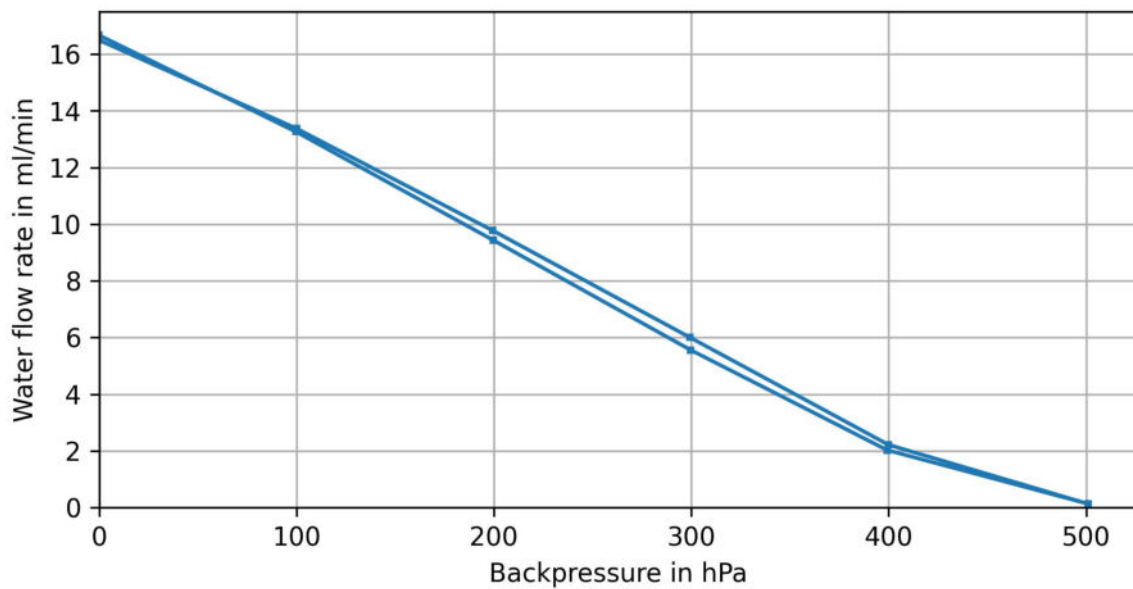


**Figure 22** Water flow backpressure test of lead-based bulk piezoelectric actuator on micro pump

This means, that the piezoelectric actuators can withstand backpressures up to  $50\text{ kPa}$  when it comes to pumping water.

For micro pumps with lead-free bulk piezoelectric actuators, operating against backpressure looks different (see Figure 23). Here we can see, that the initial water flow rate at  $0\text{ kPa}$  is as expected. Up to a pressure of  $20\text{ kPa}$  the decrease in the water flow rate is mostly linear. At higher pressures on the outlet, we see, that the measurement curve flattens and then remains close to  $0\text{ mL/min}$  at  $30\text{ kPa}$  to  $50\text{ kPa}$ .

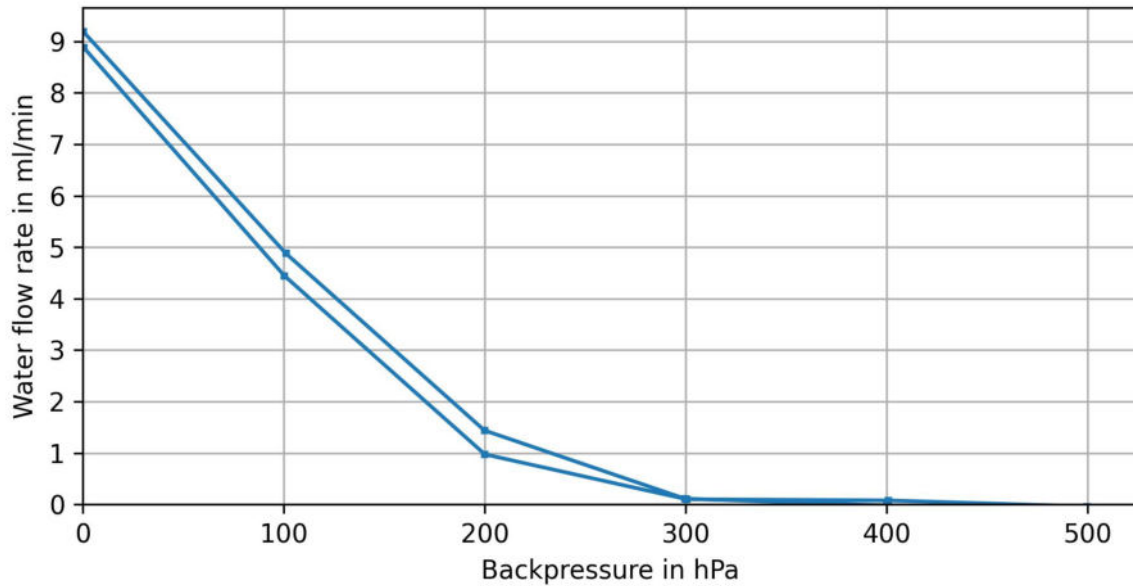


**Figure 23** Water flow backpressure test of lead-based bulk piezoelectric actuator on MMDP

All of the tested pumps show this pattern while operating against backpressure. This pattern suggests a non linear behaviour of the lead-free bulk piezoelectric actuators, which differs significantly from the behaviour of the lead-based bulk piezoelectric actuators.

The underlying reason for this typical curve can be found in the material properties of the lead-free material. These materials show lower piezoelectric coupling coefficients and a higher material stiffness, resulting in smaller actuator displacements and a lower actuator force against the backpressure. Consequently, this material reaches its performance limits at lower backpressures, where the actuator is no longer able to withstand the high opposing pressure. Especially in low flow rates and high backpressures the check valve characteristics play an important role, so that leakage at the check valves can appear. This leaking at the valves is more visible in the micro pums with the lead-free bulk piezoelectric actuators, because the generated water flow is generally lower, so that the impact of the fluidic components becomes greater.

To have a closer look at the impact of the fluidic components in the water characterisation a water leakage test is carried out.

### Water leakage test

The water leakage test is done to check the functionality of the passive check valves of the micro pumps. It must be ensured that the functionality of the passive check valves is within the manufacturing tolerance range so that they have no influence on the overall characterization

of the pump. Thermal stress in the manufacturing of the micro pumps can induce deformation of the valve foils, which can lead to a small initial gap between the valve foils and the valve seat. Through this gap, pressure loss and reverse leakage can occur.

For both variants of the micro pumps this test is done the same. There is no input signal given to the pump, just an increasing backpressure which goes from 0 kPa to 5 kPa. And so the influence of the piezoelectric actuators is not relevant.

In the following diagram we see the result for the leakage test on the micro pumps with lead-based bulk piezoelectric actuators.

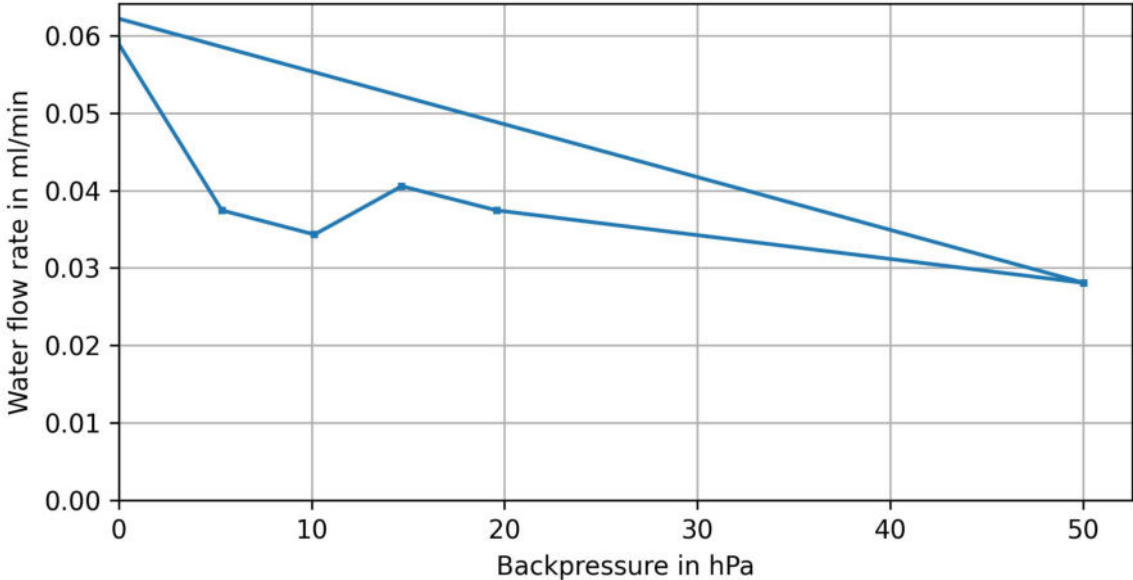


**Figure 24** Water leakage test of lead-based bulk piezoelectric actuator on micro pump

In this diagram we see that the water flow starts very low near zero and gets even lower with increasing backpressure. It is the same for micro pumps with lead-free bulk piezoelectric actuators (see Figure 25).

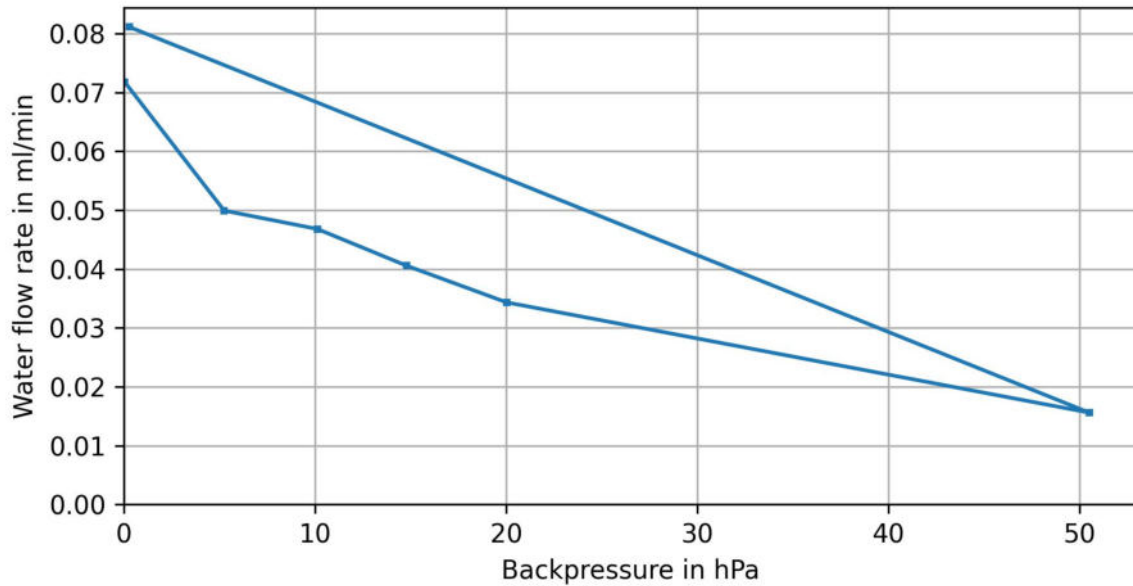


**Figure 25** Water leakage test of lead-free bulk piezoelectric actuator on MMDP

For all of the tested micro pumps, the water leakage is less than 0,1 mL/min, which is within the manufacturing tolerances.

### Conclusion water characterization

The results of the water characterization are summarized as follows:

During the frequency sweep, a maximum water flow rate of  $15,13 \pm 0,89$  mL/min was achieved at approximately 70 Hz using micro pumps equipped with lead-based bulk piezoelectric actuators. In comparison, micro pumps with lead-free bulk piezoelectric actuators achieved a maximum flow rate of  $9,59 \pm 0,66$  mL/min at 120 Hz. This corresponds to a 36,62 % lower maximum flow rate for the lead-free actuators compared to their lead-based counterparts.

Regarding the operation against backpressure, a direct comparison is more complex due to significantly different performance characteristics of the lead-free actuators. For micro pumps with lead-based bulk piezoelectric actuators, the flow rate dropped to zero at a backpressure of 50 kPa. In contrast, for micro pumps with lead-free bulk piezoelectric actuators, the flow rate approached and remained near zero at a backpressure of  $23,75 \pm 4,84$  kPa, which is 52,5 % lower than that observed with the lead-based configuration.

Overall the lead-free bulk piezoelectric actuators show about half of the operational efficiency when compared to the standard lead-based bulk piezoelectric actuators.

#### 4.2.5 Robustness test

The robustness test is conducted to evaluate the influence of mechanical stress on the performance of the lead-free bulk piezoelectric actuators on the micro pumps. For this purpose, long-term stress tests are carried out. The pumps are driven by an input signal ranging from  $-80\text{ V}$  to  $300\text{ V}$  at a frequency of  $30\text{ Hz}$ , initially for 24 hours, then extended to 48 hours, and finally to 72 hours. The goal is to simulate different high levels of mechanical stress on the piezoelectric actuators and to observe their change in performance over time.

**Table 5** Comparison of actuator behaviour under different pumping media

Parameter	Water pumping	Air pumping	Continuous pumping
Test mode	1	2	3
Outlet Configuration	Closed	Closed	Open
Flow Resistance	Higher	Lower	-
Outlet Pressure	Higher	Variable (backpressure possible)	Close to ambient
Stroke Height	Reduced	Slightly reduced	Normal
Mechanical Load	Higher	Moderate	Lower
Actuator Stress	Higher	Moderate	Lower
Mechanical Fatigue Risk	Higher	Moderate	Lower
Internal Damping Effects	Higher	Lower	Lower
Deformation at Constant Load	Possible due to stress	Not significant	Investigated (focus on ceramic deformation)

Three different test modes are defined: In test mode 1, the pump operates with water while the outlet is closed. This test mode puts the piezoelectric actuators under high mechanical stress, as the pump chamber pressure is increasing to a maximum over time and lower compressibility of water leads to a higher curvature with increased bending stress on the ceramic during driving. In test mode 2, the pump operates with air under the same outlet condition. Air has a higher compressibility than water, so that theoretically the actuator can compress the air in the pump chamber more easily in the pump cycle, causing a lower curvature of the actuator in the state, in which the fluid is pushed out of the pump. In test mode 3, continuous water pumping is performed, which is simulating a more real-world scenario for the micro pump. A detailed description of the test procedure is provided in 3.3.4 Robustness test. To illustrate

the test sequence more clearly, a flow chart of the procedure is shown in Figure 26.

Initially, two micro pumps were selected for each test mode using lead-free bulk piezoelectric actuators. Additionally, one pump equipped with lead-based bulk actuator was included in test modes 1 and 3 for comparative analysis.

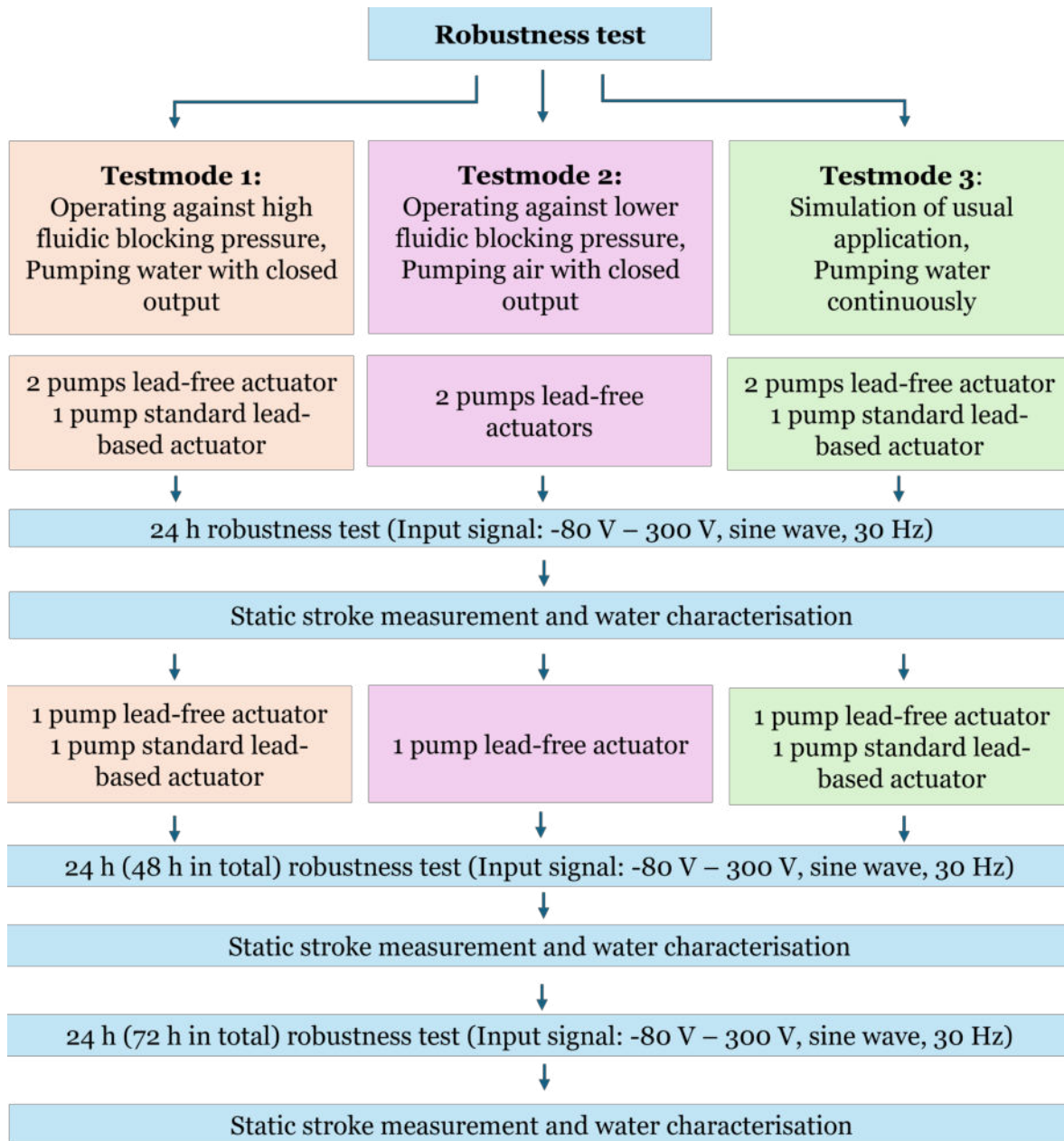


**Figure 26** Flow chart of the robustness test

After each interval of 24 h, the static stroke measurement and the water characterization are performed. The following table (Table 6) shows which pump was used for which test mode

and which piezoelectric actuator.

**Table 6** Overview of pumps and test modes in robustness test

Pump nr.	Pump configuration	Test mode
11	Lead-free bulk	High blocking pressure (water)
10	Lead-free bulk	Continuous water pumping
15	Lead-free bulk	High blocking pressure (air)
470	Lead-based bulk	High blocking pressure (water)
475	Lead-based bulk	Continuous water pumping

Table 7 shows the measurement values for the different micro pumps after every 24 h interval of the robustness test.

**Table 7** Comparison of static stroke measurement for micro pumps with lead-free and lead-based bulk piezoelectric actuators in robustness test

Pump nr.	Stroke height initially in $\mu\text{m}$	Stroke height after 24 h in $\mu\text{m}$	Stroke height after 48 h in $\mu\text{m}$	Stroke height after 72 h in $\mu\text{m}$
11	40.97	22.92	30.07	28.40
10	46.06	36.89	32.75	30.03
15	36.49	33.39	31.26	30.34
470	72.74	59.62	62.10	64.65
475	69.58	57.42	63.18	63.86

We observe that the static stroke height decreases consistently across all micro pumps and test configurations with each 24 h interval of the robustness test. A more pronounced decrease occurs after the first 24 h interval in micro pumps 11, 470, and 475, followed by an increase in static stroke height. This pattern is not observed in all pumps, suggesting that the behaviour is irregular and likely influenced by external factors. One possible explanation is the presence of residual water in these specific pumps after the robustness test, which may affect the static stroke measurements.

The number of cycles for 24 h is calculated in (1) and for 72 h in (2).

$$N_{\text{cycles}, 24} = f \cdot t = 30 \text{ Hz} \cdot 24 \text{ h} \cdot 3600 \frac{\text{s}}{\text{h}} = 2\,592\,000 \quad (1)$$

$$N_{\text{cycles}, 72} = f \cdot t = 30 \text{ Hz} \cdot 72 \text{ h} \cdot 3600 \frac{\text{s}}{\text{h}} = 7\,776\,000 \quad (2)$$

The robustness test involves millions of actuation cycles, which can induce fatigue in the piezoelectric material. Since the actuators are made from ferroelectric ceramics, repeated cycling can reduce their polarizability. Over time, the ferroelectric domains become increasingly hardened, limiting their mobility. This reduces the electromechanical coupling efficiency and consequently leads to a decrease in stroke height.

Additionally, mechanical stresses accumulated during long-term operation can lead to creep deformation in the material. This may reduce the internal pretension, weakening the restoring force and further contributing to a decline in stroke height.

To see how the robustness test impacts the actual flow rate of the micro pumps with the different piezoelectric actuators, a water characterization was done after every 24 h interval. Figure 27 shows the different curves for the frequency sweep with water for the lead-based bulk piezoelectric actuator on a micro pump for every 24 h interval. This micro pump has undergone the robustness test in test mode 1, which means continuous water pumping with closed output, which leads to high blocking pressure and high mechanical stress.

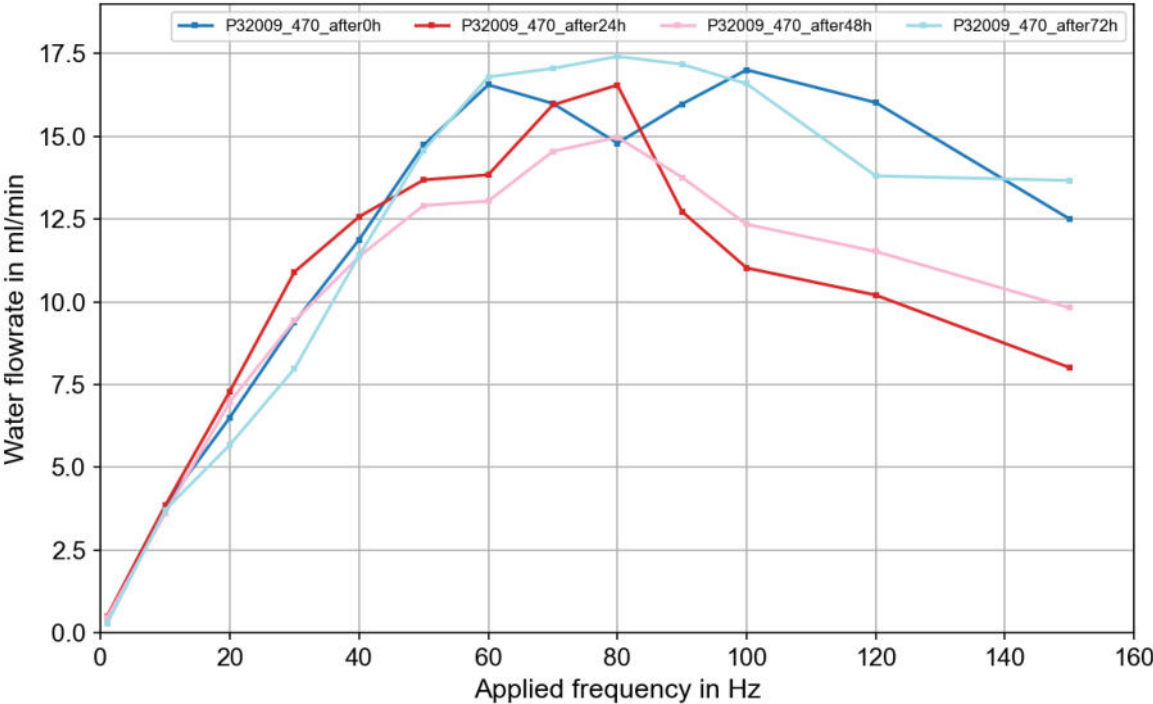


**Figure 27** Comparison of water flow rates after 72 h robustness test with high blocking pressure (water) on lead-based bulk piezoelectric actuator

The graph shows that the water flow rate is highest and most stable during the initial measurement and after the 72 h interval. Interestingly, the flow rate increased again after 72 h

of robustness testing, which may indicate an issue with the test setup. This suspicion is supported by the static stroke measurement data, where a significantly reduced stroke height is observed after the robustness test, which contradicts the higher flow rates in the water characterization. This suggests that anomalies in the test setup may be affecting the results. The test setup for water characterization includes two reservoirs: one for the water inlet and one for the outlet. Since this setup is also used for other experiments in the laboratory, variations in the water levels of the reservoirs can occur. Such changes can influence the water flow rate, as differing fill heights affect the pressure conditions within the tubing. For instance, the observed increase in water flow rate after 72 h could be attributed to a lower water level in the outlet reservoir, which reduces the backpressure in the tube the micro pump needs to overcome.

At higher frequencies of 150 Hz, the separation in water flow rates between the different robustness test time intervals become more apparent. As the frequency gets higher, additional effects like added mass, inertia and dynamic viscosity of water make it even harder for the actuator to compress the fluid properly in every pump cycle. Thus, these added effects accentuate the degradation of the piezoelectric actuator at higher frequencies more clearly. This observation is supported by the backpressure testing of this pump (see Figure 28).

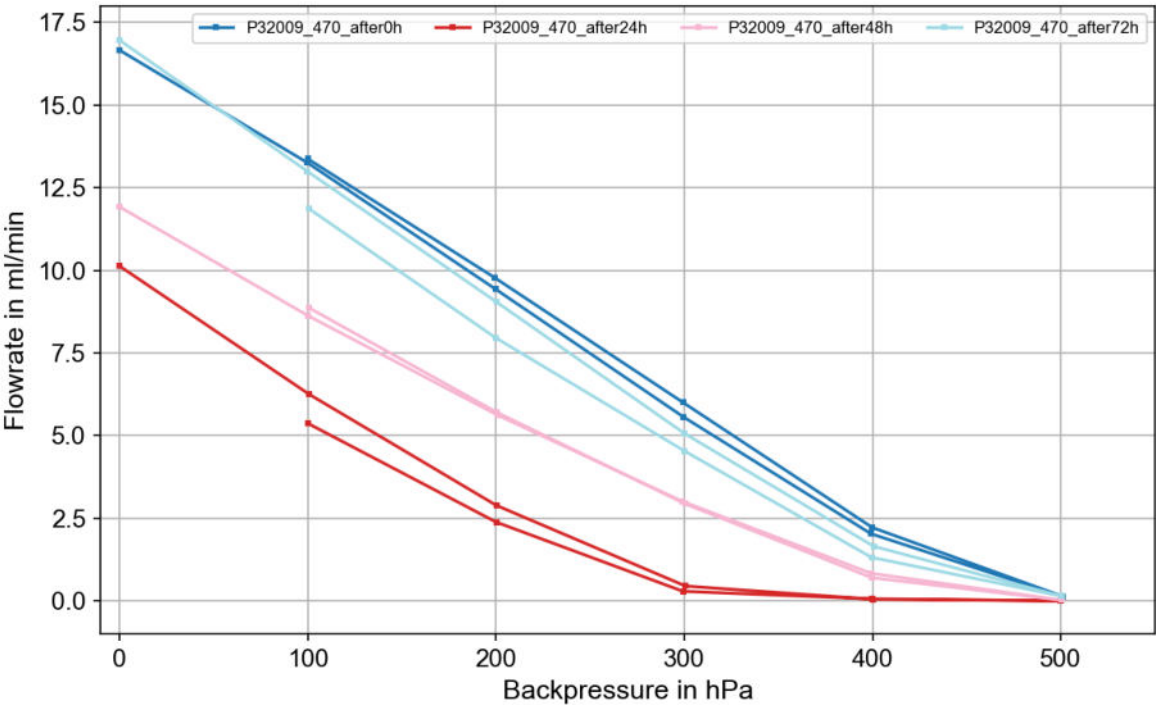


**Figure 28** Comparison of backpressure testing after 72 h robustness test with continuous water pumping with closed output on lead-based bulk piezoelectric actuator

We see a decline in the water flow rate after 24 h and 48 h but then an increased water flow rate after 72 h, which can be explained by the fill heights in the water reservoirs, which aligns with the previously discussed frequency sweep. Other possible causes could be hidden bubbles in the system or particles that got into the pump chamber. Also a recognizable difference in the characteristic curves in the backpressure test is, that after the robustness test, we see a dip in the water flow rate, that does not appear in the initial state. This is a sign for the degradation of the piezoelectric actuators, as the ability to compress the fluid in the pump chamber at higher pressures decreased.

For the lead-free bulk piezoelectric actuators the comparison of the water flow rates after each 24 h interval of the robustness test looks like the following (see Figure 29). This micro pump has undergone the robustness test in test mode 1, which is with high blocking pressure, inducing high mechanical stress.

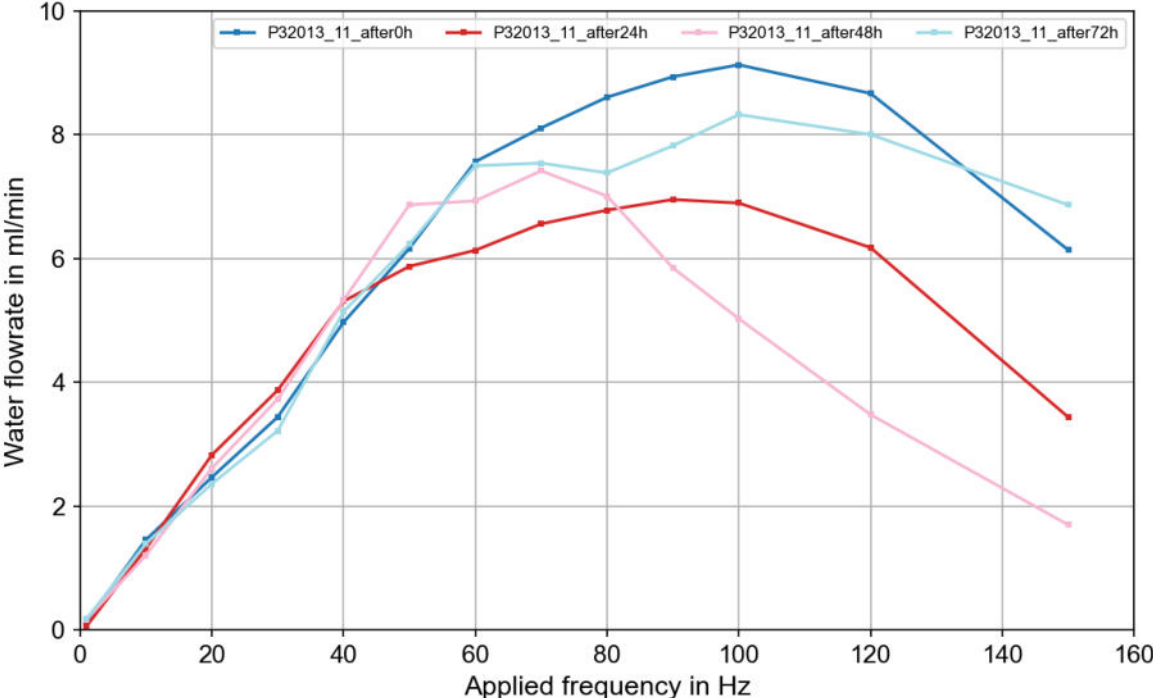


**Figure 29** Comparison of water flow rates after 72 h robustness test with high blocking pressure (water) of lead-free bulk piezoelectric actuator

Similar to lead-based bulk piezoelectric actuators, no significant differences in water flow rates are observed at lower frequencies. At higher frequencies, such as 150 Hz, where the impact of effects like added mass, inertia and dynamic viscosity changes in water, lead to a clearer separation of flow rates between the different robustness test intervals. We see that the water flow rate is highest for the initial micro pump and progressively decreases after each 24 h

interval. This trend is consistent with the static stroke measurements, which also show a gradual reduction in stroke height over time.

As previously discussed, various factors can contribute to the degradation of piezoelectric materials. In KNN-based materials in particular, which have a different internal structure compared to lead-based counterparts, degradation often manifests as microcracks along the grain boundaries. These microcracks negatively affect the electromechanical coupling, resulting in reduced stroke height and, consequently, lower flow rates. When the grain boundaries are no longer well-connected, mechanical stress cannot be effectively transferred across them, further impairing actuator performance.

This also manifests in the backpressure test of the micro pump (see Figure 30).

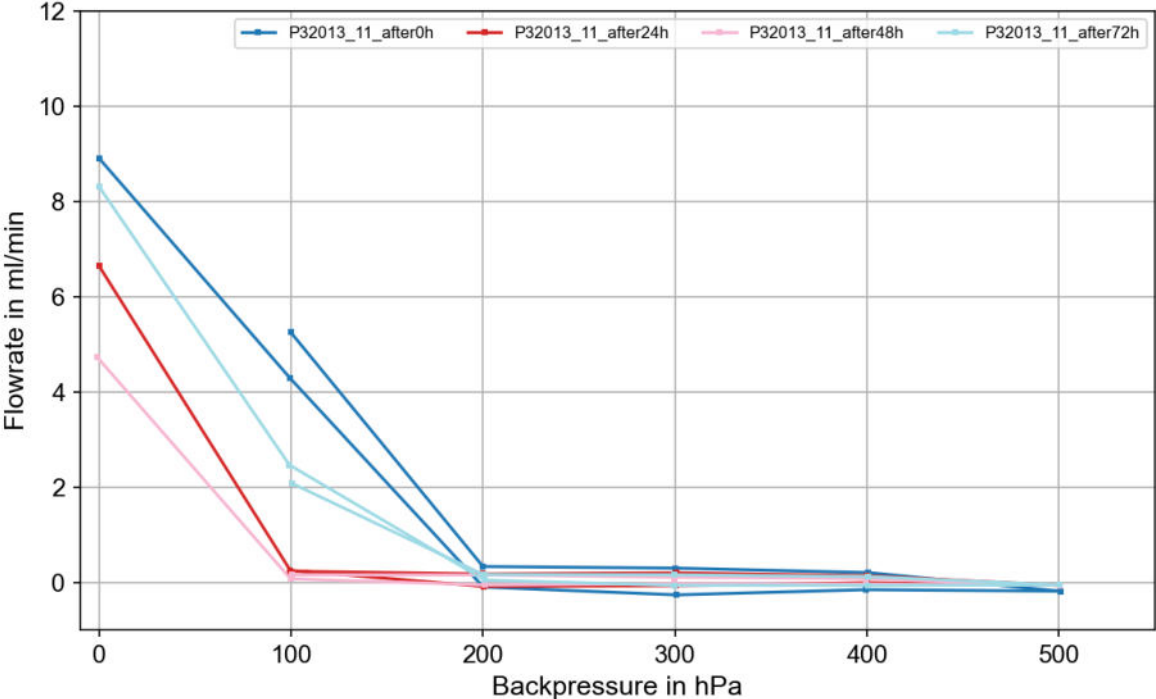


**Figure 30** Comparison of backpressure testing after 72 h robustness test with high blocking pressure (water) on lead-free bulk piezoelectric actuator

Since the backpressure test is conducted at an input frequency of 100 Hz, the initial flow rate at 0 kPa backpressure corresponds to the flow rate measured at 100 Hz in the frequency sweep. The flow rate for the micro pump prior to the robustness test decreases nearly linearly, approaching 0 g/min at a backpressure of around 20 kPa (see dark blue curve in Figure 30). After each 24 h interval of the robustness test, the backpressure at which the flow rate drops to zero is reduced to approximately 10 kPa (see red and pink curves in Figure 30).

As already observed in the frequency sweep, the flow rate for the 72 h robustness test shows

irregularities. This can likely be attributed to variations in the reservoir fill levels in the test setup. The key difference between the initial state of the micro pump and after 72 h of testing is a noticeable dip in flow rate at 10 kPa, indicating that the actuator’s performance is indeed negatively affected by the robustness testing. However, the difference between these two curves is less pronounced, likely due to test setup influences.

The shown results from above all relate to the robustness test in test mode 1, which induces the highest mechanical stress on the piezoelectric actuator. As the outlet is closed, and the pumps are continuously pumping water against a rising pressure in the pump chamber, this test shows the greatest effects on the micro pumps. In the following conclusion of the robustness test, all of the measurement data from the robustness test in the different test modes are shown.

### Conclusion robustness test

As the robustness test is a very time-consuming test and the test leads to irreparable degradation on the piezoelectric actuators on the micro pumps, only a few pumps were available for the test. Therefore, the test results from this test should rather be seen as an evaluation of a trend in the long-term application of mechanical stress on the micro pumps.

Due to the irregularities in the water characterization between the time interval of 48 h to 72 h, for the comparison, the initial measurement results and the measurement results after 48 h are depicted in the following tables(see Table 8 and Table 9).

**Table 8** Comparison of frequency sweep for the time intervals of the robustness test

	Lead-free			Lead-based	
<b>Pump nr.</b>	<b>11</b>	<b>10</b>	<b>15</b>	<b>470</b>	<b>475</b>
Test mode	1	3	2	1	2
Flow rate after 0 h in g/min at 150 Hz	6.13	10.13	8.55	12.50	13.56
Flow rate after 24 h in g/min at 150 Hz	3.43	9.61	9.53	8.01	9.39
Flow rate after 48 h in g/min at 150 Hz	1.69	8.30	6.65	9.82	6.42
Decline after 48 h in %	72.43	18.02	22.22	21.36	52.68

When examining the measurement values from the frequency sweep, it becomes evident that the largest decrease in water flow rate occurs for test mode 1 in the lead-free bulk piezoelectric

actuator. This is expected, as test mode 1 subjects the actuator to the highest mechanical stress. Additionally, the decline in flow rate over time is more pronounced for the lead-free actuators compared to the lead-based ones, indicating a higher sensitivity to mechanical stress inducing a higher degradation.

**Table 9** Comparison of backpressure test for the time intervals of the robustness test

<b>Pump nr.</b>	<b>Lead-free</b>			<b>Lead-based</b>	
	<b>11</b>	<b>10</b>	<b>15</b>	<b>470</b>	<b>475</b>
Test mode	1	3	2	1	2
Backpressure after 0 h in kPa at 100 Hz	20	20	20	50	50
Backpressure after 24 h in kPa at 100 Hz	10	20	20	40	50
Backpressure after 48 h in kPa at 100 Hz	10	20	20	40	40
Decline in %	50.00	0.00	0.00	20.00	20.00

Regarding the backpressure test, the highest decline in performance can be observed in test mode 1 on the micro pump with lead-free bulk piezoelectric actuator, inducing that the mechanical stress of this test mode is the highest on the actuator leading to the highest degradation of the material.

The following table shows the maximum stroke heights of the different tested micro pumps.

**Table 10** Comparison of max static stroke heights for the time intervals of the robustness test

<b>Pump nr.</b>	<b>Lead-free</b>			<b>Lead-based</b>	
	<b>11</b>	<b>10</b>	<b>15</b>	<b>470</b>	<b>475</b>
Test mode	1	3	2	1	2
Max static stroke height after 0 h in $\mu\text{m}$	40.97	46.06	36.49	72.74	69.58
Max static stroke height after 72 h in $\mu\text{m}$	28.40	30.03	30.34	64.65	63.86
Decline in %	30.68	34.78	16.87	11.12	8.21

In summary, it can be said that mechanical stress caused by long-term mechanical stress of the piezoelectric actuators leads to degradation of the material. The degradation of the piezoelectric actuators was higher for the lead-free bulk actuators than for the lead-based

bulk actuators, which can be attributed to the different material properties as explained and discussed above. Test modes 1 and 3 (pumping water with closed output and continuous pumping of water) affected the maximum static stroke height the most. But even after 72 h of the robustness test, functionality of the micro pumps is still given. Due to the fact, that only a small number of samples was available for the robustness test, these results show first trends of the behaviour of the micro pumps.

An important factor in the selection of micro pumps is their power consumption, operational stability, and low noise performance. To ensure reliable operation in real-world applications, it is recommended to drive the micro pumps at lower frequencies, where their behaviour is more predictable. At these lower frequencies, the influence of robustness testing is significantly reduced compared to higher frequencies, where higher flow rates may introduce greater variability. As a result, lead-free bulk piezoelectric actuators remain suitable for implantable applications, particularly when targeting flow rates around 3 mL/d, or single-use auto injectors.

In order to investigate the effect of the robustness test on the actuators even further, surface analysis of the actuators will be carried out using SEM in the following.

#### **4.2.6 Surface and structural analysis**

The primary objective of this analysis was to examine surface morphology and structural features, as well as to evaluate potential surface changes resulting from the robustness testing. Three samples were selected for this analysis. The first sample is an unused lead-free bulk piezoelectric actuator. This sample serves as a reference to assess the initial surface condition prior to any processing. The second sample is a lead-free bulk piezoelectric actuator that underwent all of the the processing steps and testing. This allows for a direct comparison to identify any changes in the surface structure due to handling, operation, and stress exposure. The last sample, that was chosen is the lead-based bulk piezoelectric actuator, that underwent all process and testing procedures. This sample was chosen to compare the influence of the processing and testing of the lead-free and the lead-based bulk piezoelectric actuators.

All the images were taken at the centre of the piezoelectric actuators, where mechanical stresses are supposed to be highest during operation. This is because the bending, and thus the strain, is most significant at the centre while the actuator is pumping.

The first picture shows the unused lead-free bulk piezoelectric actuator at a magnification of 866 x, which gives an overview of what the surface looks like (Figure 31) in the initial state.

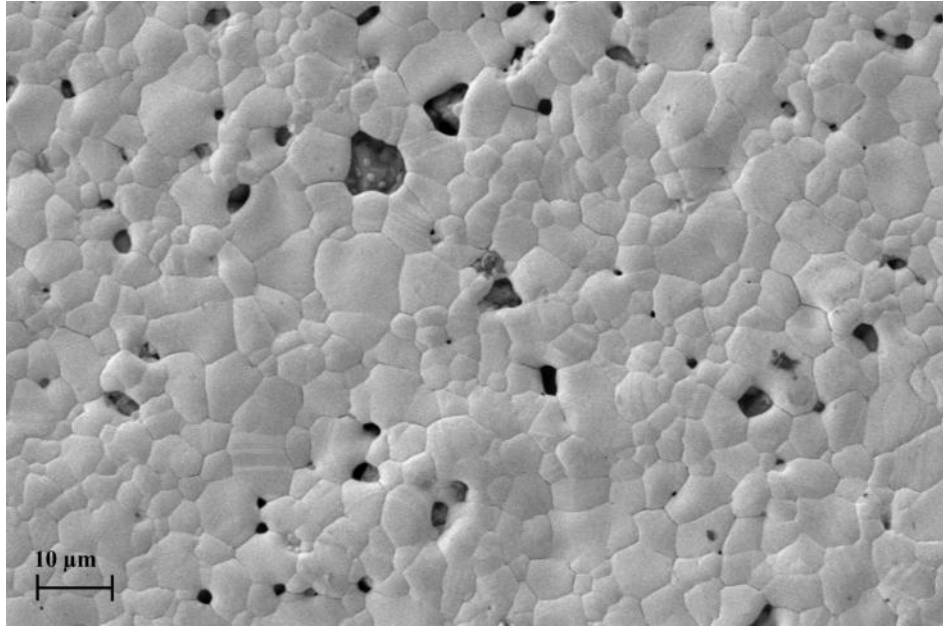


**Figure 31** SEM of lead-free bulk piezoelectric actuator before robustness testing

In this image, the grain boundaries between individual grains are clearly visible, along with several pores of varying size. The grains themselves also differ in size, indicating a non-uniform microstructure. Additionally, the surface is not completely flat but exhibits noticeable topographical variations, with slight elevations and depressions across the observed area.

In the next picture we see the lead-free bulk piezoelectric actuator, that has undergone the whole processing and testing procedure at a magnification of 800x (see Figure 32). This gives an overview of what the surface looks like after all the handling.

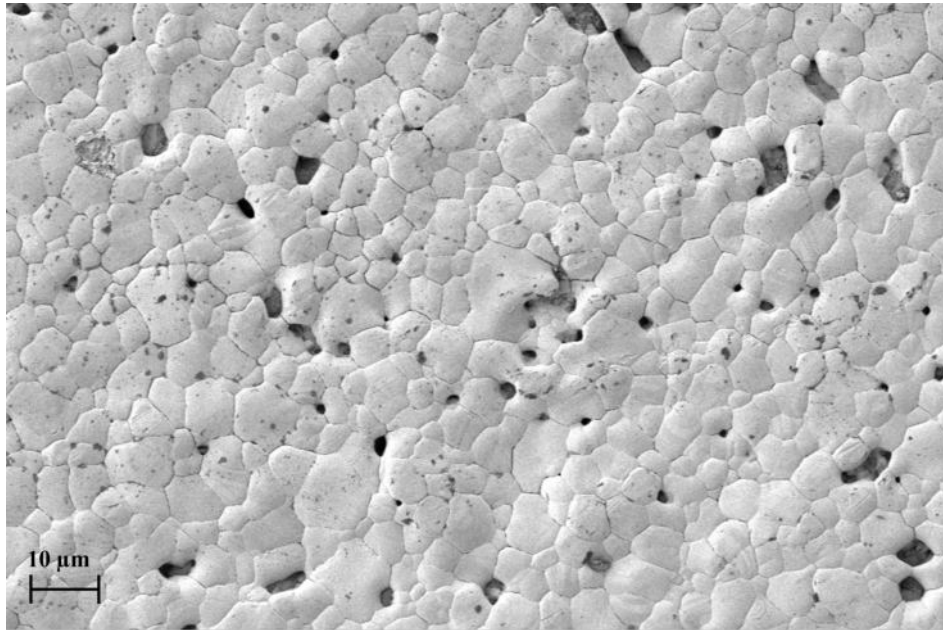
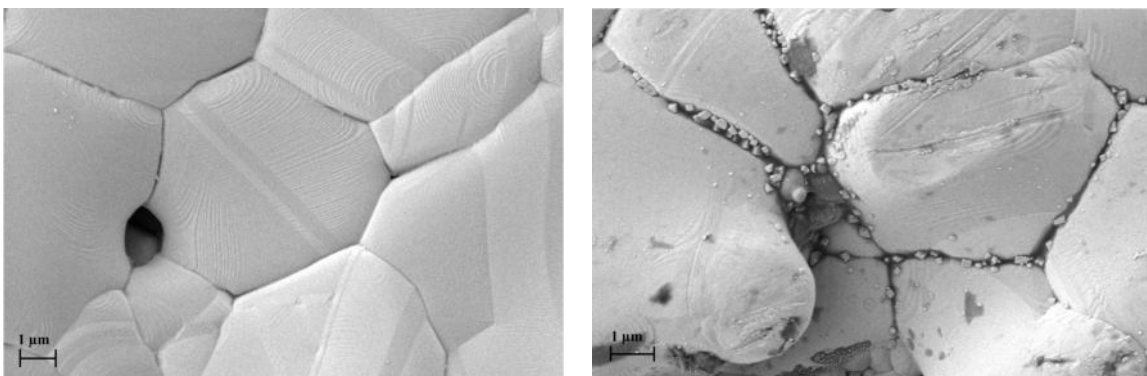


**Figure 32** SEM of lead-free bulk piezoelectric actuator after robustness testing

In this piezoelectric actuator, the grain boundaries are clearly visible, along with multiple pores of varying sizes. The grains themselves also vary in size. Additionally, some impurities can be observed. The dark spots scattered across the surface are due to pollution introduced during soldering and testing processes. Notably, some of the grain boundaries appear darker compared to those in the unused lead-free bulk piezoelectric actuator. To provide a more detailed comparison of the grain boundaries, both lead-free bulk piezoelectric actuators are shown side by side at higher magnification in Figure 33.



Before robustness testing

After robustness testing

**Figure 33** SEM side by side comparison of the lead-free bulk piezoelectric actuators before and after various processing and testing steps with a magnification of 8.000 x

In this direct comparison of the piezoelectric actuator surfaces at higher magnification, several differences become evident. On the actuator in its initial, unprocessed state, the surface appears very smooth and clean. Some grooves are visible on the grains, likely resulting from the manufacturing process. These grooves are also present on the actuator after robustness testing. However, the tested actuator shows significantly more impurities, such as very small particles, which are mostly located along the grain boundaries. Additionally, some scratches are visible on the grains themselves, likely caused by handling during fabrication of the pump. The grain boundaries also appear slightly darker, which may indicate that they are no longer as tightly bonded as before testing. This degradation could help explain the reduced performance of the piezoelectric actuators following the robustness tests.

The final sample selected for surface and structural analysis is the lead-based bulk piezoelectric actuator that underwent the full processing and testing procedure. Figure 34 provides an overview of its surface. The structure of the PZT material appears noticeably different from that of the previously examined KNN sample. The grains exhibit a distinct texture, and the grain boundaries are clearly visible, with grains varying in size. While some pores are present, their number is generally lower compared to the lead-free bulk KNN material.

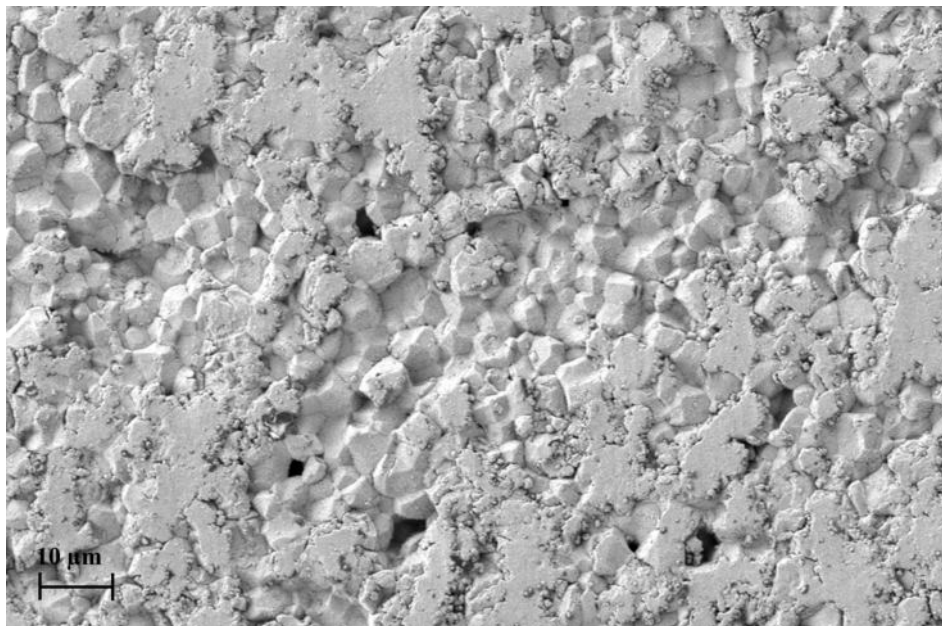


**Figure 34** SEM of lead-based bulk piezoelectric actuator after robustness testing with a magnification of 829 x

Surface features resembling pressure marks are visible, likely resulting from the actuator being pressed during the mounting process onto the micro metal diaphragm pump base. Since the PZT material is softer than the KNN material used in the lead-free actuator, this could explain why such pressing marks are observed on the lead-based PZT sample but not on the KNN

sample.

At a higher magnification of 5.56k x on the same actuator, the surface structure becomes more apparent. Similar to the lead-free piezoelectric actuators, impurities can be observed on the surface. However, unlike the dark spot-like impurities seen on the lead-free material, these appear more like distinct particles resting on the surface.

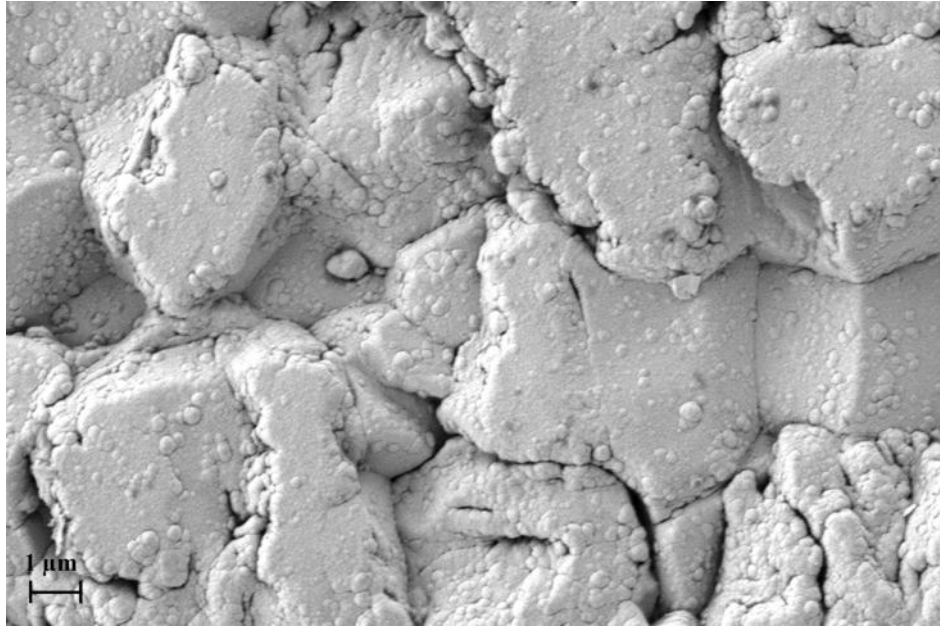


**Figure 35** SEM of lead-based bulk piezoelectric actuator after robustnesstesting (high magnitude)

In this closer examination of the surface, some grain boundaries appear darker; however, most still appear well-defined and tightly bonded.

In conclusion, the surface and structural analysis revealed distinct differences between the lead-free bulk piezoelectric actuators before and after processing and testing. Initially, the surface appears very smooth and clean, with visible grain boundaries that seem well-connected. A notable number of pores are also present, which may slightly affect actuator performance, as they can reduce both the piezoelectric response and mechanical coupling.

After processing and robustness testing, the surface shows increased contamination, with impurities primarily accumulating along the grain boundaries. These boundaries appear darker and deeper, indicating possible degradation. Such changes likely contribute to a reduction in the piezoelectric effect, thereby lowering the performance of the micro pump.

It is important to note that this SEM analysis does not reveal potential subsurface microcracks, which may still be present. These microcracks, typically induced by high mechanical stress, could also significantly reduce actuator performance.

### **4.3 Evaluation of lead-based stack piezoelectric actuators with self-sensing properties**

To evaluate the lead-based stack piezoelectric actuators with self-sensing abilities, at first the micro pumps fabrication process needs to be adapted, due to the different properties of these actuators. After that, the electro mechanical characterization was conducted followed by the examination of the self-sensing properties.

#### **4.3.1 Optimization of the micro pump fabrication process**

Since the novel stack piezoelectric actuators differ in several characteristics from those previously used, and in order to simplify the fabrication process, two steps in the manufacturing of micro pumps have been adapted.

On the one hand, the process can be streamlined by using an adhesive epoxy film instead of the conventional method of dosing adhesive when bonding the piezoelectric actuators. On the other hand, during pump fabrication, it was found that the self-sensing pads of the piezoelectric actuators are sensitive to thermal stress. For this reason, a conductive adhesive was tested as an alternative to soldered connections.

#### **Using Adhesive Epoxy Film Instead of Liquid Adhesive for Mounting the Piezoelectric Actuators**

As described in Chapter 3.2.2 Mounting of the piezoelectric actuators onto the micro pumps, the standard procedure in micro pump manufacturing involves bonding the piezoelectric actuators to the micro pump base body using liquid adhesive. This adhesive is usually applied via an automated dispensing machine. However, the process often results in variations in the amount of adhesive dispensed. In some cases, excessive adhesive was applied, which would leak out at the edges of the actuators after curing in the oven. Additionally, entrapped bubbles in the glue can compromise bonding strength.

To address this issue and improve the bonding process between the piezoelectric actuator and the micro pump base body, an adhesive epoxy film is proposed as an alternative. This film allows for more precise and consistent application as they offer uniform thickness, eliminate the risk of entrapped air bubbles and enable more precise and consistent application. They are also easy to handle and provide reliable electrical insulation.

The adhesive epoxy film is stored in a refrigerator and can be cut into the required shape using a punch shortly before use (see Figure 36, a). As the epoxy film warms to room temperature, it becomes tacky and can be easily positioned on the pump base bodies with improved alignment and bonding quality (see Figure 36, b).



a) Punching out of the epoxy foil



b) Epoxy foil on pump base bodies

**Figure 36** Mounting of the piezoelectric actuators on the pump base bodies

To analyze the final result of the piezomounting with the epoxy foil, a profile scan of the pump is conducted to evaluate the thickness of the foil after curing. Figure 37 shows the scanned profile line on the pump with the actuator.

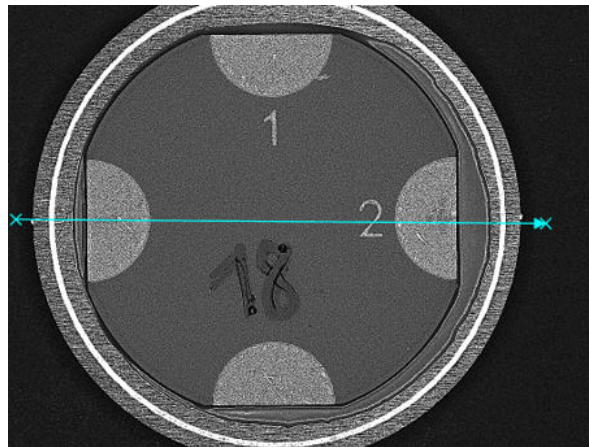


**Figure 37** Micro pump with actuator with scan line for the profile scan

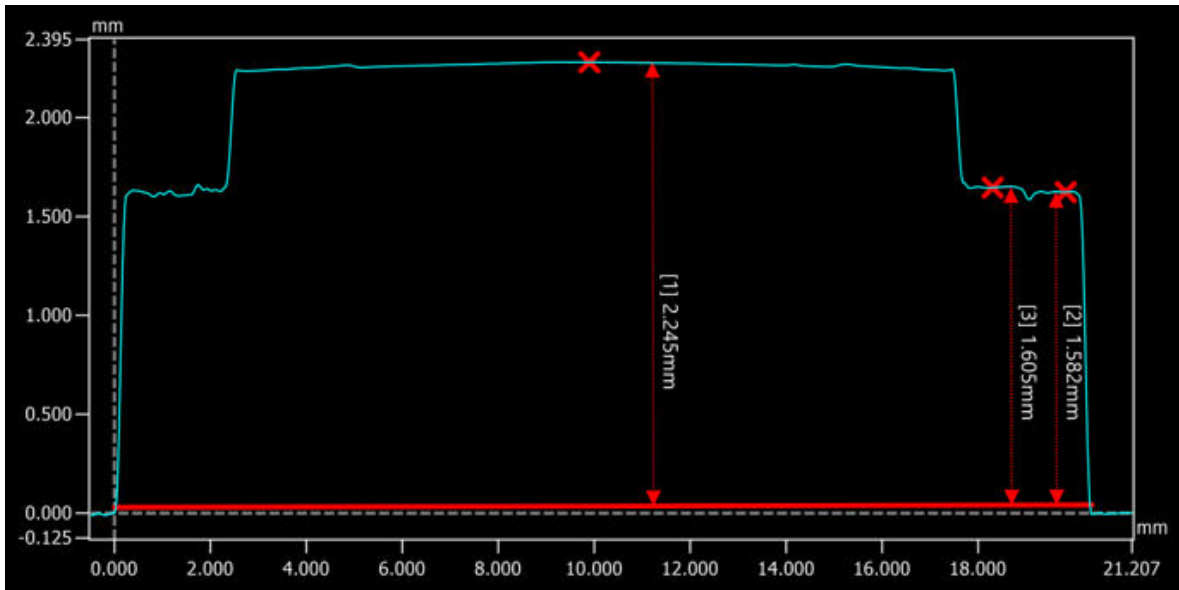


**Figure 38** Profile scan over the piezoelectric Actuator on the micro pumps using epoxy foil for mounting

In the profile scan (see Figure 38) we can see, that the epoxy foil after curing is very thin. Even thinner as before the curing. The thickness comes out at around 20 nm.

Using the adhesive epoxy film instead of liquid adhesive significantly simplified the mounting process. The preparatory steps typically required for handling and applying the glue, including setup and calibration of the dosing machine, which are no longer necessary, resulting in considerable time savings, which is mostly important for batch manufacturing. Additionally, punching the epoxy film into the desired shape ensures consistent geometry, leading to uniform bonding quality across all units.

### **Using conductive adhesive instead of soldering the contacts on the micro pumps**

During initial trials of fabricating micro pumps with piezoelectric stack actuators featuring self-sensing pads, it was observed that soldering the contacts from the PCB to the self-sensing pads caused damage to the pads. The soldered wires were prone to detachment even with minimal movement, and thermal stress further contributed to the delamination of both the actuation and self-sensing pads.

As an alternative, a conductive liquid adhesive was tested. This adhesive should be stored in a refrigerator and brought to room temperature before use. Prior to application, it must be thoroughly stirred to ensure a homogeneous distribution of the silver particles. The wires used to connect the PCB to the piezoelectric actuators should be handled with gloves to avoid contamination from skin oils.

Since the adhesive is not tacky in its uncured state, the wires were temporarily fixed in position

using tape to ensure accurate placement. It is important to apply a sufficient amount of adhesive to the contact area, as the adhesion improves with increased material volume. While different curing temperatures and durations are recommended depending on the application, they also depend on the amount of adhesive applied and its initial condition. For our specific use case, a curing process at 80 °C for 8 h yielded good results.

### 4.3.2 Electro mechanical characterisation - static stroke measurement

A total of five micro pumps with these actuators were fabricated, incorporating recent improvements such as the use of epoxy foil instead of conventional glue, and conductive adhesive instead of soldering for connecting the contacts to the PCB.

Due to differences in material properties, such as the thickness of the piezoelectric elements and the stacked layer structure, these actuators require a modified input signal. The signal used is the same as described in 3.3.1 Electro mechanical characterization , featuring a voltage range from -12 V to 88 V.

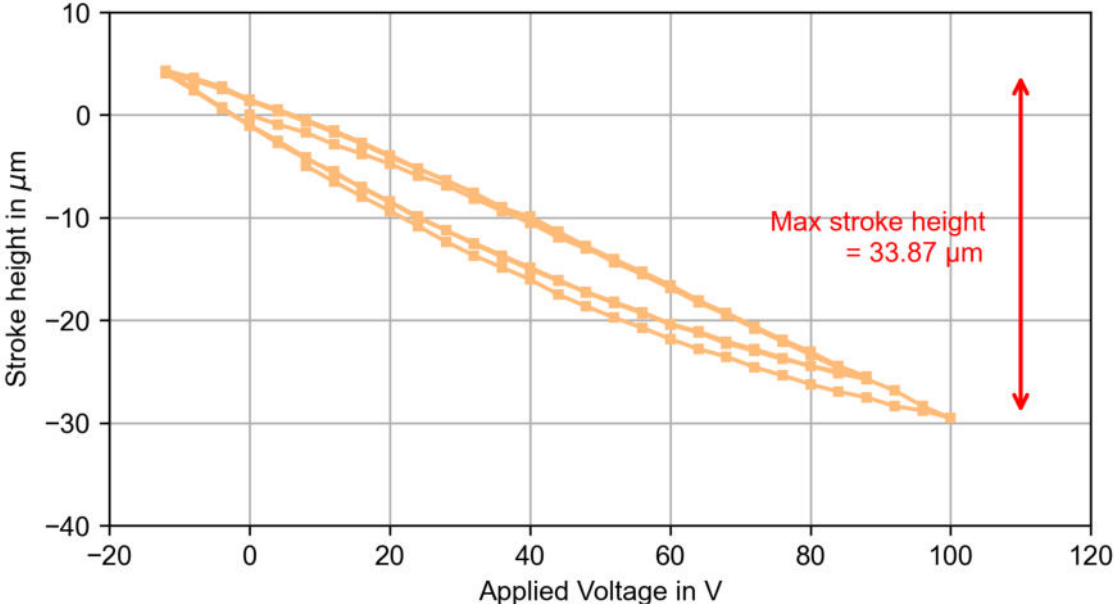


**Figure 39** Stroke measurement for lead-based stack piezoelectric actuator on micro pump

The measurement results indicate a similar hysteresis pattern to that observed in previous piezoelectric actuators. However, the maximum stroke height is reduced. This reduction is attributed to the increased stiffness of the actuator due to its greater thickness, which limits bending.

**Table 11** Measurement results for the static stroke measurement for the micro pumps with lead-based stack piezoelectric actuators

Pump nr.	max stroke 1 in $\mu\text{m}$	max stroke 2 in $\mu\text{m}$	max stroke 3 in $\mu\text{m}$	mean max stroke in $\mu\text{m}$
1	33.8	33.55	33.43	33.59
2	33.0	33.13	33.43	33.18
3	33.13	33.01	28.42	31.52
4	33.19	32.70	32.58	32.82
5	32.58	32.33	32.32	32.41

The mean maximum stroke height for all of the pumps is  $32,71 \mu\text{m} \pm 0,71 \mu\text{m}$ .

### 4.3.3 Evaluation of the self-sensing properties

Detecting bubbles or blockages in the micro dosing system is crucial, as even minor irregularities can cause significant errors in the dosing volume. To address this, a novel piezoelectric actuator with self-sensing capabilities is being evaluated to determine its suitability for detecting such anomalies and thus minimizing dosing errors.

To assess the self-sensing properties of the lead-based stack piezoelectric actuators, a series of measurements were conducted. In particular, dynamic stroke measurements were performed to correlate the actuator's mechanical movement with the self-sensing output signal. These tests were carried out under varying input frequencies and with different excitation waveforms, including sine and square waves, to comprehensively evaluate the actuator's response.

In the following graph, we see the dynamic stroke height measurement as well as the output voltage of the self-sensing signal, while the piezoelectric actuator is actuated with an input signal of  $-12 \text{ V}$  to  $88 \text{ V}$  at a frequency of  $1 \text{ Hz}$  with sine wave signal.

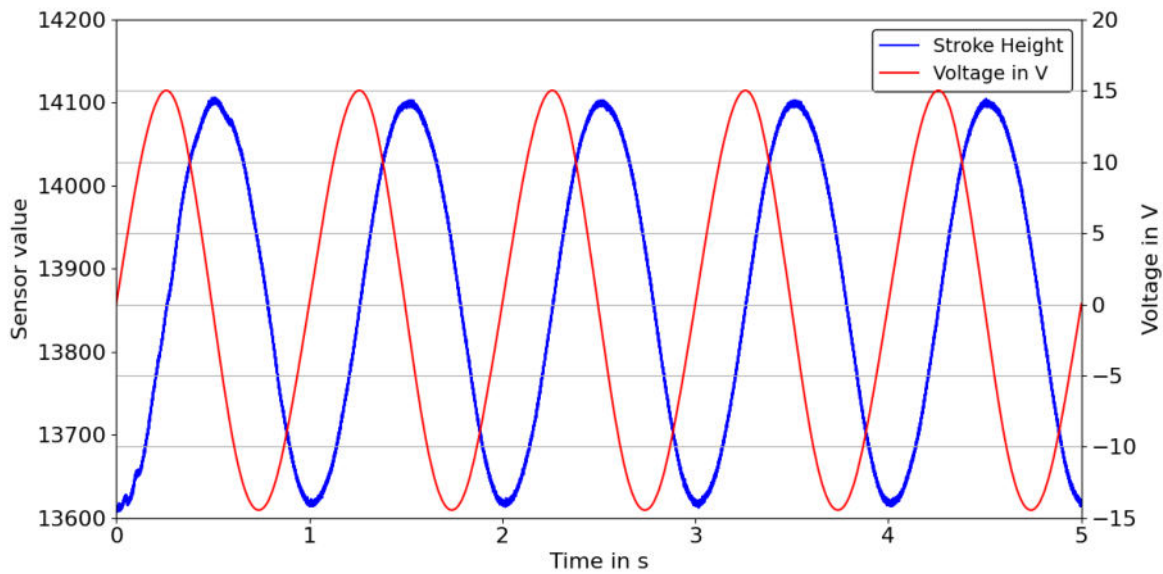


**Figure 40** Comparison of stroke height and output voltage of self-sensing pads while actuation

For this input frequency, the output voltage of the self-sensing pads ranges from approximately  $-15\text{ V}$  to  $15\text{ V}$ . Because the measurement cannot be started at the same time due to the conditions on site in the laboratory, the two curves for the output signal from the self-sensing pads and the stroke height of the actuator were superimposed as would be expected according to theory (see 2.3 Self-Sensing in micro pumps). Since the piezoelectric actuator generates a maximum voltage due to the direct piezoelectric effect when the mechanical movement of the actuator is at its highest, the output voltage at the self-sensing pad shows a maximum when the stroke height experiences the maximum gradient. Overall, it is visible that the output signal is very even and shows no fluctuations, even if the dynamic measurement of the stroke height shows slight fluctuations.

To evaluate the self-sensing properties, different test scenarios for real-world use were simulated. The micro pump is driven at a frequency of  $100\text{ Hz}$ . One important scenario is the clogging of the micro pump or the tubes while pumping water, to see if this is recognizable by the self-sensing properties of the pump. This is simulated by closing the outlet with a clamp, to increase the pressure in the pump chamber, as it would happen with clogged micro pump or tubes. The outlet voltage of the self-sensing pads for this scenario is shown in the following graph.

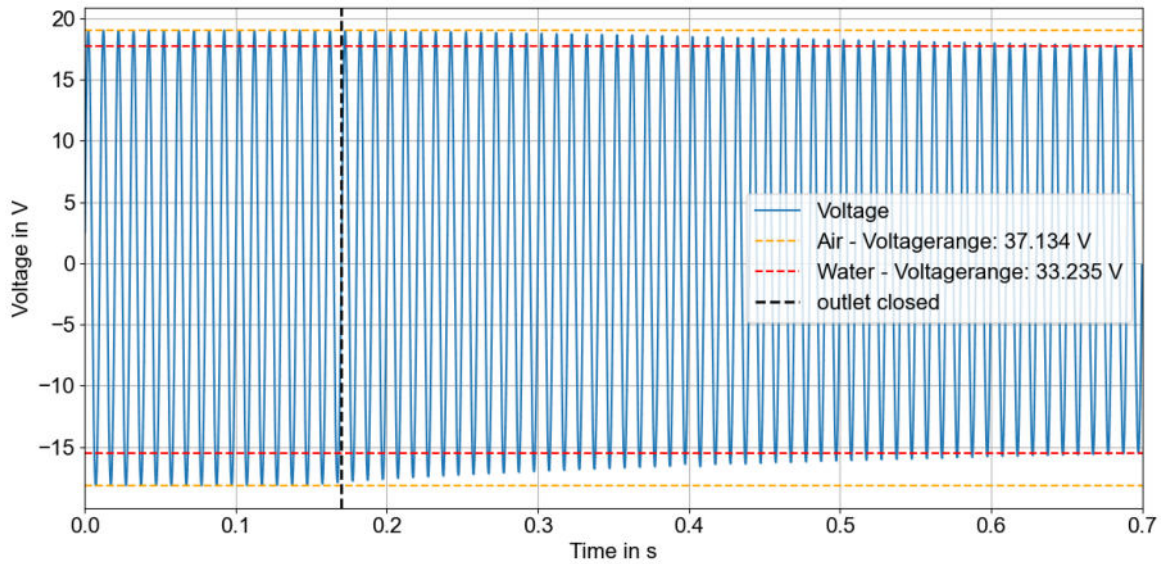


**Figure 41** Self-Sensing output voltage over time pumping water with closed output after 0.27 seconds

In the graph, we see the sine wave of the output voltage from the self-sensing pads, which is generated by the direct piezoelectric effect, through the movement of the pump. Because of the high input frequency of 100 Hz, the oscillation is accordingly fast. At 0,17s, the outlet was closed with a clamp (see black line in Figure 23). After closing the outlet, we see a slow decrease in the amplitude of the voltage signal. Initially, the amplitude has a value of 37,13 V and after 0,7s the amplitude decreased to 33,24 V, which makes a difference of 3,88 V. The slow decrease in the amplitude refers to the slow building up of pressure in the pump chamber. As long tubes were used in this test setup, the dampening effect of the tubes plays a role as well. The piezoelectric actuator has to push against that pressure, which leads to a smaller movement range. As the movement range gets smaller, the direct piezoelectric effect leads to a smaller output voltage. As the building up of the pressure in the pump chamber and the tubes needs some micro seconds, the recognition from the self-sensing pads would also need the same time.

Another very important test scenario is the detection of fluid change pumping through the micro pump. Sometimes bubbles get into the water stream. To test this scenario and see if bubbles are detectable with the self-sensing properties of the piezoelectric actuators, the micro pump was driven with alternating water and air.

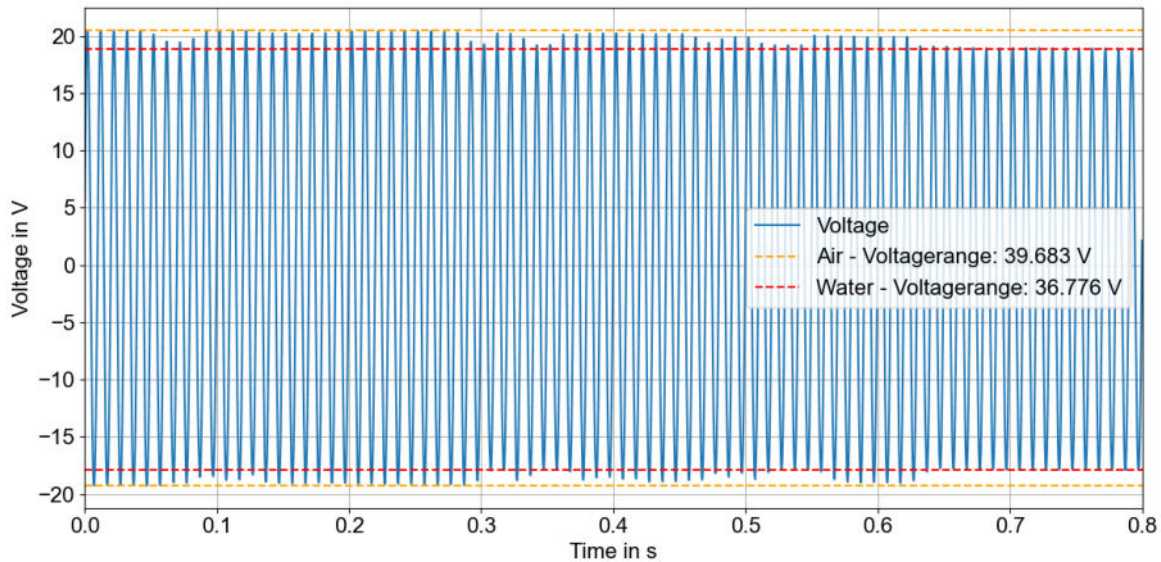


**Figure 42** Self-Sensing output voltage over time pumping air with water droplets

For the change of the fluid, that is going through the pump, we see differing voltage ranges from the self-sensing pads. For the pumping of air, we see a voltage range of 39,68 V and for pumping water 36,78 V. As the air has a much lower viscosity and is much better compressible than water, the piezoelectric actuator can reach higher stroke heights, which leads to a faster movement of the piezoelectric actuator, thus a higher output voltage of the self-sensing pads. Even after the pump chamber is wetted with water, we still see the difference in the output voltage of the self-sensing pads.

Voltage fluctuations between pumping air and water are visible within the microsecond range. There is no significant difference when switching from water to air or from air to water, making the output signal well-suited for detecting air bubbles in a stream of water or water in a stream of air.

With this piezoelectric actuator, no additional sensors are needed, making this actuator a uncomplicated solution for detecting errors in the dosing in real-time by building a closed loop system.

#### 4.4 Failure mode and effects

##### Tightness of the micro pumps

One of the challenges encountered during the fabrication and testing of micro pumps is the tightness of the pumps. It was observed that leaks occur at two different points. On the one hand, leaks occur at the inlet and outlet of the pump in the housing, and on the other hand, leaks occur in the pump body itself.

Regarding the leakage within the housing at the pump's inlet and outlet it is most likely due to insufficient sealing. The inlet and outlet of the pump are build by sealing rings, that connect the inlet and outlet of the pump to the housing. The leaking issue can be caused by particles getting trapped between the sealing rings. Another possible cause is the degradation of sealing rings with time, where the plastic material becomes porous or the surface becomes rough, allowing fluids to pass through. Additionally, it is crucial that the PCB applies adequate pressure to the pump to ensure that that that it is firmly pressed against the sealing rings, securing a tight and reliable seal.

Looking at the leakage, that happens in the pump body itself, it most likely happens on top of the laser weld. The difficulty lies in welding thin metal foils, which form both the valves and the pump chamber, to the base body. This process is carried out using laser beam welding, which requires extremely high precision due to the delicate nature of the foils. A critical aspect of laser beam welding is finding the right parameters: sufficient heat must be applied to achieve a reliable bond between the metal layers, while excessive energy input must be avoided, as it can lead to material degradation such as burning, porosity, or warping. Identifying optimal welding parameters is particularly challenging as the results can vary significantly even when the same settings are used. In addition, small variations in equipment or setup can have a substantial impact on welding outcome.

For example, leaks have been observed in the welding seams of micro pumps equipped with bulk piezoelectric actuators. In these cases, leakage typically occurs at the top of the pump, where a 100  $\mu\text{m}$  thick actuator membrane is used. An example of such a defective porous weld is shown in Figure 43.

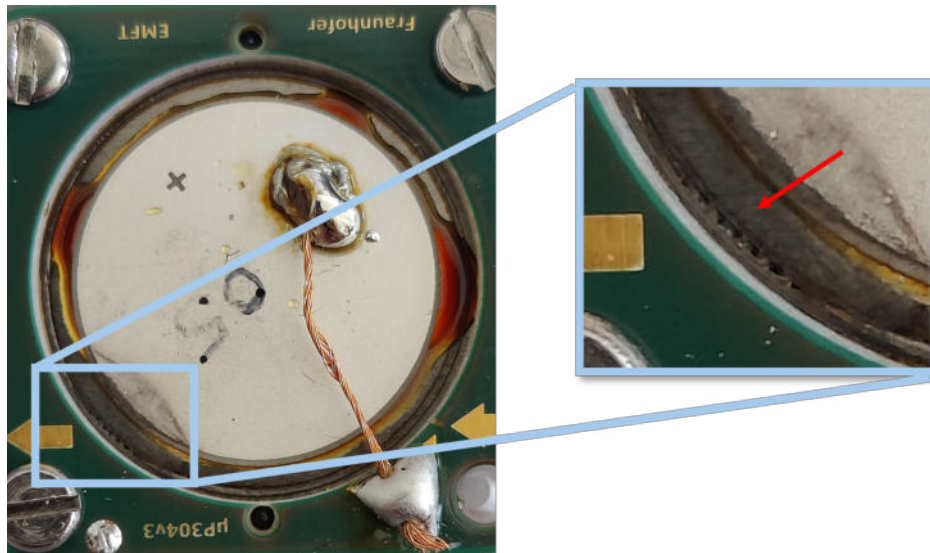


**Figure 43** Micro pump with damaged welding seam on 100  $\mu\text{m}$  thick actuator membrane

In contrast, for micro pumps using stack actuators with a 150  $\mu\text{m}$  thick actuator membrane, leakage tends to occur between the valve foils. In these cases, the leakage is visible at the bottom of the pump, near the PCB, as illustrated in Figure 44.

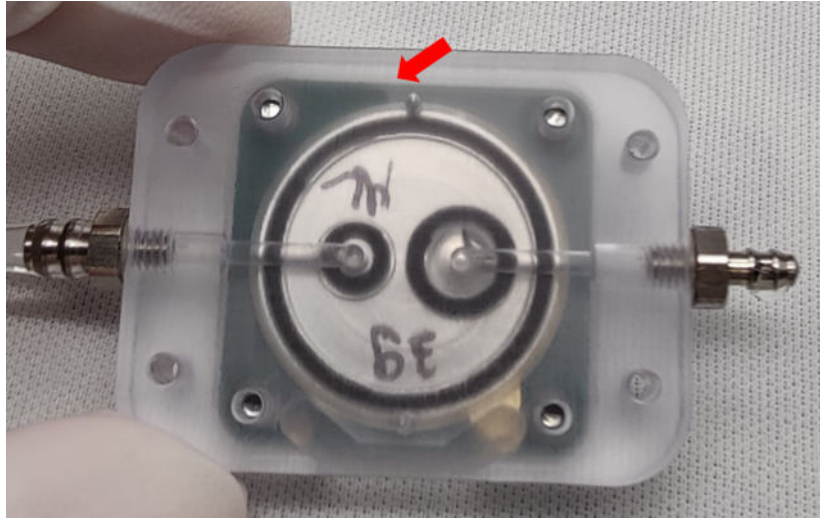


**Figure 44** Micro pump with leakage under PCB

Of course, these seams must be completely leak proof to preserve the integrity of the pump chamber and allow effective fluid pumping.

#### **Soldering of the contacts on the pump**

To establish electrical contact with the piezoelectric actuators on the pumps, a soldered connection is made from the PCB to the actuator. This approach presents two main challenges: thermal stress caused by the high soldering temperature (typically around 360  $^{\circ}\text{C}$ ), and the inherent brittleness of the resulting connection.

Thermal stress is particularly problematic for stack self-sensing piezoelectric actuators. The elevated temperature during soldering can damage the thin active layers of an actuator and may also negatively affect the self-sensing pads. Attempts to reduce the soldering temperature to 320  $^{\circ}\text{C}$  in order to minimize thermal stress resulted in insufficient melting of the solder, preventing the formation of a reliable connection. This issue is illustrated in Figure 45, where the solder joint on the top electrode failed to form properly. After soldering the wire to the sensing pad, even minimal mechanical stress caused the wire to detach, highlighting the fragility of the connection.

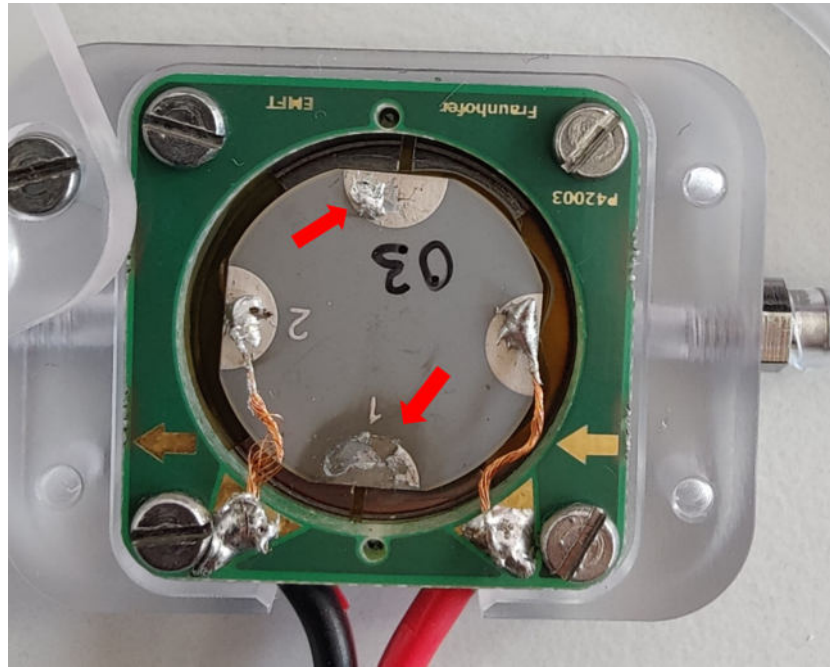


**Figure 45** Lead-based stack piezoelectric actuator with detached sensor pad from thermal stress

On the lower electrode in Figure 45, it can be seen that not only did the solder connection detach due to minimal mechanical stress, but parts of the sensing pad were also lifted or damaged in the process.

These manufacturing related challenges were identified during the development stage, and suitable measures were implemented to address potential failure mechanisms in the manufacturing process.

## 5 Summary and outlook

In the following, all results of this work are summarized and an outlook on possible future developments is provided. This Master's thesis aimed to evaluate novel piezoelectric actuators for micro pumps, in order to further improve the performance of existing models. For this purpose, two novel piezoelectric actuators were investigated: a lead-free bulk piezoelectric actuator and a lead-based stack piezoelectric actuator with integrated self-sensing capabilities.

### Lead-free bulk piezoelectric actuator

As part of the electromechanical characterization of the lead-free bulk piezoelectric actuators, static stroke measurements were carried out. The maximum stroke is a characteristic parameter of each pump and is directly related to the volume of the pump chamber. Micro pumps equipped with lead-free bulk actuators exhibited a mean maximum stroke of  $40,93 \mu\text{m} \pm 3,24 \mu\text{m}$ . Compared to the standard lead-based bulk actuators, this corresponds to a reduction of 53,34 % in maximum stroke.

In the dynamic stroke measurement, the behaviour of the lead-free bulk actuators was found to be similar to that of the lead-based counterparts. Upon application of pressure to the pump chamber, the height of the actuators increased, while the stroke amplitude remained unchanged, showing that the actuators can withstand pressures up to 50 kPa inside the pump chamber.

In the air characterization, different tests were conducted: a frequency sweep and the operation against backpressure. During the frequency sweep, a maximum air flow rate of  $58,15 \text{ mL/min} \pm 9,21 \text{ mL/min}$  was measured at 550 Hz. At 200 Hz, the lead-free bulk actuators achieved a mean air flow rate of  $25,75 \text{ mL/min} \pm 6,27 \text{ mL/min}$ , which is 51,74 % lower than that of the lead-based actuators. While operating against backpressure, the lead-free actuators withstood a maximum backpressure of  $12,46 \text{ kPa} \pm 4,54 \text{ kPa}$  at 30 Hz input frequency, which is 66,58 % lower than the lead-based reference actuators.

In the water characterization, the same two tests were conducted: a frequency sweep and the operation against backpressure. In the frequency sweep, the micro pumps with lead-free bulk actuators achieved a mean maximum water flow rate of  $9,59 \text{ g/min} \pm 0,66 \text{ g/min}$  at 120 Hz. In comparison, the lead-based actuators reached a mean of  $15,13 \text{ g/min} \pm 0,89 \text{ g/min}$  at 70 Hz. In the backpressure test, the lead-free actuators reached a mean maximum backpressure of  $23,75 \text{ kPa} \pm 4,84 \text{ kPa}$ , which is 52,5 % lower than that of the lead-based actuators.

The robustness test revealed a clear trend in the performance degradation of the micro pumps. Due to the limited number of available samples, the results are considered indicative rather than conclusive. Across the different test modes, it became evident that the robustness test significantly impacted the pump's performance for both actuator types, but did not lead to complete functional degradation, even after 72 h. Static stroke measurements before and

after the test showed reductions in maximum stroke after 72 h ranging from 31,30 % to 18,85 % for the lead-free bulk actuators, depending on the specific test mode. The test mode using water with a closed output had the most pronounced negative effect on pump performance, as it induces the highest stress. The backpressure resistance of the pumps was also reduced following the robustness test.

Surface and structural analyses demonstrated that both the fabrication processes and the various test procedures had a considerable impact on the actuator surfaces. For the lead-free bulk piezoelectric actuators, an increased number of surface impurities and deeper grain boundaries were observed compared to their initial state.

Future work could include further robustness testing for the piezoelectric actuators. As the fabrication process of the micro pumps, including the welding of the base bodies, is very delicate, only a few samples were qualified to undergo further processing and testing.

To enhance the performance of micro pumps and mitigate the effects observed during robustness testing, future improvements in pump design are essential. Overall pump quality could benefit from an optimized welding process, while the valve design also offers potential for refinement. To increase backpressure capability, employing a thicker actuator foil and a thicker piezoelectric actuator could be advantageous. These modifications would result in a stiffer membrane, thereby enabling the micro pump to generate greater force and better withstand increased resistance in the fluid path.

### **Lead-based stack piezoelectric actuator with self-sensing properties**

Due to the different structural and material characteristics of these piezoelectric actuators, the fabrication process was optimized accordingly. One significant improvement was the use of adhesive epoxy foil for mounting the piezoelectric actuators onto the pump. Another enhancement involved using conductive adhesive instead of soldering to attach the electrical contacts. Both modifications proved to be successful and functional in the tested setups.

In the static stroke measurement, the lead-based stack piezoelectric actuators achieved a mean maximum stroke of  $28,55 \mu\text{m} \pm 0,34 \mu\text{m}$  across five tested pumps.

To assess the self-sensing capabilities, two different test scenarios were conducted. The first scenario simulated a blockage within the pump, while the second simulated the passage of air bubbles through the system. In the blockage simulation, a gradual decrease in the output voltage from the self-sensing electrodes was observed, indicating that blockages within the tubing can be detected via the self-sensing function. Additionally, the transition between air and water flow through the pump chamber also resulted in a measurable signal change, confirming the potential of these actuators to distinguish between different fluids and detect flow interruptions.

Since this work focused on initial tests with novel piezoelectric actuators, there are some ideas for further evaluations and improvements.

Another step to further improve the micro pumps with self-sensing capabilities would be a new design of the micro pumps to align with the properties of the novel piezoelectric actuators. This would include a new design of the housing for the pumps, as these actuators have four pads that need to be connected. The current design only plans for two connections. Also for the self-sensing properties of the piezoelectric actuators, future work could include automated systems, which detect the sensing of bubbles in the water stream automatically.

## List of Figures

1	Schematic of bulk (single-layer) vs. stack (multi-layer) piezoelectric actuators [16] . . . . .	4
2	Perovskite structure of PT before and after polarization [31] . . . . .	6
3	Schematic design of bulk piezoelectric actuators [27] . . . . .	7
4	Schematic design of stack piezoelectric actuator [27] . . . . .	8
5	Schematic cross-section of a micro pump in its non-functional state. Pump components: 1) piezoelectric actuator 2) Diaphragm 3) 1st valve foil 4) 2nd valve foil 5) Metal base plate 6) Sealing rings 7) Housing 8) Inlet 9) Outlet . . . . .	9
6	Schematic cross-section of a metal micro diaphragm pump with applied voltages	10
7	Overview of selected piezoelectric disc actuators used in this work . . . . .	11
8	Components of the micro pump base body [50] . . . . .	15
9	Fixture for holding pump base bodies for use in the Vieweg glue dispensing machine . . . . .	17
10	Housing materials for the metal micro pumps . . . . .	18
11	Experimental setup for robustness testing of micro pumps in closed-outlet configuration . . . . .	23
12	Static stroke measurement for lead-based bulk piezoelectric actuator on micro pump . . . . .	28
13	Stroke measurement for lead-free piezoelectric actuator on metal micro diaphragm pump . . . . .	30
14	Deflection of the lead-free bulk piezoelectric actuator in dependence of the adjacent pressure and time in dynamic stroke measurement with sine wave input signal . . . . .	31
15	Deflection of the lead-free bulk piezoelectric actuator in dependence of the adjacent pressure and time in dynamic stroke measurement with square wave input signal . . . . .	33
16	Frequency sweep for lead-based bulk piezoelectric actuator on MMDP with air	34
17	Frequency sweep for lead-free bulk piezoelectric actuator on MMDP with air .	35
18	Air flow backpressure test of lead-based bulk piezoelectric actuator on micro pump . . . . .	37
19	Air flow backpressure test of lead-free bulk piezoelectric actuator on MMDP . .	38
20	Frequency sweep for lead-based bulk piezoelectric actuator on micro pump with water . . . . .	40
21	Frequency sweep for lead-free bulk piezoelectric actuator on micro pump with water . . . . .	41

22	Water flow backpressure test of lead-based bulk piezoelectric actuator on micro pump . . . . .	43
23	Water flow backpressure test of lead-based bulk piezoelectric actuator on MMDP	44
24	Water leakage test of lead-based bulk piezoelectric actuator on micro pump . .	45
25	Water leakage test of lead-free bulk piezoelectric actuator on MMDP . . . . .	46
26	Flow chart of the robustness test . . . . .	48
27	Comparison of water flow rates after 72 h robustness test with high blocking pressure (water) on lead-based bulk piezoelectric actuator . . . . .	50
28	Comparison of backpressure testing after 72 h robustness test with continuous water pumping with closed output on lead-based bulk piezoelectric actuator . .	51
29	Comparison of water flow rates after 72 h robustness test with high blocking pressure (water) of lead-free bulk piezoelectric actuator . . . . .	52
30	Comparison of backpressure testing after 72 h robustness test with high blocking pressure (water) on lead-free bulk piezoelectric actuator . . . . .	53
31	SEM of lead-free bulk piezoelectric actuator before robustness testing . . . . .	57
32	SEM of lead-free bulk piezoelectric actuator after robustness testing . . . . .	58
33	SEM side by side comparison of the lead-free bulk piezoelectric actuators before and after various processing and testing steps with a magnification of 8.000 x .	58
34	SEM of lead-based bulk piezoelectric actuator after robustness testing with a magnification of 829 x . . . . .	59
35	SEM of lead-based bulk piezoelectric actuator after robustnesstesting (high magnitude . . . . .	60
36	Mounting of the piezoelectric actuators on the pump base bodies . . . . .	62
37	Micro pump with actuator with scan line for the profile scan . . . . .	62
38	Profile scan over the piezoelectric Actuator on the micro pumps using epoxy foil for mounting . . . . .	63
39	Stroke measurement for lead-based stack piezoelectric actuator on micro pump	64
40	Comparison of stroke height and output voltage of self-sensing pads while actuation . . . . .	66
41	Self-Sensing output voltage over time pumping water with closed output after 0.27 seconds . . . . .	67
42	Self-Sensing output voltage over time pumping air with water droplets . . . . .	68
43	Micro pump with damaged welding seam on 100 $\mu\text{m}$ thick actuator membrane	69
44	Micro pump with leakage under PCB . . . . .	70
45	Lead-based stack piezoelectric actuator with detached sensor pad from thermal stress . . . . .	71

## List of Tables

1	Comparison of properties of different piezoelectric actuators used in this work [45] . . . . .	13
2	Results for the static stroke measurement for micro pumps with lead-free bulk piezoelectric actuators . . . . .	29
3	Measurement results for the backpressure testing for lead-free bulk piezoelectric actuators on micro pumps . . . . .	39
4	Measurement results for frequency sweep with lead-free bulk piezoelectric actuators on micro pumps with water . . . . .	41
5	Comparison of actuator behaviour under different pumping media . . . . .	47
6	Overview of pumps and test modes in robustness test . . . . .	49
7	Comparison of static stroke measurement for micro pumps with lead-free and lead-based bulk piezoelectric actuators in robustness test . . . . .	49
8	Comparison of frequency sweep for the time intervals of the robustness test . .	54
9	Comparison of backpressure test for the time intervals of the robustness test . .	55
10	Comparison of max static stroke heights for the time intervals of the robustness test . . . . .	55
11	Measurement results for the static stroke measurement for the micro pumps with lead-based stack piezoelectric actuators . . . . .	65
12	Material data for the lead-based PZT bulk piezoelectric actuator [45] . . . . .	I
13	Material data for the lead-free KNN bulk piezoelectric actuator [45] . . . . .	II
14	Material data for the lead-based PZT stack piezoelectric actuator [45] . . . . .	III
15	Thickness measurement of the PZT piezoelectric actuators at various points . .	IV
16	Weight measurement and capacitance measurement of the PZT piezoelectric actuators . . . . .	V
17	Thickness measurement of the lead-free piezoelectric actuators at various points	VI
18	Weight measurement and capacitance measurement of lead-free piezoelectric actuators . . . . .	VII
19	Thickness measurement of the multi layer self sensing piezoelectrics at various points . . . . .	VIII
20	Weight measurement and capacitance measurement on both sensor pads of the multi layer piezoelectric . . . . .	X

## References

- [1] Y.-x. Sun, L. Wang, and J.-g. Gao, “Study on the key technology of urban rail train automatic operation system,” *Science in China Series E: Technological Sciences*, vol. 52, no. 12, pp. 3528–3535, 2009. DOI: 10.1007/s11431-009-0283-1. [Online]. Available: <https://link.springer.com/article/10.1007/s11431-009-0283-1>.
- [2] J.-W. Thies, P. Kuhn, B. Thürmann, S. Dübel, and A. Dietzel, “Microfluidic quartz-crystal-microbalance (qcm) sensors with specialized immunoassays for extended measurement range and improved reusability,” *Microelectronic Engineering*, vol. 179, pp. 25–30, 2017. DOI: 10.1016/j.mee.2017.04.023. [Online]. Available: <https://www.sciencedirect.com/science/article/pii/S0167931717301570>.
- [3] V. Singhal and S. V. Garimella, “Induction electrohydrodynamics micropump for high heat flux cooling,” *Sensors and Actuators A: Physical*, vol. 134, pp. 650–659, 2007. DOI: 10.1016/j.sna.2006.05.007. [Online]. Available: <https://www.sciencedirect.com/science/article/pii/S0924424706003566>.
- [4] J. Smits, “Piezoelektrische mikropumpe,” European patent application EP0134614A1, Aug. 1983. [Online]. Available: <https://patents.google.com/patent/EP0134614A1/en>.
- [5] A. Nisar, N. Afzulpurkar, B. Mahaisavariya, and A. Tuantranont, “Mems-based micropumps in drug delivery and biomedical applications,” *Sensors and Actuators B: Chemical*, vol. 130, no. 2, pp. 917–942, 2008. DOI: 10.1016/j.snb.2007.10.064. [Online]. Available: <https://www.sciencedirect.com/science/article/pii/S0925400507009148>.
- [6] Y.-N. Wang and L.-M. Fu, “Micropumps and biomedical applications – a review,” *Microelectronic Engineering*, vol. 195, pp. 121–138, 2018. DOI: 10.1016/j.mee.2018.04.008. [Online]. Available: <https://www.sciencedirect.com/science/article/pii/S0167931718301527>.
- [7] X. Y. Wang, Y. T. Ma, G. Y. Yan, and Z. H. Feng, “A compact and high flow-rate piezoelectric micropump with a folded vibrator,” *Smart Materials and Structures*, vol. 23, no. 11, p. 115005, 2014. DOI: 10.1088/0964-1726/23/11/115005. [Online]. Available: <https://iopscience.iop.org/article/10.1088/0964-1726/23/11/115005>.
- [8] N. A. Hamid, B. Y. Majlis, J. Yunas, A. R. Syafeeza, Y. C. Wong, and M. Ibrahim, “A stack bonded thermo-pneumatic micro-pump utilizing polyimide based actuator membrane for biomedical applications,” *Microsystem Technologies*, vol. 22, no. 5, pp. 1209–1216, 2016. DOI: 10.1007/s00542-016-2951-y. [Online]. Available: <https://link.springer.com/article/10.1007/s00542-016-2951-y>.

- [9] A. Lee and B. Smith, “A study on piezoelectric micropumps,” *Journal of Microfluidics*, vol. 12, pp. 123–130, 2016.
- [10] S. Spieth, A. Schumacher, T. Holtzman, *et al.*, “An intra-cerebral drug delivery system for freely moving animals,” *Biomedical Microdevices*, vol. 14, no. 5, pp. 799–809, 2012. DOI: 10.1007/s10544-012-9659-2.
- [11] K. G. Sravani, D. Ramakrishna, P. Chandh, K. Sathvik, and K. S. Rao, “Design of micropump with two stacked ring type piezoelectric actuators for drug delivery,” *Journal of Micro-Bio Robotics*, vol. 17, no. 2, pp. 69–78, 2022. DOI: 10.1007/s12213-022-00146-1. [Online]. Available: <https://link.springer.com/article/10.1007/s12213-022-00146-1>.
- [12] S. Fournier and E. Chappel, “Dynamic simulations of a piezoelectric driven mems micropump,” in *Proceedings of the 30th Eurosensors Conference*, vol. 168, 2016, pp. 860–863. DOI: 10.1016/j.proeng.2016.11.291. [Online]. Available: <https://www.sciencedirect.com/science/article/pii/S1877705816336049>.
- [13] R. K. Haldkar, V. K. Gupta, and T. Sheorey, “Modeling and flow analysis of piezoelectric based micropump with various shapes of microneedle,” *Journal of Mechanical Science and Technology*, vol. 31, no. 6, pp. 2933–2941, 2017. DOI: 10.1007/s12206-017-0536-z. [Online]. Available: <https://link.springer.com/article/10.1007/s12206-017-0536-z>.
- [14] Z. Zhang, J. w. Kan, S. Wang, H. Wang, J. Ma, and Y. Jiang, “Development of a self-sensing piezoelectric pump with a bimorph transducer,” *Journal of Intelligent Material Systems and Structures*, vol. 27, no. 5, pp. 581–591, 2016, ISSN: 1045-389X. DOI: 10.1177/1045389X15575082.
- [15] P.-H. Cazorla, O. Fuchs, M. Cochet, S. Maubert, Y. Fouillet, and E. Defay, “A low voltage silicon micro-pump based on piezoelectric thin films,” *Sensors and Actuators A: Physical*, vol. 250, pp. 35–39, 2016. DOI: 10.1016/j.sna.2016.05.042. [Online]. Available: <https://www.sciencedirect.com/science/article/pii/S1877705816336049>.
- [16] Unictron Technologies Co., Ltd., *Multilayer piezoelectric actuators*, <https://www.unictron.com/news/multilayer-piezoelectric-actuators/>, Zugriff am 12. Juni 2025, 2025.
- [17] R. Hu, L. He, D. Hu, Y. Hou, and G. Cheng, “Recent studies on the application of piezoelectric pump in different fields,” *Microsystem Technologies*, vol. 29, no. 5, pp. 663–682, 2023. DOI: 10.1007/s00542-023-05453-6. [Online]. Available: <https://link.springer.com/article/10.1007/s00542-023-05453-6>.

- [18] A. Angelou, C. Norman, N. Miran, S. Albers, R. Moradi-Dastjerdi, and K. Behdinin, “An eco-friendly, biocompatible and reliable piezoelectric nanocomposite actuator for the new generation of microelectronic devices,” *The European Physical Journal Plus*, vol. 136, no. 6, 2021. DOI: 10.1140/epjp/s13360-021-01653-z.
- [19] Y. Meng, G. Chen, and M. Huang, “Piezoelectric materials: Properties, advancements, and design strategies for high-temperature applications,” *Nanomaterials (Basel)*, vol. 12, no. 7, p. 1171, Apr. 2022. DOI: 10.3390/nano12071171.
- [20] A. Dahiya, O. P. Thakur, and J. K. Juneja, “Sensing and actuating applications of potassium sodium niobate: Use of potassium sodium niobate in sensor and actuator,” pp. 383–386, DOI: 10.1109/ICSensT.2013.6727680.
- [21] S. Kawada, H. Hayashi, H. Ishii, *et al.*, “Potassium sodium niobate-based lead-free piezoelectric multilayer ceramics co-fired with nickel electrodes,” *Materials (Basel, Switzerland)*, vol. 8, no. 11, pp. 7423–7438, 2015, ISSN: 1996-1944. DOI: 10.3390/ma8115389.
- [22] Y. Zhang, Q. Hang, D. Zheng, F. Lin, and C. Chen, “Fabrication of a laminated actuator with excellent linearity using ground potassium sodium niobate-based ceramic sheets,” *Inorganics*, vol. 12, no. 1, p. 18, 2024. DOI: 10.3390/inorganics12010018.
- [23] F. Hubert, *Piezelektrische EMV-Filter*. Wiesbaden: Springer Fachmedien Wiesbaden, 2023. DOI: 10.1007/978-3-658-41858-8.
- [24] L. Guo, S.-T. Han, and Y. Zhou, “Electromechanical coupling effects for data storage and synaptic devices,” *Nano Energy*, vol. 77, p. 105156, 2020, ISSN: 2211-2855. DOI: <https://doi.org/10.1016/j.nanoen.2020.105156>. [Online]. Available: <https://www.sciencedirect.com/science/article/pii/S2211285520307345>.
- [25] R. Hinchet, U. Khan, C. Falconi, and S.-W. Kim, “Piezoelectric properties in two-dimensional materials: Simulations and experiments,” *Materials Today*, vol. 21, no. 6, pp. 611–630, 2018, ISSN: 1369-7021. DOI: <https://doi.org/10.1016/j.mattod.2018.01.031>. [Online]. Available: <https://www.sciencedirect.com/science/article/pii/S1369702117306715>.
- [26] M. Gall, “Experimentelle und numerische untersuchungen zur lebensdauer von flächigen piezokeramischen sensor- & aktor-modulen,” Dissertation, Karlsruher Institut für Technologie (KIT), Karlsruhe, Deutschland, 2012.
- [27] X. Zhou, S. Wu, X. Wang, *et al.*, “Review on piezoelectric actuators: Materials, classifications, applications and recent trends,” *Frontiers of Mechanical Engineering*, vol. 19, no. 1, p. 6, 2024, Kapitel 2: Piezoelectric effects. DOI: 10.1007/s11465-023-0772-0.

- [28] A. Aabid, M. A. Raheman, Y. E. Ibrahim, *et al.*, “A systematic review of piezoelectric materials and energy harvesters for industrial applications,” *Sensors*, vol. 21, no. 12, 2021, ISSN: 1424-8220. DOI: 10.3390/s21124145. [Online]. Available: <https://www.mdpi.com/1424-8220/21/12/4145>.
- [29] W. Heywang, K. Lubitz, and W. Wersing, *Piezoelectricity: Evolution and Future of a Technology* (Springer Series in Materials Science). Springer, 2008, vol. 114, ISBN: 978-3-540-68683-5. DOI: 10.1007/978-3-540-68683-5.
- [30] D.-J. Shin, S. Jeong, C.-E. Seo, K. H. Cho, and [Autoren], “Multi-layered piezoelectric energy harvesters based on pzt ceramic actuators,” *Ceramics International*, vol. 41, no. 6, p. 6, 2015. DOI: 10.1016/j.ceramint.2015.03.180.
- [31] A. K. Zak, S. T. Yazdi, M. E. Abrishami, and A. M. Hashim, “A review on piezoelectric ceramics and nanostructures: Fundamentals and fabrications,” *Journal of the Australian Ceramic Society*, vol. 60, no. 3, pp. 723–753, 2024. DOI: 10.1007/s41779-024-00990-3.
- [32] W. P. Chen, H. L. W. Chan, F. C. H. Yiu, K. M. W. Ng, and P. C. K. Liu, “Water-induced degradation in lead zirconate titanate piezoelectric ceramics,” *Applied Physics Letters*, vol. 80, no. 19, pp. 3587–3589, 2002. DOI: 10.1063/1.1479205.
- [33] N. Sezer and M. Koç, “A comprehensive review on the state-of-the-art of piezoelectric energy harvesting,” *Nano Energy*, vol. 80, p. 105567, 2021. DOI: 10.1016/j.nanoen.2020.105567.
- [34] G. H. Khorrami, A. Kompany, and A. K. Zak, “Structural and optical properties of knn nanocubes synthesized by a green route using gelatin,” *Functional Materials Letters*, vol. 8, no. 2, p. 1550030, 2015. DOI: 10.1142/S1793604715500307.
- [35] Kyocera Corporation. “Piezoelectric element (single plate) – energy conversion devices.” Zugriff am 13. Juni 2025. (2025).
- [36] Motion Control Tips, *Faq: What are stacked piezo actuators and what do they do?* <https://www.motioncontroltips.com/faq-what-are-stacked-piezo-actuators-and-what-do-they-do/>, Zugriff am 13. Juni 2025.
- [37] K. Axelsson, M. Sheikhsarraf, P. Höllein, D. Lewke, and M. Richter, “Self-sensing micropump with gas bubble detection for improved dosing reliability,” in *Proceedings of the 14th International Fluid Power Conference*, River Publishers, 2024. DOI: 10.13052/rp-9788770042222C42. [Online]. Available: [https://www.riverpublishers.com/research\\_article\\_details.php?book\\_id=1139&cid=42](https://www.riverpublishers.com/research_article_details.php?book_id=1139&cid=42).
- [38] Z. Zhang, J. Kan, G. Cheng, H. Wang, and Y. Jiang, “A piezoelectric micropump with an integrated sensor based on space-division multiplexing,” *Sensors and Actuators A: Physical*, vol. 203, pp. 29–36, 2013, ISSN: 09244247. DOI: 10.1016/j.sna.2013.08.027.

- [39] “Method for manufacturing a bending transducer, a micro pump and a micro valve, micro pump and micro valve,” 20130055889, Mar. 2013. [Online]. Available: <https://www.freepatentsonline.com/y2013/0055889.html>.
- [40] A. B. Bußmann, C. P. Durasiewicz, S. H. A. Kibler, and C. K. Wald, “Piezoelectric titanium based microfluidic pump and valves for implantable medical applications,” *Sensors and Actuators A: Physical*, vol. 323, p. 112649, 2021, ISSN: 0924-4247. DOI: <https://doi.org/10.1016/j.sna.2021.112649>. [Online]. Available: <https://www.sciencedirect.com/science/article/pii/S0924424721001114>.
- [41] A. B. Bußmann, “Biomedical application of piezoelectric micro diaphragm pumps,” Veröffentlicht am 09. Mai 2022; 140 Seiten, Dissertation, Karlsruher Institut für Technologie (KIT), Fakultät für Chemieingenieurwesen und Verfahrenstechnik, May 2022. DOI: 10.5445/IR/1000145645. [Online]. Available: <https://doi.org/10.5445/IR/1000145645>.
- [42] T. Thalhofer, A. Bussmann, C. Durasiewicz, and O. Hayden, “Effect of actuation signal on single stroke volume in metal micro diaphragm pumps,” in *ACTUATOR; International Conference and Exhibition on New Actuator Systems and Applications 2021*, 2021, pp. 1–4.
- [43] C. P. Durasiewicz, “Development of a metal-based microfluidic mems platform for medical applications,” Eingereicht am 09.06.2022, mündliche Prüfung am 12.12.2022, PhD Dissertation, Technische Universität München, München, Deutschland, 2022. [Online]. Available: <https://mediatum.ub.tum.de/?id=1660219>.
- [44] P. Instrumente, *Fertigungstechnologie - presstechnik*, Accessed: 2025-04-24, 2024. [Online]. Available: <https://www.physikinstrumente.de/de/expertise/technologie/piezotechnologie/fertigungstechnologie/presstechnik>.
- [45] PI Ceramic GmbH, *Material data*, Accessed: 2025-04-22, Aug. 2024. [Online]. Available: <https://www.piceramic.com/en/?type=5600&downloadUId=1385&downloadFileUId=1255>.
- [46] P.-E. GmbH, “Elecolit® 3661: Technisches Datenblatt,” Panacol-Elosol GmbH, Stierstädter Straße 4, 61449 Steinbach, Germany, Tech. Rep. Revision 7, Aug. 2024, Stand: 16.09.2024. Technisches Datenblatt für elektrisch leitfähigen 1K-Epoxidklebstoff. [Online]. Available: <https://www.panacol.de>.
- [47] H. Corporation, “LOCTITE ABLESTIK 563K: Thermally Conductive Epoxy Film Adhesive,” Henkel Corporation, Tech. Rep., Nov. 2019, Technical Data Sheet, Revision from November 2019. Film adhesive with 1.1 W/(m·K) thermal conductivity and 97°C glass transition temperature. [Online]. Available: <https://www.henkel.com/electronics>.

- [48] Rohde & Schwarz GmbH & Co. KG, *R&S® RTB2000 oszilloskop*, [https://www.rohde-schwarz.com/de/produkte/messtechnik/oszilloskope/rs-rtb2000-oszilloskop\\_63493-266306.html](https://www.rohde-schwarz.com/de/produkte/messtechnik/oszilloskope/rs-rtb2000-oszilloskop_63493-266306.html), Digitales Oszilloskop mit 10-Bit A/D-Konverter, 10Msample Speicher und 10.1 Touchscreen :contentReference[oaicite:1]index=1, Munich, Germany: Rohde&Schwarz GmbH&Co.KG, 2025.
- [49] Digilent Inc., *Analog Discovery 3: 125MS/s USB Oscilloscope, Logic Analyzer, Waveform Generator & Power Supply*, <https://digilent.com/shop/analog-discovery-3/>, Portable USB-C-powered Multifunktionsgerät (125MS/s, 14-Bit, 30 MHz BW, 16 I/O, 800 mA Versorgung) :contentReference[oaicite:1]index=1, Pullman, WA, USA: Digilent Inc., 2025.
- [50] Fraunhofer-Institut für Elektronische Mikrosysteme und Festkörper-Technologien EMFT, *Piezoelektrisch angetriebene mikropumpen*, <https://www.emft.fraunhofer.de/de/kompetenzen/mikropumpen/piezo-mikropumpe-piezoelektrizitaet.html>, Accessed: 2025-06-15, München, Germany, 2025.
- [51] F. GmbH, *Bedienungsanleitung frt microprof*, Version 2.237, FRT GmbH, Bergisch Gladbach, Deutschland, 2017.
- [52] Keysight Technologies, *33500b und 33600a trueform waveform-generatoren – datenblatt*, <https://www.keysight.com/us/en/assets/7018-05928/data-sheets/5992-2572.pdf>, Zugegriffen am 20. Mai 2025, 2017.
- [53] piezosystem jena GmbH, *SVR 1000/1 analog piezo amplifier – bedienungsanleitung*, Manual page 8: technical specifications and usage instructions, Stockholmer Str. 12, 07747 Jena, Germany, n.d. [Online]. Available: <https://www.manualslib.de/manual/297131/Piezosystemjena-Svr-1000-1.html>.
- [54] Bronkhorst High-Tech B.V., *LOW-P-FLOW Massedurchflussmesser/-regler mit geringem Druckabfall und für korrosive Gase*, <https://www.dex.cz/uploads/2017/06/lowdpg.pdf>, Zugegriffen am 20. Mai 2025, 2017.
- [55] Bronkhorst High-Tech B.V., *Mass flow / pressure meters and controllers for gases and liquids*, Manual No. 9.17.001, 2016. [Online]. Available: <https://www.bronkhorst.com/media/imqj1fz1/917001-manual-mass-flow-pressure-meters-and-controllers-for-gases-and-liquids.pdf?v=1dbaeb21f9287b0>.
- [56] WIKA Alexander Wiegand SE & Co. KG, *Betriebsanleitung: Pneumatischer High-Speed Druckcontroller CPC3000*, German, Version 1.1, Dokumentnummer 11498162.01, Klingenberg, Deutschland, 2009. [Online]. Available: [https://www.mensor.com/media/Operating-instructions/Operating-instructions/Calibration/Pressure-controllers/oi\\_cpc3000\\_archived\\_de.pdf](https://www.mensor.com/media/Operating-instructions/Operating-instructions/Calibration/Pressure-controllers/oi_cpc3000_archived_de.pdf).

- [57] Bronkhorst High-Tech B.V., *mini CORI-FLOW™ – Coriolis Massendurchflussmesser und -regler*, Dokumentennummer 961071, Ruurlo, Niederlande, 2025. [Online]. Available: <https://prod-bronkhorst-products-cdn-cdwbfhmd0gfecfb.a02.azurefd.net/media/gphlnonz/961071-mini-cori-flow-de.pdf>.
- [58] W. Zhou and Z. L. Wang, Eds., *Scanning Microscopy for Nanotechnology: Techniques and Applications*. Boston, MA: Springer, 2007, ISBN: 978-0-387-39620-0. DOI: 10.1007/978-0-387-39620-0. [Online]. Available: <https://link.springer.com/book/10.1007/978-0-387-39620-0>.
- [59] Carl Zeiss AG, *ZEISS GeminiSEM Produktfamilie*, <https://www.zeiss.com/microscopy/de/produkte/sem-und-fib-sem/sem/die-geminisem-produktfamilie.html>, Zugriff am 14. Mai 2025, 2025.
- [60] KEYENCE Deutschland GmbH, *Datenblatt: 3D-Profilometer VR-6000*, <https://www.keyence.de/products/3d-measure/roughness-measure/vr-6000/models/vr-6000/>, Zugriff am 14. Mai 2025, 2025.

## 6 Appendix

### 6.1 Material data for different piezoelectric actuators

**Table 12** Material data for the lead-based PZT bulk piezoelectric actuator [45]

PZT - PIC151	Unit	Sign	Value
<b>Physical and dielectric properties</b>			
Diameter	$mm$	$d$	16
Weight	$mg$	$m$	300
Thickness	$\mu m$	$t$	200
Density	$g/cm^3$	$\rho$	7.8
Curie temperature	$^{\circ}C$	$T_C$	250
Coercive field strength	$kV/mm$	$E_C$	1.0
<b>Electro-mechanical properties</b>			
Piezoelectric charge coefficient	$10^{-12}C/N$	$d_{31}$	-210
		$d_{32}$	500
		$d_{33}$	610
Coupling factor		$k_p$	0.62
		$k_t$	0.53
		$k_{31}$	0.35
		$k_{32}$	0.69
<b>Acousto-mechanical properties</b>			
Elastic compliance coefficient	$10^{-12}m^2/N$	$S_{11}^E$	16.4
		$S_{33}^E$	19.4
Elastic stiffness coefficient	$10^{-10}N/m^2$	$C_{11}^D$	15.7

**Table 13** Material data for the lead-free KNN bulk piezoelectric actuator [45]

<b>KNN - PIC753</b>	<b>Unit</b>	<b>Sign</b>	<b>Value</b>
<b>Physical and dielectric properties</b>			
Diameter	$mm$	$d$	16
Weight	$mg$	$m$	appr. 200
Thickness	$\mu m$	$t$	200
Density	$g/cm^3$	$\rho$	4.8
Curie temperature	$^{\circ}C$	$T_C$	300
Coercive field strength	$kV/mm$	$E_C$	1.1
<b>Electro-mechanical properties</b>			
Piezoelectric charge coefficient	$10^{-12}C/N$	$d_{31}$	-118
		$d_{32}$	241
		$d_{33}$	316
Coupling factor		$k_p$	0.53
		$k_t$	0.45
		$k_{31}$	0.30
		$k_{32}$	0.59
<b>Acousto-mechanical properties</b>			
Elastic compliance coefficient	$10^{-12}m^2/N$	$S_{11}^E$	12.2
		$S_{33}^E$	13.6
Elastic stiffness coefficient	$10^{-10}N/m^2$	$C_{11}^D$	17.2

**Table 14** Material data for the lead-based PZT stack piezoelectric actuator [45]

<b>PZT - PIC252</b>	<b>Unit</b>	<b>Sign</b>	<b>Value</b>
<b>Physical and dielectric properties</b>			
Diameter	<i>mm</i>	<i>d</i>	16
Weight	<i>mg</i>	<i>m</i>	appr. 886
Thickness	$\mu m$	<i>t</i>	570
Density	$g/cm^3$	$\rho$	7.8
Curie temperature	$^{\circ}C$	$T_C$	350
Coercive field strength	$kV/mm$	$E_C$	1.5
<b>Electro-mechanical properties</b>			
Piezoelectric charge coefficient	$10^{-12}C/N$	$d_{31}$	-180
		$d_{32}$	400
		$d_{33}$	550
Coupling factor		$k_p$	0.62
		$k_t$	0.47
		$k_{31}$	0.35
		$k_{33}$	0.69
<b>Acousto-mechanical properties</b>			
Elastic compliance coefficient	$10^{-12}m^2/N$	$S_{11}^E$	16
		$S_{33}^E$	19
Elastic stiffness coefficient	$10^{-10}N/m^2$	$C_{11}^D$	15.4

## 6.2 Measurement results of the preliminary examination of the piezoelectric actuators

**Table 15** Thickness measurement of the PZT piezoelectric actuators at various points

<b>Actuator</b>	<b>Thickness 1</b> in $\mu\text{m}$	<b>Thickness 2</b> in $\mu\text{m}$	<b>Thickness 3</b> in $\mu\text{m}$	<b>Average thickness</b> in $\mu\text{m}$
1	197	197	197	197,0
2	197	196	196	196,3
3	197	198	198	197,7
4	198	198	198	198,0
5	199	197	199	198,3
6	198	198	198	198,0
7	198	199	198	198,3
8	199	199	199	199,0
9	198	198	198	198,0
10	198	199	199	198,7
11	197	197	198	197,3
12	198	198	198	198,0
13	197	199	197	197,7
14	197	198	197	197,3
15	198	198	197	197,7
16	199	198	198	198,3
17	198	198	198	198,0
18	199	199	201	199,7
19	198	198	201	199,0
20	197	197	199	197,7
21	198	198	198	198,0
22	198	198	197	197,7
23	198	200	198	198,7
24	198	198	199	198,3
25	197	202	201	200,0

**Table 16** Weight measurement and capacitance measurement of the PZT piezoelectric actuators

<b>Actuator</b>	<b>Weight in mg</b>	<b>Capacity in nF</b>
1	311	2,21
2	309	2,22
3	311	2,19
4	310	2,18
5	310	2,15
6	311	2,15
7	311	2,14
8	312	2,17
9	311	2,17
10	311	2,16
11	310	2,15
12	312	2,15
13	311	2,18
14	310	2,14
15	310	2,15
16	310	2,16
17	310	2,16
18	312	2,16
19	311	2,17
20	310	2,15
21	309	2,17
22	310	2,15
23	311	2,15
24	311	2,17
25	310	2,19

**Table 17** Thickness measurement of the lead-free piezoelectric actuators at various points

<b>Actuator</b>	<b>Thickness 1</b> in $\mu\text{m}$	<b>Thickness 2</b> in $\mu\text{m}$	<b>Thickness 3</b> in $\mu\text{m}$	<b>Average thickness</b> in $\mu\text{m}$
1	207,8	206,8	207,1	207,2
2	215	215,6	226,9	219,2
3	203	204,15	204,15	203,8
4	204,3	204,75	204,15	204,4
5	205,9	204,2	205,35	205,2
6	213,15	213,6	214,4	213,7
7	206,6	205,8	205,5	206
8	207,9	208,5	210,2	208,9
9	205,5	205,7	204,7	205,3
10	205,5	206,9	205,9	206,1
11	201,2	201,4	202,5	201,7
12	209,8	211	212,9	211,2
13	207,05	206	206,9	206,7
14	206,3	206,4	206,15	206,3
15	207,2	207,4	207,4	207,3
16	205,5	203	204,4	204,3
17	204,6	205,5	204,8	205
18	205,1	209,6	204,7	206,5
19	211	209,7	210,2	210,3
20	208,9	206,4	207,6	207,6
21	201,35	203,7	206,1	203,7
22	207,8	207,1	208	207,6
23	212,4	211,75	213,8	212,7
24	207,7	208,5	208,3	208,2
25	209,4	205,9	206,6	207,3

**Table 18** Weight measurement and capacitance measurement of lead-free piezoelectric actuators

<b>Actuator</b>	<b>Weight in mg</b>	<b>Capacity in nF</b>
1	202,2	9,30
2	208,7	9,07
3	201,2	9,39
4	199,1	9,41
5	199,2	9,32
6	204,5	9,28
7	201,4	9,28
8	199,8	9,45
9	199,9	9,43
10	201,1	9,15
11	197,5	9,33
12	205,2	9,09
13	201,5	9,37
14	201,1	9,27
15	201,7	9,29
16	197,6	9,44
17	200,1	9,40
18	199,6	9,47
19	200,9	9,51
20	200,7	9,22
21	197,9	9,64
22	200,7	9,22
23	205,2	9,23
24	203,7	9,24
25	200,3	9,40

**Table 19** Thickness measurement of the multi layer self sensing piezoelectrics at various points

<b>Actuator</b>	<b>Thickness 1</b> in $\mu\text{m}$	<b>Thickness 2</b> in $\mu\text{m}$	<b>Thickness 3</b> in $\mu\text{m}$	<b>Average thickness</b> in $\mu\text{m}$
1	578,95	587	592	586,0
2	573,95	573,65	569,7	572,4
3	561,3	575,1	575,3	570,6
4	580,75	586,05	582,75	583,2
5	581,9	596,2	592,15	590,1
6	569,15	577,5	576,55	574,4
7	579,2	581,1	583	581,1
8	579,4	586,95	583,55	583,3
9	573,95	586,55	572,75	577,8
10	580,9	594,05	587,5	587,5
11	584,7	585,55	587,45	585,9
12	576,25	580,85	592,05	583,1
13	578,95	574,55	577,1	576,9
14	563,6	567,3	570,55	567,2
15	578,85	579,65	583,55	580,7
16	580,5	581,05	580,95	580,8
17	567,8	583,5	587,9	579,7
18	580,7	571,25	575,55	575,8
19	571,45	585,7	588,1	581,8
20	576,5	578,35	581,65	578,8
21	578,5	583,15	583,2	581,6
22	581,7	574,3	581,55	579,2
23	578,9	572,85	580,35	577,4
24	585,75	589,95	585,1	586,9
25	577,55	578,35	583,25	579,7
26	573,85	581,15	581,95	579,0
27	581,6	573,6	572,85	576,0
28	569,65	567,05	567,5	568,1
29	561,3	566,4	569,8	565,8
30	576,45	570,35	571,9	572,9
31	582,15	586,6	575	581,3
32	582,15	584,65	575,25	580,7
33	590,4	580,65	593,3	588,1
34	565,85	580,4	571,3	572,5
35	580,4	578,4	589,65	582,8
36	573,1	577,1	592,95	581,1
37	579,9	580,6	586,5	582,3
38	576,95	573,35	574,6	575,0
39	572,05	577,65	578,65	576,1
40	585,6	589,6	588,3	587,8

<b>Actuator</b>	<b>Thickness 1</b> in $\mu\text{m}$	<b>Thickness 2</b> in $\mu\text{m}$	<b>Thickness 3</b> in $\mu\text{m}$	<b>Average thickness</b> in $\mu\text{m}$
41	586,9	599,3	583,3	589,8
42	568,6	572,45	584,4	575,2
43	565,25	597,45	573,4	578,7
44	567,9	584	588,4	580,1
45	570,3	569,75	573,55	571,2
46	564,75	580,35	568,75	571,3
47	562,2	585,9	574,85	574,3
48	562,15	561,7	569,55	564,5
49	561,25	569,35	564,9	565,2
50	576,7	579,6	575,9	577,4

**Table 20** Weight measurement and capacitance measurement on both sensor pads of the multi layer piezoelectric

Actuator	Weight in mg	Capacity sensor pad 1 in nF	Capacity sensor pad 1 in nF
1	886,7	141,60	1240,00
2	887,1	143,50	1253,00
3	884,5	142,10	1254,00
4	882,7	141,80	1233,00
5	887,9	141,50	1235,00
6	884,5	141,90	1261,00
7	886,4	141,50	1233,00
8	884,2	142,50	1238,00
9	887,5	141,90	1256,00
10	888,5	140,40	1229,00
11	886,6	139,10	1218,00
12	887,0	142,10	1239,00
13	882,4	142,70	1243,00
14	882,4	143,20	1238,00
15	886,3	142,30	1239,00
16	887,2	141,30	1238,00
17	885,9	141,40	1243,00
18	887,4	142,30	1234,00
19	885,1	142,40	1239,00
20	885,1	142,80	1240,00
21	888,9	137,90	1211,00
22	886,0	142,30	1235,00
23	887,2	142,80	1236,00
24	888,2	142,30	1235,00
25	883,9	142,10	1238,00
26	888,0	141,30	1223,00
27	887,7	139,80	1228,00
28	883,2	140,20	1237,00
29	886,5	142,90	1236,00
30	887,9	141,50	1229,00
31	887,2	143,20	1236,00
32	889,5	142,10	1222,00
33	890,6	139,00	1195,00
34	885,5	142,70	1237,00
35	886,9	139,10	1203,00
36	882,5	143,20	1245,00
37	886,3	142,70	1243,00
38	884,9	142,70	1241,00
39	883,6	142,30	1243,00
40	885,2	141,60	1239,00

<b>Actuator</b>	<b>Weight in mg</b>	<b>Capacity sensor pad 1 in nF</b>	<b>Capacity sensor pad 1 in nF</b>
41	885,5	142,30	1237,00
42	888,4	141,60	1230,00
43	886,9	143,70	1254,00
44	884,1	142,30	1239,00
45	889,1	140,60	1238,00
46	885,6	141,90	1240,00
47	890,2	139,50	1230,00
48	886,7	142,90	1259,00
49	887,1	141,60	1249,00
50	885,9	142,10	1249,00